

**DOT/FAA/AR-03/44**

Office of Aviation Research  
Washington, D.C. 20591

# **Statistical Loads Data for Bombardier CRJ100 Aircraft in Commercial Operations**

June 2003

Final Report

This document is available to the U.S. public  
through the National Technical Information  
Service (NTIS), Springfield, Virginia 22161.



U.S. Department of Transportation  
**Federal Aviation Administration**

## **NOTICE**

This document is disseminated under the sponsorship of the U.S. Department of Transportation in the interest of information exchange. The United States Government assumes no liability for the contents or use thereof. The United States Government does not endorse products or manufacturers. Trade or manufacturer's names appear herein solely because they are considered essential to the objective of this report. This document does not constitute FAA certification policy. Consult your local FAA aircraft certification office as to its use.

This report is available at the Federal Aviation Administration William J. Hughes Technical Center's Full-Text Technical Reports page: [actlibrary.tc.faa.gov](http://actlibrary.tc.faa.gov) in Adobe Acrobat portable document format (PDF).

# Technical Report Documentation Page

1. Report No. DOT/FAA/AR-03/44		2. Government Accession No.		3. Recipient's Catalog No.	
4. Title and Subtitle  STATISTICAL LOADS DATA FOR BOMBARDIER CRJ100 AIRCRAFT IN COMMERCIAL OPERATIONS				5. Report Date  June 2003	
				6. Performing Organization Code	
7. Author(s) John W. Rustenburg, Donald A. Skinn, and Daniel O. Tipps				8. Performing Organization Report No. UDR-TR-2002-00108	
9. Performing Organization Name and Address University of Dayton Research Institute Structural Integrity Division 300 College Park Dayton, OH 45469-0120				10. Work Unit No. (TRAIS) RPD-510	
				11. Contract or Grant No. Grant No. 00-G-015	
12. Sponsoring Agency Name and Address U.S. Department of Transportation Federal Aviation Administration Office of Aviation Research Washington, DC 20591				13. Type of Report and Period Covered Final Report	
				14. Sponsoring Agency Code ANM-100	
15. Supplementary Notes  The Federal Aviation Administration William J. Hughes Technical Center COTR was Thomas DeFiore.					
16. Abstract  The University of Dayton is supporting Federal Aviation Administration (FAA) research on the structural integrity requirements for the U.S. commercial transport airplane fleet. The primary objective of this research is to develop new and improved methods and criteria for processing and presenting commercial transport airplane flight and ground loads usage data. The scope of activities performed involves (1) defining the service-related factors that affect the operational life of commercial aircraft; (2) designing an efficient software system to reduce, store, and process large quantities of optical quick-access recorder data; and (3) reducing, analyzing, and providing processed data in statistical formats that will enable the FAA to reassess existing certification criteria. Equally important, these new data will also enable the FAA, the aircraft manufacturers, and the airlines to better understand and control those factors that influence the structural integrity of commercial transport aircraft. Presented herein are Bombardier CRJ100 aircraft operational usage data collected from 467 flights, representing 607.2 flight hours, as recorded by a single airline operator. Statistical data are presented on the aircraft's usage, flight and ground loads data, and systems operational data. The data presented in this report will provide the user with information about the accelerations, speeds, altitudes, flight duration and distance, thrust reverser usage, and gust velocities encountered by the Bombardier CRJ100 during actual operational usage.					
17. Key Words  Optical quick-access recorder, Flight profiles, Flight loads, Ground loads, Systems operational data, Statistical loads data			18. Distribution Statement  This document is available to the public through the National Technical Information Service (NTIS), Springfield, Virginia 22161.		
19. Security Classif. (of this report) Unclassified		20. Security Classif. (of this page) Unclassified		21. No. of Pages 97	
				22. Price	

## PREFACE

This research was performed by the Flight Systems Integrity Group of the Structural Integrity Division of the University of Dayton Research Institute under Federal Aviation Administration (FAA) Grant No. 00-G-015 entitled “An Assessment of CRJ100 Operational Loads and Usage Characteristics and Automated Systems Effects.” The Program Manager for the FAA was Mr. Thomas DeFiore of the FAA William J. Hughes Technical Center at Atlantic City International Airport, New Jersey, and the Program Technical Advisor was Mr. John Howford of the FAA Aircraft Certification Office. Additional support was provided by Mr. Anthony Linsdell of Bombardier and Mr. Jack Grabowski of Transport Canada. Mr. Daniel Tipps was the Principal Investigator for the University of Dayton, who provided overall technical direction for this effort, and assisted in preparation of the final report. Mr. Donald Skinn developed the data reduction algorithms, programmed the data reduction criteria, and performed the data reduction. Mr. John Rustenburg performed the data analysis, created the graphical presentations, and prepared the final report.

## TABLE OF CONTENTS

	Page
EXECUTIVE SUMMARY	xi
1. INTRODUCTION	1
2. AIRCRAFT DESCRIPTION	1
3. AIRLINE DATA COLLECTION AND GROUND PROCESSING SYSTEMS	2
4. UNIVERSITY OF DAYTON RESEARCH INSTITUTE DATA PROCESSING	3
4.1 Recorded Data Parameters	4
4.2 Computed Parameters	4
4.2.1 Atmospheric Density	4
4.2.2 Equivalent Airspeed	5
4.2.3 Dynamic Pressure ( $q$ )	5
4.2.4 Derived Gust Velocity ( $U_{de}$ )	6
4.2.4.1 Derived Vertical Gust Velocity	6
4.2.4.2 Derived Lateral Gust Velocity	7
4.2.5 Continuous Gust Intensity ( $U_{\sigma}$ )	7
4.2.6 Flight Distance	8
4.2.7 Rate of Climb	9
4.3 Data Reduction Operations	9
4.3.1 Initial Quality Screening	10
4.3.2 Time History Files	10
4.3.3 Relational Database	10
4.3.4 Permanent Data Files	10
4.3.5 Loads Data Reduction	10
4.4 Data Reduction Criteria	11
4.4.1 Phases of Flight Profile	12
4.4.1.1 Ground Phases	13
4.4.1.2 Airborne Phases	13
4.4.2 Specific Events	13
4.4.2.1 Liftoff	14
4.4.2.2 Landing Touchdown	15

4.4.2.3	Thrust Reverser Deployment and Stowage	15
4.4.2.4	Runway Turnoff	15
4.4.3	Sign Conventions	16
4.4.4	Peak Selection Technique	16
4.4.5	Separation of Maneuver and Gust Load Factors	17
4.4.6	Flap Detents	17
5.	DATA PRESENTATION	18
5.1	Aircraft Usage Data	21
5.1.1	Altitude, Duration, and Speed Data	21
5.1.2	Attitude and Rate Data	24
5.2	Ground Loads Data	24
5.2.1	Lateral Load Factor Data	24
5.2.2	Longitudinal Load Factor Data	25
5.2.3	Vertical Load Factor Data	26
5.3	Flight Loads Data	26
5.3.1	Gust Vertical Load Factor Data	27
5.3.2	Derived Gust Velocity Data	27
5.3.3	Continuous Gust Intensity Data	28
5.3.4	Gust V-n Diagram Data	29
5.3.5	Maneuver Vertical Load Factor Data	29
5.3.6	Maneuver V-n Diagram Data	29
5.3.7	Combined Maneuver and Gust Vertical Load Factor Data	30
5.3.8	Combined Maneuver and Gust Lateral Load Factor Data	30
5.4	Systems Operational Data	30
5.4.1	Flap Usage Data	30
5.4.2	Landing Gear Data	31
5.4.3	Thrust Reverser Data	31
5.4.4	Propulsion Data	31
6.	CONCLUSIONS	31
7.	REFERENCES	33
APPENDIX A—DATA PRESENTATION		

## LIST OF FIGURES

Figure		Page
1	Bombardier CRJ100 Three-View Drawing	2
2	Airline Recording and Editing System	3
3	Data Processing Flow Chart	9
4	Description of Flight Profile Phases	12
5	Sketch of Ground Phases and Specific Events	14
6	Sign Convention for Airplane Accelerations	16
7	The Peak-Between-Means Classification Criteria	17

## LIST OF TABLES

Table		Page
1	Bombardier CRJ100 Aircraft Characteristics	2
2	Recorded Parameters Provided to UDRI	4
3	Parameter Editing Values	11
4	Flight Phase Criteria	12
5	Summary of Specific Events Criteria	14
6	Flap Detents (Bombardier CRJ100)	18
7	Statistical Data Formats	19

## LIST OF SYMBOLS AND ABBREVIATIONS

$\bar{A}$	aircraft PSD gust response factor
$a$	speed of sound (ft/sec)
$a_0$	speed of sound at sea level (ft/sec)
$a_t$	vertical tail lift curve slope per radian
$\bar{c}$	wing mean geometric chord (ft)
$\bar{C}$	aircraft discrete gust response factor
$C_{L\alpha}$	aircraft lift curve slope per radian
$C_{L_{\max}}$	maximum lift coefficient
$c.g.$	center of gravity
$D$	integrated flight distance
$F(PSD)$	continuous gust alleviation factor
$g$	gravity constant, 32.17 ft/sec <sup>2</sup>
$H_p$	pressure altitude, (ft)
$K$	radius of gyration in yaw, (ft)
$K_g$	discrete gust alleviation factor, $0.88 \mu / (5.3 + \mu)$
$kts$	knots
$L$	turbulence scale length (ft)
$l_t$	distance from airplane center of gravity to lift center of vertical tail
$M$	Mach number
$N$	number of occurrences for $U_\sigma$ (PSD gust procedure)
$N_0$	number of zero crossings per nautical mile (PSD gust procedure)
$N_1$	fan (low-pressure compressor) rotor speed (percentage of normal maximum turbine speed.)
$N_2$	turbine (high-pressure compressor) rotor speed (percentage of normal maximum turbine speed)
$nm$	nautical mile
$n_x$	longitudinal load factor (g)
$n_y$	lateral load factor (g)
$n_z$	vertical load factor (g)
$q$	dynamic pressure (lbs/ft <sup>2</sup> )
$RC$	rate of climb (ft/sec)
$S$	wing area (ft <sup>2</sup> )
$S_t$	vertical tail area (ft <sup>2</sup> )
$U_{de}$	derived gust velocity (ft/sec, EAS)
$U_\sigma$	continuous turbulence gust intensity (ft/sec, TAS)
$V_e$	equivalent airspeed
$V_{MO}$	maximum airspeed at altitude
$V_T$	true airspeed
$W$	gross weight (lbs)
$\Delta n_z$	incremental vertical load factor, $n_z - 1$
$\Delta n_{z_{man}}$	incremental maneuver load factor

$\Delta n_{z_{gust}}$	incremental gust load factor
$\Delta t$	time increment
$\mu$	airplane mass ratio for vertical gust calculation, $\frac{2W / S}{\rho g \bar{c} C_{L\alpha}}$
$\mu_t$	airplane mass ratio for vertical gust calculation, $\frac{2W / S_t}{\rho g c_t a_t} \left( \frac{K}{l_t} \right)$
$\rho$	air density, slugs/ft <sup>3</sup> (at altitude)
$\rho_0$	standard sea level air density, 0.0023769 slugs/ft <sup>3</sup>

## EXECUTIVE SUMMARY

The University of Dayton is supporting Federal Aviation Administration (FAA) research on the structural integrity requirements for the U.S. commercial transport airplane fleet. The primary objective of this research is to develop new and improved methods and criteria for processing and presenting commercial transport airplane flight and ground loads usage data. The scope of activities performed involves (1) defining the service-related factors that affect the operational life of commercial aircraft; (2) designing an efficient software system to reduce, store, and process large quantities of optical quick-access recorder data; and (3) reducing, analyzing, and providing processed data in statistical formats that will enable the FAA to reassess existing certification criteria. Equally important, these new data will also enable the FAA, the aircraft manufacturers, and the airlines to better understand and control those factors that influence the structural integrity of commercial transport aircraft. Presented herein are Bombardier CRJ100 aircraft operational usage data collected from 467 flights, representing 607.2 flight hours, as recorded by a single airline operator. Statistical data are presented on the aircraft's usage, flight and ground loads data, and systems operations. The data presented in this report will provide the user with information about the accelerations, speeds, altitudes, flight duration and distance, thrust reverser usage, and gust velocities encountered by the Bombardier CRJ100 during actual operational usage.

## 1. INTRODUCTION.

The Federal Aviation Administration (FAA) has an ongoing operational loads monitoring research program to collect, process, and evaluate statistical flight and ground loads data from transport aircraft used in normal commercial airline operations. The objectives of this program are (1) to acquire, evaluate, and use typical operational in-service data for comparison with the prior data used in the design and qualification testing of civil transport aircraft and (2) to provide a basis to improve the structural criteria and methods of design, evaluation, and substantiation of future airplanes. The University of Dayton Research Institute (UDRI) supports the FAA's efforts by developing the technology for reducing, processing, analyzing, and reporting on the operational flight and ground loads data received from the airlines participating in the FAA program and by conducting research studies.

Since the inception of the FAA's Operational Loads Monitoring Research Program, the scope of the Flight Loads Program has steadily expanded to include research on data collected from several aircraft operators and on aircraft models such as the B-737-400, B-767-200ER, B-747-400, MD-82/83, A-320, and BE-1900D. While current program research efforts are tailored primarily to support the FAA and the aircraft structural design community in evaluating design criteria related to the strength, durability, and damage tolerance of the basic airframe structure, much of the data that are available, when provided in meaningful statistical formats, can provide the aircraft operator with some valuable insight into how his aircraft and aircraft systems are being used during normal flight and ground operations. In an effort to improve the data content and to disseminate meaningful data to the larger community of designers, regulators, and aircraft operators, UDRI has made changes, deletions, and additions to the statistical data formats as presented in past reports. These changes occur throughout the data presentation section of this report.

This report presents flight and ground loads data obtained from Bombardier CRJ100 aircraft representing 467 flights and 607.2 hours of airline operations from a single carrier.

## 2. AIRCRAFT DESCRIPTION.

The CRJ100 is a twin turbofan regional transport aircraft with conventional and power-assisted primary flight controls and electronically controlled/hydraulically actuated spoiler surfaces. Figure 1 presents a three-view drawing showing front, top, and side views of the aircraft. Table 1 presents certain operational characteristics and major physical dimensions of the Bombardier CRJ100 aircraft.

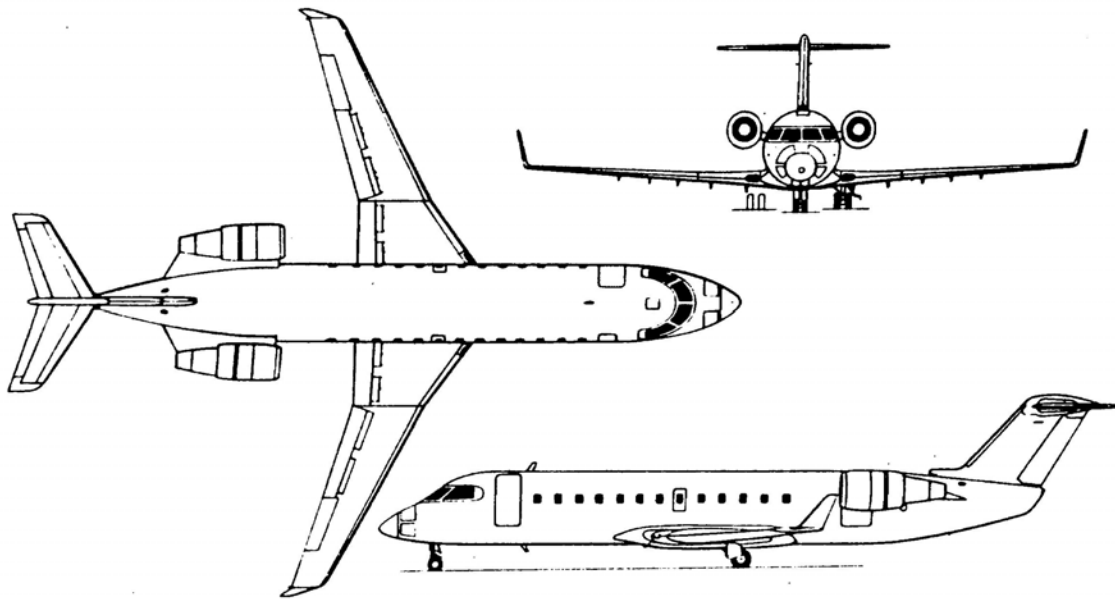


FIGURE 1. BOMBARDIER CRJ100 THREE-VIEW DRAWING

TABLE 1. BOMBARDIER CRJ100 AIRCRAFT CHARACTERISTICS

Maximum Taxi Weight	53,250 lbs
Maximum Takeoff Weight	53,000 lbs
Maximum Landing Weight	47,000 lbs
Maximum Zero-Fuel Weight	44,000 lbs
Fuel Capacity	13,984 lbs @ 6.55 lbs/U.S. gallon
GE Turbo Fan CF34-3A1	@ 8479 lbs static thrust @ sea level each
Wing Span	70.33 ft
Wing Reference Area	520.17 ft <sup>2</sup>
Wing MAC	99.43 inches
Wing Sweep	24.76 degrees
Length	88 ft 5 in
Height	20 ft 8 in
Tread	10 ft 5 in
Wheel Base	37 ft 5 in

### 3. AIRLINE DATA COLLECTION AND GROUND PROCESSING SYSTEMS.

The systems used for the onboard data collection, retrieval, and initial ground processing of the recorded flight and ground loads parameters for the CRJ100 aircraft are the property and responsibility of the participating airline. UDRI has very little specific information about the equipment an airline chooses to use; however, a typical airborne system consists of a Digital

Flight Data Acquisition Unit (DFDAU) and a Flight Data Recorder (FDR). The DFDAU collects signals from the onboard sensors and sends these data signals to the FDR, which is equipped with a storage device (disk, tape, etc.) that can store several hours of operational flight and ground loads data. A typical airline ground processing station consists of a drive mechanism, computer, and software systems that are capable of interrogating the stored raw data. The software converts the recorded raw data into engineering units and formats that are suitable for processing by UDRI. The software also performs the important function of desensitizing the data prior to it being forwarded to UDRI for flight loads processing and analysis. A schematic showing the typical interface between these systems, the airline, and UDRI are shown in figure 2.

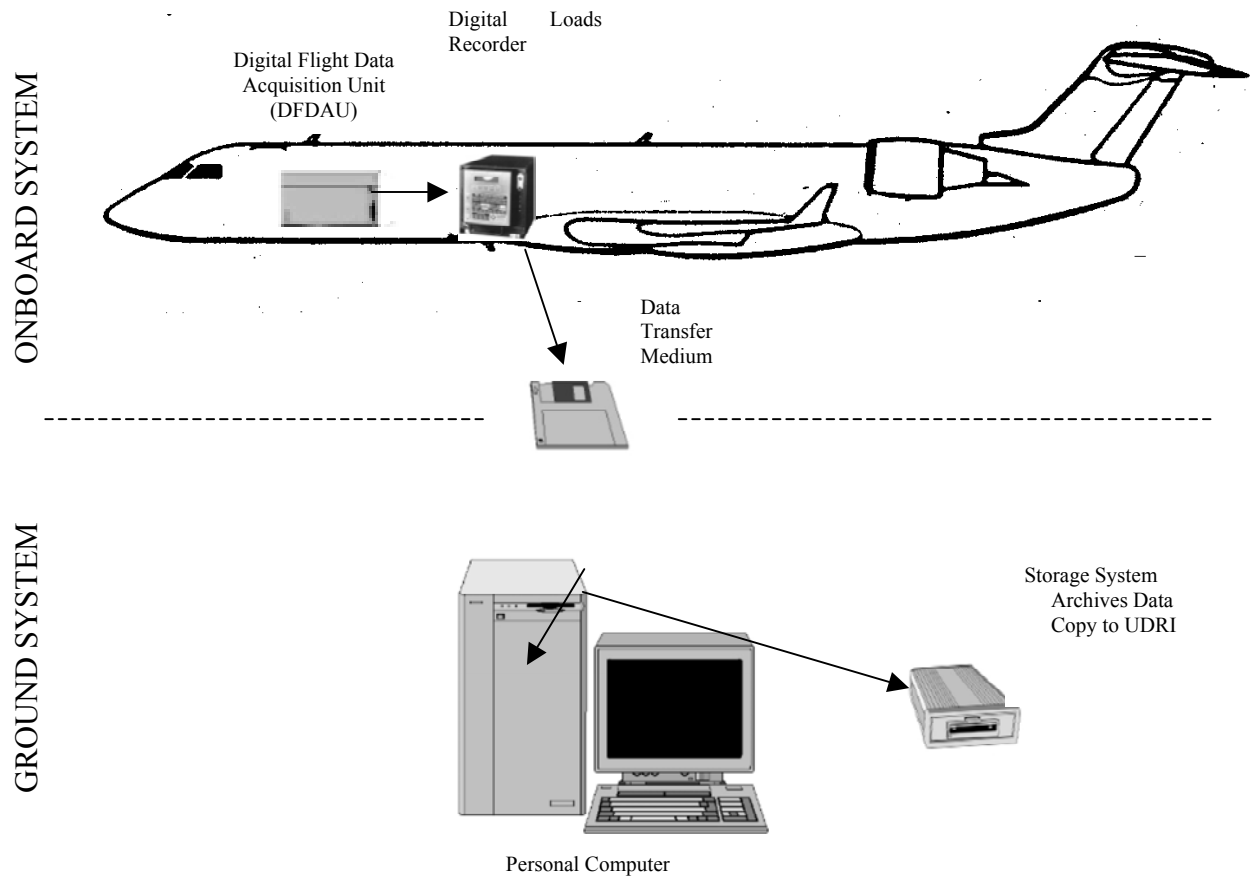


FIGURE 2. AIRLINE RECORDING AND EDITING SYSTEM

#### 4. UNIVERSITY OF DAYTON RESEARCH INSTITUTE DATA PROCESSING.

The recorded flight and ground loads parameter data are provided by the airline to UDRI on compact disks containing binary files for multiple flights for different airplanes. This section lists the recorded parameters received from the airline, identifies those parameters processed by UDRI, describes the methods used to extract or compute parameters that are not recorded, and describes how these data are then processed by UDRI through a series of computer software programs to extract the final data required to develop the statistical data formats.

#### 4.1 RECORDED DATA PARAMETERS.

Table 2 lists the recorded data parameters provided by the airline to UDRI for each recorded flight.

However, not all parameters listed in table 2 are used for statistical analysis and data presentation. Those recorded parameters that are used by UDRI to create time history files, compressed onto magneto-optical (MO) disks, and processed through the data reduction software for statistical analysis and data presentation are highlighted in table 2.

TABLE 2. RECORDED PARAMETERS PROVIDED TO UDRI

Parameter	Sampling Rate	Parameter	Sampling Rate
Vertical Acceleration	8 per second	Pressure Altitude	1 per second
Lateral Acceleration	4 per second	N1 Engine—Right and Left	1 per second each
Longitudinal Acceleration	4 per second	N2 Engine—Right and Left	1 per 2 seconds each
Aileron Position—Right and Left	2 per second each	Thrust Reverser Status, Engine 1 and 2	1 per second each
Elevator Position—Right and Left	2 per second each	Interturbine Temperature, Right and Left	1 per second
Rudder Position	2 per second	Fuel Flow—Right and Left	1 per 2 seconds
Horizontal Stabilizer Position	1 per 4 second	Bank Angle	2 per second
Flap Position, Right and Left	1 per second	Pitch Angle	4 per second
Flight Spoiler, Right and Left	1 per second each	Magnetic Heading	1 per second
Ground Spoiler, Right and Left	1 per second	Total Air Temperature	1 per second
Speed Brake Position	1 per second	Radio Altitude	1 per 2 seconds
Squat Switch—Main, Right and Left and Nose	1 per second each	Autopilot	1 per second
Brake Pressure	1 per 2 seconds	Landing Gear	1 per second
Calibrated Airspeed	1 per second	Wind Direction	1 per 4 seconds
Ground Speed	1 per second	Wind Speed	1 per 4 seconds

#### 4.2 COMPUTED PARAMETERS.

Certain information and parameters needed in subsequent data reduction are not recorded and need to be extracted or derived from available time history data. Derived gust velocity,  $U_{de}$ , and continuous gust intensity,  $U_{\sigma}$ , are important statistical load parameters, which are derived from measured vertical accelerations. This derivation of  $U_{de}$  and  $U_{\sigma}$  requires knowledge of atmospheric density, equivalent airspeed, and dynamic pressure. These values are calculated using equations that express the rate of change of density as a function of altitude based on the International Standard Atmosphere.

##### 4.2.1 Atmospheric Density.

For altitudes below 36,089 feet, the density ( $\rho$ ) is expressed as a function of altitude by

$$\rho = \rho_0 (1 - 6.876 \times 10^{-6} \times H_p)^{4.256} \quad (1)$$

where  $\rho_0$  is air density at sea level (0.0023769 slugs/ft<sup>3</sup>) and  $H_p$  is pressure altitude (ft). Pressure altitude is a recorded parameter.

#### 4.2.2 Equivalent Airspeed.

Equivalent air speed ( $V_e$ ) is a function of true air speed ( $V_T$ ) and the square root of the ratio of air density at altitude ( $\rho$ ) to air density at sea level ( $\rho_0$ ) and is expressed as

$$V_e = V_T \sqrt{\frac{\rho}{\rho_0}} \quad (2)$$

True airspeed ( $V_T$ ) is derived from Mach number ( $M$ ) and speed of sound ( $a$ ):

$$V_T = Ma \quad (3)$$

Mach number is dimensionless. The speed of sound ( $a$ ) is a function of pressure altitude ( $H_p$ ), and the speed of sound at sea level and is expressed as

$$a = a_0 \sqrt{(1 - 6.876 \times 10^{-6} \times H_p)} \quad (4)$$

Substituting equations 1 and 4 into equation 2 gives

$$V_e = M \times a_0 \times (1 - 6.876 \times 10^{-6} \times H_p)^{0.5} \times (1 - 6.876 \times 10^{-6} \times H_p)^{2.128} \quad (5)$$

which simplifies to

$$V_e = M \times a_0 \times (1 - 6.876 \times 10^{-6} \times H_p)^{2.626} \quad (6)$$

where the speed of sound at sea level  $a_0$  is 1116.4 fps or 661.5 knots.

Unfortunately, equivalent airspeed and Mach Number were parameters that were not provided for the CRJ100 to UDRI—only calibrated airspeed was made available. As a consequence, it was assumed that calibrated airspeed equalled equivalent airspeed. This is not entirely correct, because the calibrated airspeed should be corrected for compressibility effects. Because the proper algorithm to account for the compressibility effects was not available, this was not done for this report, but will be accomplished in any future efforts. The resulting error would be a maximum of approximately 5%. True airspeed was derived using the relationship of equation 2.

#### 4.2.3 Dynamic Pressure ( $q$ ).

The dynamic pressure ( $q$ ) is calculated from the air density and velocity as

$$q = \frac{1}{2} \rho V^2 \quad (7)$$

where

$$\begin{aligned}\rho &= \text{air density at altitude (slugs/ft}^3\text{)} \\ V &= \text{true air speed (ft/sec)}\end{aligned}$$

#### 4.2.4 Derived Gust Velocity ( $U_{de}$ ).

The derivation of gust velocity from measured acceleration is similar for the vertical and lateral case.

##### 4.2.4.1 Derived Vertical Gust Velocity.

The derived vertical gust velocity ( $U_{de}$ ) is computed from the peak values of gust incremental vertical acceleration as

$$U_{de} = \frac{\Delta n_z}{\bar{C}} \quad (8)$$

where  $\Delta n_z$  is gust peak incremental vertical acceleration and  $\bar{C}$  is the aircraft response factor, considering the plunge-only degree of freedom and is calculated from

$$\bar{C} = \frac{\rho_0 V_e C_{L_\alpha} S}{2W} K_g \quad (9)$$

where

$$\begin{aligned}\rho_0 &= 0.002377 \text{ slugs/ft}^3, \text{ standard sea level air density} \\ V_e &= \text{equivalent airspeed (ft/sec)} \\ C_{L_\alpha} &= \text{aircraft lift-curve slope per radian} \\ S &= \text{wing reference area (ft}^2\text{)} \\ W &= \text{gross weight (lbs)} \\ K_g &= \frac{0.88\mu}{5.3 + \mu} = \text{gust alleviation factor}\end{aligned}$$

$$\mu = \frac{2W}{\rho g \bar{c} C_{L_\alpha} S}, \text{ dimensionless}$$

$$\begin{aligned}\rho &= \text{air density, slug/ft}^3, \text{ at pressure altitude } (H_p), \text{ from equation 1} \\ g &= 32.17 \text{ ft/sec}^2 \\ \bar{c} &= \text{wing mean geometric chord (ft)}\end{aligned}$$

#### 4.2.4.2 Derived Lateral Gust Velocity.

The derived lateral gust velocity ( $U_{de}$ ) is computed from the peak values of lateral acceleration as

$$U_{de} = \frac{n_y}{\bar{C}} \quad (8)$$

where  $n_y$  is peak lateral acceleration and  $\bar{C}$  is the aircraft lateral response factor calculated from

$$\bar{C} = \frac{\rho_0 V_e a_t S_t}{2W} K_{gt} \quad (9)$$

where

$\rho_0$  = 0.002377 slugs/ft<sup>3</sup>, standard sea level air density

$V_e$  = equivalent airspeed (ft/sec)

$a_t$  = vertical tail lift-curve slope per radian

$S_t$  = vertical tail reference area (ft<sup>2</sup>)

$W$  = gross weight (lbs)

$K_g = \frac{0.88\mu}{5.3 + \mu}$  = gust alleviation factor

$\mu_{gt} = \frac{2W}{\rho c_t a_t S_t g} \left( \frac{K}{l_t} \right)^2$

$\rho$  = air density, slug/ft<sup>3</sup>, at pressure altitude ( $H_p$ ), from equation 1

$g$  = 32.17 ft/sec<sup>2</sup>

$c_t$  = vertical tail mean geometric chord (ft)

$K$  = Radius of gyration in yaw, ft

$l_t$  = distance from airplane cg to lift center of vertical surface

#### 4.2.5 Continuous Gust Intensity ( $U_\sigma$ ).

Power spectral density (PSD) functions provide a turbulence description in terms of the probability distribution of the root-mean-square gust velocities. The root-mean-square gust velocities or continuous gust intensities ( $U_\sigma$ ) are computed from the peak gust value of vertical acceleration using the power spectral density technique as described in reference 1 as

$$U_\sigma = \frac{\Delta n_z}{\bar{A}} \quad (10)$$

where

$\Delta n_z$  = gust peak incremental vertical acceleration

$\bar{A}$  = aircraft PSD gust response factor =  $\frac{\rho_0 V_e C_{L\alpha} S}{2W} F(PSD)$  in  $\frac{1}{ft/sec}$  (11)

$\rho_0$  = 0.002377 slugs/ft<sup>3</sup>, standard sea level air density  
 $V_e$  = equivalent airspeed (ft/sec)  
 $C_{L_\alpha}$  = aircraft lift-curve slope per radian  
 $S$  = wing reference area (ft<sup>2</sup>)  
 $W$  = gross weight (lbs)

$$F(PSD) = \frac{11.8}{\sqrt{\pi}} \left[ \frac{\bar{c}}{2L} \right]^{\frac{1}{3}} \sqrt{\frac{\mu}{110 + \mu}}, \text{ dimensionless} \quad (12)$$

$\bar{c}$  = wing mean geometric chord (ft)  
 $L$  = turbulence scale length, 2500 ft

$$\mu = \frac{2W}{\rho g \bar{c} C_{L_\alpha} S}, \text{ dimensionless} \quad (13)$$

$\rho$  = air density (slugs/ft<sup>3</sup>)  
 $g$  = 32.17 ft/sec<sup>2</sup>

To determine the number of occurrences ( $N$ ) for  $U_\sigma$ , calculate

$$N = \frac{N_0(o)_{ref}}{N_0(o)} = \frac{\pi \bar{c}}{203} \left[ \frac{\rho}{\rho_0} \mu \right]^{0.46}, \text{ dimensionless} \quad (14)$$

where  $\bar{c}$ ,  $\rho$ ,  $\rho_0$ , and  $\mu$  are defined above. Then each  $U_\sigma$  peak is counted as  $N$  counts at that  $U_\sigma$  value. This number of counts is used to determine the number of counts per nautical mile (nm), or

$$\frac{\text{counts}}{\text{nm}} = \left( \frac{N}{\text{distance flown in counting interval}} \right) \quad (15)$$

Finally, the number of such counts is summed from the largest plus or minus value toward the smallest to produce the cumulative counts per nautical mile.

#### 4.2.6 Flight Distance.

Because longitude and latitude data were not available for the CRJ100, the flight distance was obtained by numerical integration of speed as a function of time. The integrated flight distance  $D$  is obtained from the time at liftoff ( $t_0$ ) to the time of touchdown ( $t_n$ ), and  $V_T$  is the average true velocity during  $\Delta t$ .

$$D = \sum_{t_0}^{t_n} \Delta t \cdot V_T \quad (16)$$

#### 4.2.7 Rate of Climb.

Although the rate of climb was a recorded value on the Bombardier CRJ100, it was not always a recorded value on other aircraft; therefore, UDRI continued its previous practice of calculating these values. The rate of climb is obtained by numerical differentiation of the change in pressure altitude with time.

$$RC = \sum_{t_1}^{t_2} \frac{\Delta H_p}{\Delta t} \quad (17)$$

#### 4.3 DATA REDUCTION OPERATIONS.

The data reduction phase retrieves the data from the compact disks provided by the airline, processes it through a series of computer programs that convert the data to UDRI-compatible formats, and provides statistical information on aircraft usage, ground loads, flight loads, and systems operation. The data processing flow chart is illustrated in figure 3, and the flow of the processed data is discussed in subsequent paragraphs.

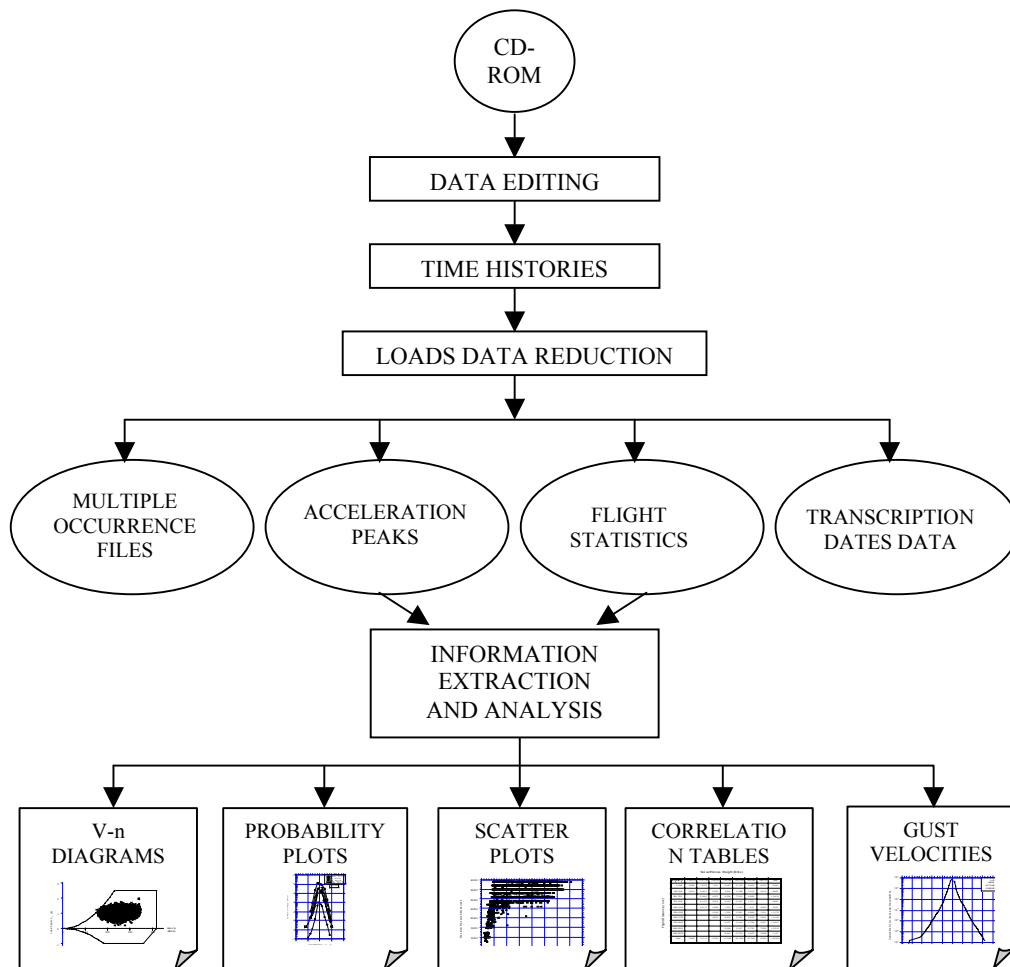


FIGURE 3. DATA PROCESSING FLOW CHART

#### 4.3.1 Initial Quality Screening.

All incoming data files are screened for acceptability. Individual flights are edited to remove erroneous or meaningless data such as discontinuous elapsed time data, evidence of nonfunctional channels or sensors, incomplete flight phases, and duplicate data sets. Files with missing, incomplete, or duplicate data are identified. For certain flights, the ground speed data was not provided by the airline. As a consequence, these flights were deleted from further data processing involving ground operations.

#### 4.3.2 Time History Files.

Each CD-ROM provided by the airline contains multiple flights, which are separated into individual parameter time history files for each flight. Then, these time history files are compressed and stored on 230-MB magneto-optical disks for later recall by the flight loads processing software. Data editing and verification are performed on the data as the time histories are being prepared. Message alerts indicate that obviously erroneous data have been removed and that questionable data have been retained but need to be manually reviewed prior to their acceptance. Table 3 lists the limits against which the data are compared. Some of the parameters from table 1 are edited and retained even though they are not currently being used. No limits were given to UDRI for the parameters provided by the airline. Therefore, the range checking applied to each parameter was very liberal, but still somewhat constrained based on past experience from other aircraft.

#### 4.3.3 Relational Database.

Important characteristics about each set of flights received from the airline are recorded in a relational database. The airline identifier, aircraft code, and disk identifier of the disk received from the airline are in the data. Each flight is assigned a unique flight sequence number. The flight sequence number assigned to the first flight of the set and the number of flights in the set are also entered. Also recorded is the disk identifier of the MO disk that contains the compressed time history files of all flights in the set.

#### 4.3.4 Permanent Data Files.

In addition to the time history files, two other files are created and permanently stored with the time history files. The first file contains the chronologically sorted list of the phases of flight and their corresponding starting times. This file provides the means to separate flight-by-flight phases in subsequent data analysis processing. The second file contains the accumulated time and distance for various combinations of phase of flight and altitude band. This file provides the capability to present data results in terms of normalized unit time and distance.

#### 4.3.5 Loads Data Reduction.

The loads data reduction program uses the compressed time history files to derive statistical information on aircraft usage, ground loads, flight loads, and systems operations. These data are then reduced in accordance with specific data reduction criteria.

TABLE 3. PARAMETER EDITING VALUES

Item		Min	Max
	VARIABLE		
1	Total Air Temperature	-300°	+300°
2	Radio Altitude		<4090 ft
3	Pressure Altitude (Hp)	-2000 ft	45,000 ft
4	Calibrated Airspeed	0 kts	500 kts
5	Ground Speed	0 kts	600 kts
6	Vertical Acceleration	-2.0 g	+4.0 g
7	Lateral Acceleration	-1.5 g	+1.5 g
8	Longitudinal Acceleration	-1.5 g	+1.5 g
9	Flap Position	-60°	60°
10	Elevator Position	-51°	+40°
11	Aileron Position	-26°	+26°
12	Rudder Position	-60°	+60°
13	Horizontal Stabilizer Position	-30°	+30°
14	Flight Spoiler Position	-70°	+70°
15	Pitch Attitude	-20°	+35°
16	Bank Attitude	-40°	+40°
17	Engine N <sub>1</sub>	0%	140%
18	Engine N <sub>2</sub>	0%	140%
19	Fuel Flow	As is	As is
20	Inter Turbine Temperature	As is	As is
21	Wind Speed	-800 kts	+800 kts
22	Wind Direction	-360°	360°
23	Magnetic Heading	-360°	360°
24	Brake Pressure		<32,000 psi
	DISCRETE		
25	Thrust Reverser	no	yes
26	Ground Spoiler Extended	no	yes
27	Auto Pilot	off	on
28	Squat Switch	off	on
29	Landing Gear Position	no	yes
30	Landing Gear Door	no	yes

#### 4.4 DATA REDUCTION CRITERIA.

To process the measured data into statistical loads formats, specific data reduction criteria were developed for separating the phases of ground and flight operations, identifying specific events associated with operation of the aircraft and its onboard systems, assigning sign conventions, determining maximum and minimum values and load cycles, and distinguishing between gust and maneuver load factors. These criteria are discussed in the following paragraphs.

#### 4.4.1 Phases of Flight Profile.

The ground and flight phases were determined by UDRI from the recorded data. Each time history profile was divided into nine phases—four ground phases (taxi-out, takeoff roll, landing roll with and without thrust reverser deployed, and taxi-in) and five airborne phases (departure, climb, cruise, descent, and approach). Figure 4 shows these nine phases of a typical flight profile.

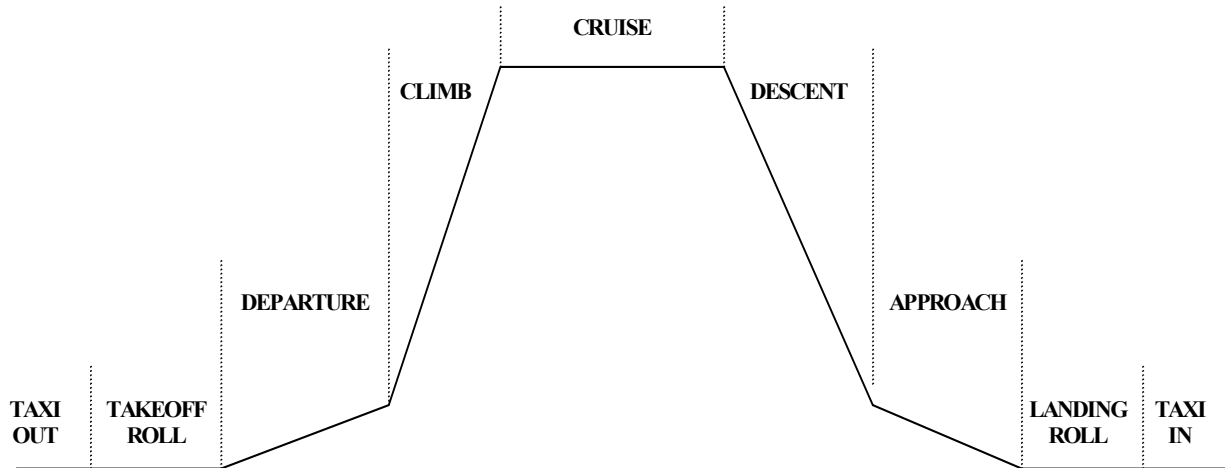


FIGURE 4. DESCRIPTION OF FLIGHT PROFILE PHASES

The criteria used to define each of these phases are summarized in table 4 and discussed in more detail in the following sections.

TABLE 4. FLIGHT PHASE CRITERIA

Phase of Flight	Defining Condition at Start of Phase
Taxi-Out	From initial aircraft movement.
Takeoff Roll	Ground acceleration $>1$ kts/sec in a 13-second duration sequence.
Departure	Liftoff, squat switch off.
Climb	Rate of climb $\geq 250$ ft/min maintained for at least 1 minute with flaps retracted.
Cruise	Rate of climb is between $\pm 250$ ft/min and flaps retracted.
Descent	Rate of descent $\geq 250$ ft/min occurs for at least 1 minute and flaps retracted.
Approach	Rate of descent $\leq 250$ ft/min occurs for at least 1 minute with flaps extended.
Landing Roll	Touchdown, squat switch on.
Taxi-In	End of landing roll to parked at the gate or recorder shutdown.

#### 4.4.1.1 Ground Phases.

Specific data reduction criteria were developed and used to identify the beginning and end of each ground phase of operation (taxi-out, takeoff roll, landing roll with and without thrust reverser deployed, and taxi-in).

The taxi-out phase begins when the ground speed exceeds 1 knot. All aircraft movement until the aircraft begins its takeoff roll is defined as being taxi-out.

The beginning of the takeoff roll is found by searching for ground speeds that accelerated at rates greater than 1 kts/sec for a minimum duration of 13 seconds. Then, when these values are found, the beginning of the takeoff roll is assigned as being the time slice where the first ground speed rate change greater than 1 kts/sec for that sequence occurred. The takeoff roll ends at liftoff with the squat switch off signal.

The landing roll phase is defined as beginning when the squat switch signaled that the landing touchdown had occurred and ending when the aircraft begins its turnoff from the active runway. The criterion for the turnoff is based on a change in the magnetic heading following landing and is discussed further in section 4.4.2.4.

Taxi-in is defined from the point where the aircraft began its turnoff from the active runway after its landing roll to the point when the aircraft was either parked at the gate or the recorder has shut down. The criterion for completion of the turnoff uses magnetic heading to identify when the aircraft has either returned to taxiing in a straight line or has turned in the opposite direction and is also discussed further in section 4.4.2.4.

#### 4.4.1.2 Airborne Phases.

The airborne portion of each flight profile was separated into phases called departure, climb, cruise, descent, and approach. These phases occur between the time that the squat switch turns off at liftoff until it turns on again at landing touchdown. The beginning of each flight phase is defined based on combinations of the squat switch position, flap settings, and the calculated rate of climb or descent over a period of at least 1 minute, as shown in table 4. Also, by definition, the departure phase cannot be less than 1 minute in length.

It should be noted that an airborne phase could occur several times per flight because it is determined by the rate of climb and the position of the flaps. When this occurs, the flight loads data are combined and presented as a single flight phase. The UDRI software then creates a file that chronologically lists the phases of flight and their corresponding starting times.

#### 4.4.2 Specific Events.

In addition to the ground and airborne phases, a unique set of criteria was also required to identify certain specific events such as liftoff, landing touchdown, thrust reverser deployment and stowage, and start of turnoff from the active runway after landing. Figure 5 shows a sketch depicting these phases and events.

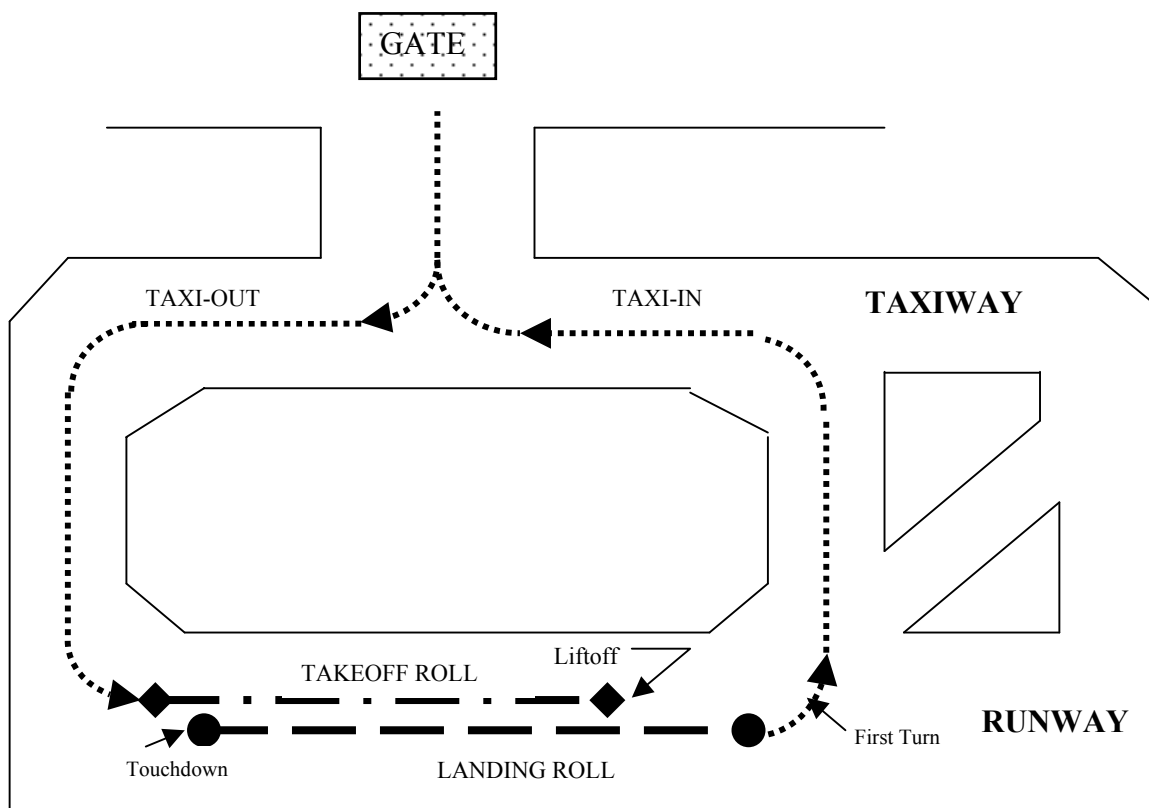


FIGURE 5. SKETCH OF GROUND PHASES AND SPECIFIC EVENTS

The criteria used to define each of the specific events are summarized in table 5 and discussed in more detail in reference 2 and the following paragraphs.

TABLE 5. SUMMARY OF SPECIFIC EVENTS CRITERIA

Phase/Event	Defining Conditions
Liftoff	Point at which the squat switch opens.
Landing Touchdown	From 5 seconds prior to squat switch on to 1 second afterwards.
Thrust Reverser Deployment/Stowage	Thrust reverser switch on for deployment and off for stowage.
Runway Turnoff	From first sequential magnetic heading change in same direction from runway centerline and heading sequence changes $>13.5$ degrees to a straight line heading or turn in opposite direction.

#### 4.4.2.1 Liftoff.

As in most earlier reports, liftoff was defined as the time when the squat switch opened. Because the squat switch reading is not always an accurate indicator of liftoff, this criterion may result in pitch angles that exceed the clearance angle necessary to avoid a tail strike. A recent study has shown that a criterion that is based on changes in radio altitude provides a better estimate of the

instant of liftoff for the determination of pitch angle. Such a criterion uses an algorithm that identifies liftoff as the first reading in a series of increasing radio altitude values that are greater than a fixed level above the average radio altitude calculated during the takeoff roll. For the algorithm to be dependable, the fixed level above the runway is sensitive to the aircraft type. Time restraints prevented the determination of the correct fixed radio altitude level to be used in the algorithm for this report.

#### 4.4.2.2 Landing Touchdown.

Previous experience has shown that the squat switch is not an accurate indicator of when touchdown actually occurs. To ensure that the maximum vertical and side load factors associated with touchdown were identified, the actual touchdown event was deemed to occur within a time frame from 5 seconds prior to, until 1 second following squat switch closure. UDRI decided that it was more important to ensure capturing the touchdown event even if the 5-second time prior to squat switch closure resulted in some minor loss of flight data. The 1-second time after squat switch was chosen somewhat arbitrarily, but was intended to ensure that sufficient time was allowed for the aircraft to respond to the touchdown and for the vertical and side load accelerations to build to their maximum values.

#### 4.4.2.3 Thrust Reverser Deployment and Stowage.

An on/off switch identifies when deployment or stowage of the thrust reverser occurs. Thus, by identifying when this occurs as a special event, load factor acceleration data can be obtained at the instant of thrust reverser deployment and during the time of thrust reverser usage and stowage.

#### 4.4.2.4 Runway Turnoff.

Changes in the aircraft's magnetic heading were used to identify the beginning of the aircraft's turnoff from the active runway after the landing roll. After the aircraft touched down, subsequent magnetic heading readings were averaged and this average heading was defined as the runway centerline. Subsequent magnetic heading changes were then tested to identify continuous movement in the same direction away from this centerline. When the aircraft's sequential magnetic heading change exceeded 13.5 degrees from the direction of the landing centerline, the time slice associated with the first sequential heading change from the landing centerline in the direction of the turn was defined as the beginning of the turnoff from the runway.

An alternate method was used to identify runway turnoffs involving shallow turns from the runway, i.e., turns that did not exceed the 13.5 degree turn criteria. This method uses aircraft ground speed and magnetic heading to calculate the aircraft's position relative to the runway centerline by identifying when the aircraft's position perpendicular to the runway centerline exceeded 150 feet. The time slice associated with the first aircraft movement away from the landing centerline in the direction of the turn was defined as the beginning of the aircraft's turnoff from the runway.

#### 4.4.3 Sign Conventions.

Acceleration data are recorded in three directions: vertical (z), lateral (y), and longitudinal (x). As shown in figure 6, the positive z direction is up; the positive y direction is airplane starboard; and the positive x direction is forward.

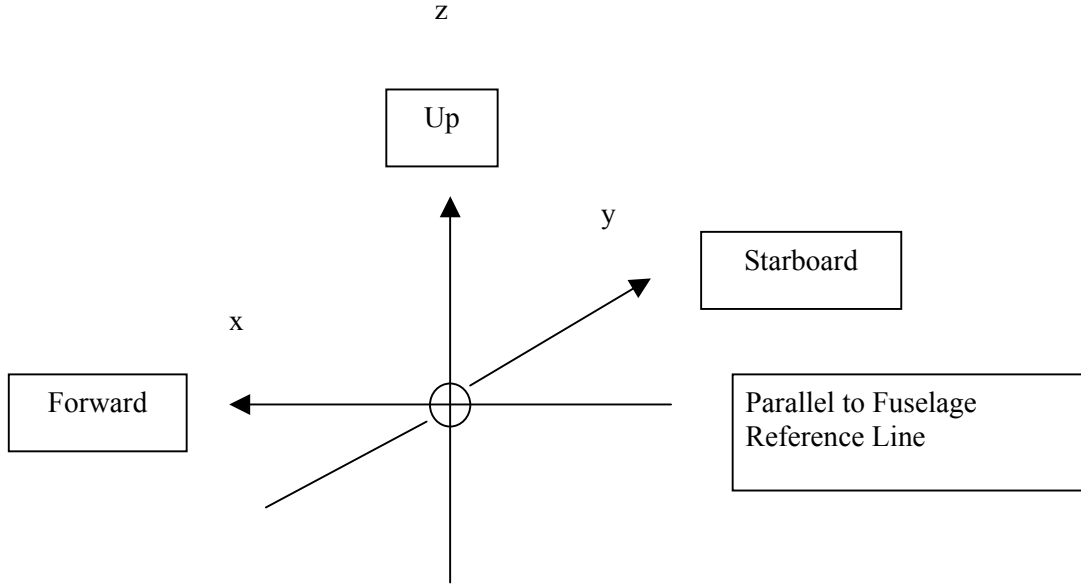


FIGURE 6. SIGN CONVENTION FOR AIRPLANE ACCELERATIONS

#### 4.4.4 Peak Selection Technique.

The peak-between-means method presented in reference 1 is used to identify positive and negative peaks in the acceleration data. This method is consistent with past practices and pertains to all accelerations ( $n_x$ ,  $n_y$ ,  $\Delta n_z$ ,  $\Delta n_{z_{gust}}$ ,  $\Delta n_{z_{man}}$ ). A brief description of the peak-between-means technique follows.

One peak is identified between each two successive crossings of the mean acceleration, which is the 0-g condition for lateral, longitudinal, and incremental vertical accelerations. Peaks greater than the mean are considered positive and those less than the mean negative. A threshold zone is defined around the mean, within which acceleration peaks are ignored because they have been shown to be irrelevant. The threshold zone is  $\pm 0.05$  g for the vertical accelerations  $\Delta n_z$ ,  $\Delta n_{z_{gust}}$ ,  $\Delta n_{z_{man}}$ ,  $\pm 0.005$  g for lateral acceleration  $n_y$ , and  $\pm 0.0025$  g for longitudinal acceleration  $n_x$ .

Figure 7 demonstrates the acceleration peak selection technique. The sample acceleration trace contains eight zero crossings, which are circled, set off by vertical dashed lines, and labeled as  $C_i$ ,  $i = 0$  to 7. For each of the seven intervals between successive mean crossings,  $C_{i-1}$  to  $C_i$ ,  $i = 1$  to 7, one peak, which is located at  $P_i$ , is identified. Those peaks lying outside of the threshold zone ( $P_1$ ,  $P_2$ ,  $P_5$ ,  $P_6$ , and  $P_7$ ) are accepted and retained; whereas, those peaks lying inside the threshold zone ( $P_3$  and  $P_4$ ) are ignored.

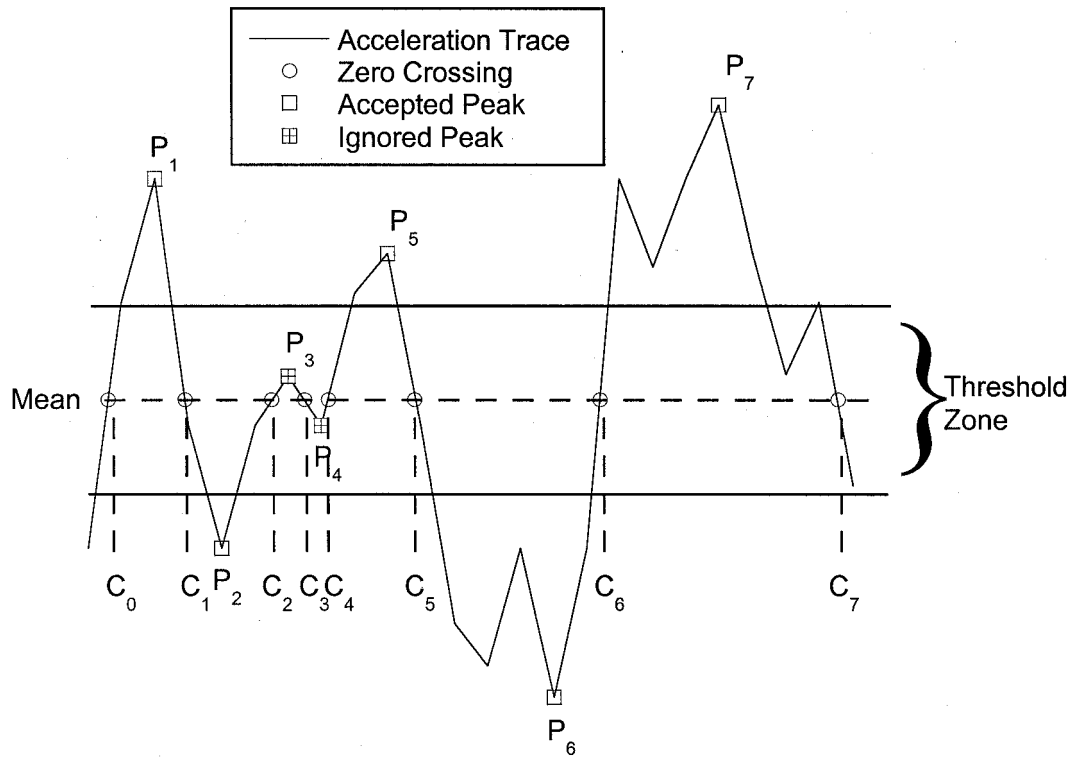


FIGURE 7. THE PEAK-BETWEEN-MEANS CLASSIFICATION CRITERIA

#### 4.4.5 Separation of Maneuver and Gust Load Factors.

Vertical acceleration ( $n_z$ ) is measured at the center of gravity (c.g.) of the aircraft and incremental vertical acceleration ( $\Delta n_z$ ) results from removing the 1-g condition from  $n_z$ . The incremental acceleration measured at the c.g. of the aircraft in flight may be the result of either maneuvers or gusts. In order to derive gust and maneuver statistics, the maneuver-induced acceleration ( $\Delta n_{z_{man}}$ ) and the gust response acceleration ( $\Delta n_{z_{gust}}$ ) must be separated from the total acceleration history. Reference 3 reported the results of a UDRI study to evaluate methods of separating maneuver and gust load factors from measured acceleration time histories. As a result of this study, UDRI uses a cycle duration rule to differentiate maneuver-induced acceleration peaks from those peaks caused by gust loading. Review of the CRJ100 response characteristics has shown that a cycle duration of 2.0 seconds is appropriate for the CRJ100 aircraft and, thus, was used.

#### 4.4.6 Flap Detents.

When flaps are extended, the effective deflection is considered to be that of the applicable detent, as indicated in table 6. The flap deflection ranges and placard speeds reflect the flap operational limits, as provided by Bombardier Inc. Flap design speeds are higher than the operational speeds shown.

TABLE 6. FLAP DETENTS (BOMBARDIER CRJ100)

Flap Detent	Minimum Flap Setting	Maximum Flap Setting	Operational Airspeed Limit (KCAS)
0	0	$\leq 0$	330
8	$> 0$	$\leq 8$	215
20	$> 8$	$\leq 20$	215
30	$> 20$	$\leq 30$	185
45	$> 30$	$\leq 45$	170

## 5. DATA PRESENTATION.

The statistical data presented in this section provide the FAA, aircraft manufacturers, and the operating airline with the information that is needed to assess how the CRJ100 aircraft is actually being used in operational service versus its original design or intended usage. The statistical data presented herein can be used by the FAA as a basis to evaluate existing structural certification criteria, to improve requirements for the design, evaluation, and substantiation of existing aircraft, and to establish design criteria for future generations of new aircraft. The aircraft manufacturer can use these data to assess the aircraft's structural integrity by comparing the actual in-service usage of the CRJ100 aircraft versus its originally intended design usage. It can also use these data to derive typical flight profiles and to update structural strength, durability, and damage tolerance analyses in order to establish or revise maintenance and inspection requirements for critical airframe and structural components. The airline/aircraft operator can use these data to evaluate the aircraft's current usage with respect to established operational procedures and placard limitations. It can also use these data to identify where changes in current operational procedures could provide additional safety margins, increase the service life of structural components, and improve on the economics of its operations.

Table 7 lists all the statistical data formats for which data were processed. The various data formats have been grouped together within the table in an attempt to categorize the CRJ100 data being presented on the basis of whether it pertains to aircraft usage, ground or flight loads data, or systems operational data. The aircraft usage data column of table 7 describes the aircraft's operational usage in terms of distributions of flight lengths, flight duration, flight phase, flight altitudes, flight speeds, takeoff and landing gross weights, fuel flows, etc. The loads and system data section describes the flight and ground environment and the induced system cyclic loadings experienced by the aircraft while the aircraft performs its intended usage.

Figures A-1 through A-87 are presented in appendix A. For ease of understanding, most of the figures in appendix A are presented in graphical form with a minimum of numerical summaries. In an effort to make the data presentation of a more comprehensive nature, some figures include both cumulative and relative probability or frequency distribution histograms, as well as line plots. Scatter plots are also included, where appropriate, to show the relationship between coincident parameters that are considered to be of interest and to show visible evidence of relationships, outliers, or suspicious data.

TABLE 7. STATISTICAL DATA FORMATS

Data Description	Figure
AIRCRAFT USAGE DATA	
ALTITUDE AND SPEED DATA	
Percent of Flights vs Flight Duration	A-1
Percent of Flights vs Maximum Flight Altitude	A-2
Correlation of Maximum Altitude and Flight Duration	A-3
Cumulative Probability of Maximum Ground Speed During Taxi	A-4
Probabilities of Wind Speed Parallel to Runway at Touchdown	A-5
Relative Probability of Wind Speed Across Runway at Touchdown	A-6
Mean Yaw Angle Before Touchdown vs Crosswind at Touchdown	A-7
Mean Bank Angle Before Touchdown vs Crosswind at Touchdown	A-8
Yaw Angle vs Crosswind at Touchdown	A-9
Bank Angle vs Crosswind at Touchdown	A-10
Coincident Parallel and Crosswind Speeds at Touchdown	A-11
Maximum Calibrated Airspeed and Coincident Altitude, All Flight Phases	A-12
Cumulative Probability of Airspeed at Liftoff and Touchdown	A-13
ATTITUDE AND RATE DATA	
Cumulative Probability of Pitch Angle at Liftoff and Touchdown	A-14
Cumulative Probability of Maximum Pitch Angle During Departure and Approach	A-15
GROUND LOADS DATA	
LATERAL LOAD FACTOR, $n_y$	
Maximum Lateral Load Factor and Coincident Incremental Vertical Load Factor at Touchdown	A-16
Cumulative Frequency of Maximum Lateral Load Factor During Ground Turns	A-17
Cumulative Frequency of Maximum Lateral Load Factor at Touchdown	A-18
Maximum Lateral Load Factor and Coincident Longitudinal Load Factor During Ground Turns, Taxi-Out	A-19
Maximum Lateral Load Factor and Coincident Longitudinal Load Factor During Ground Turns, Taxi-In	A-20
Maximum Lateral Load Factor and Coincident Yaw Angle at Touchdown	A-21
Maximum Lateral Load Factor and Coincident Bank Angle at Touchdown	A-22
Maximum Lateral Load Factor vs Parallel Wind Speed at Touchdown	A-23
Maximum Lateral Load Factor vs Crosswind Speed at Touchdown	A-24
LONGITUDINAL LOAD FACTOR, $n_x$	
Cumulative Frequency of Longitudinal Load Factor During Taxi Operations	A-25
Cumulative Frequency of Longitudinal Load Factor at Touchdown and During Landing Roll	A-26
VERTICAL LOAD FACTOR, $n_z$	
Cumulative Frequency of Incremental Vertical Load Factor During Taxi Operations	A-27
Cumulative Frequency of Incremental Vertical Load Factor During Takeoff Roll	A-28
Cumulative Frequency of Incremental Load Factor at Spoiler Deployment and at Touchdown	A-29
Cumulative Frequency of Incremental Vertical Load Factor During Landing Roll	A-30
Maximum Incremental Vertical Load Factor vs Coincident Airspeed at Touchdown	A-31
FLIGHT LOADS DATA	
GUST VERTICAL LOAD FACTOR DATA	
Cumulative Occurrences of Incremental Vertical Gust Load Factor per 1000 Hours by Flight Phase	A-32
Cumulative Occurrences of Incremental Vertical Gust Load Factor per 1000 Hours, Combined Flight Phases	A-33
DERIVED GUST VELOCITY DATA	
Incremental Vertical Load Factor vs Derived Vertical Gust Velocity for 100-150 KIAS	A-34
Incremental Vertical Load Factor vs Derived Vertical Gust Velocity for 150-200 KIAS	A-35
Incremental Vertical Load Factor vs Derived Vertical Gust Velocity for 200-250 KIAS	A-36
Incremental Vertical Load Factor vs Derived Vertical Gust Velocity for 250-300 KIAS	A-37

TABLE 7. STATISTICAL DATA FORMATS (Continued)

Data Description	Figure
DERIVED GUST VELOCITY DATA (Cont'd.)	
Incremental Vertical Load Factor vs Derived Vertical Gust Velocity for 300-350 KIAS	A-38
Lateral Load Factor vs Derived Lateral Gust Velocity for 100-150 KIAS	A-39
Lateral Load Factor vs Derived Lateral Gust Velocity for 150-200 KIAS	A-40
Lateral Load Factor vs Derived Lateral Gust Velocity for 200-250 KIAS	A-41
Lateral Load Factor vs Derived Lateral Gust Velocity for 250-300 KIAS	A-42
Lateral Load Factor vs Derived Lateral Gust Velocity for 300-350 KIAS	A-43
Lateral Load Factor vs Derived Lateral Gust Velocity for 400-450 KIAS	A-44
Cumulative Occurrences of Derived Vertical Gust Velocity per 1000 Hours—Climb, Cruise, and Descent Phases	A-45
Cumulative Occurrences of Derived Lateral Gust Velocity per 1000 Hours—Climb, Cruise, and Descent Phases	A-46
Cumulative Occurrences of Derived Gust Velocity per Nautical Mile, < 500 Feet Above Airport	A-47
Cumulative Occurrences of Derived Gust Velocity per Nautical Mile, 500-1500 Feet Above Airport	A-48
Cumulative Occurrences of Derived Gust Velocity per Nautical Mile, < 500 Feet	A-49
Cumulative Occurrences of Derived Gust Velocity per Nautical Mile, 500-1500 Feet	A-50
Cumulative Occurrences of Derived Gust Velocity per Nautical Mile, 1500-4500 Feet	A-51
Cumulative Occurrences of Derived Gust Velocity per Nautical Mile, 4500-9500 Feet	A-52
Cumulative Occurrences of Derived Gust Velocity per Nautical Mile, 9,500-19,500 Feet	A-53
Cumulative Occurrences of Derived Gust Velocity per Nautical Mile, 19,500-29,500 Feet	A-54
Cumulative Occurrences of Derived Gust Velocity per Nautical Mile, 29,500-39,500 Feet	A-55
Cumulative Occurrences of Derived Gust Velocity per Nautical Mile, Flaps Extended	A-56
Cumulative Occurrences of Derived Gust Velocity per Nautical Mile, Flaps Retracted	A-57
CONTINUOUS GUST INTENSITY DATA	
Cumulative Occurrences of Continuous Gust Intensity per Nautical Mile, Flaps Extended	A-58
Cumulative Occurrences of Continuous Gust Intensity per Nautical Mile, Flaps Retracted	A-59
GUST V-n DIAGRAM DATA	
Gust Load Factor and Coincident Speed vs V-n Diagram for Flaps Retracted	A-60
Gust Load Factor and Coincident Speed vs V-n Diagrams for Flaps Extended, Detents 8, 20, 30, and 45	A-61
MANEUVER VERTICAL LOAD FACTOR DATA	
Cumulative Occurrences of Incremental Vertical Maneuver Load Factor per 1000 Hours During Departure by Altitude	A-62
Cumulative Occurrences of Incremental Vertical Maneuver Load Factor per 1000 Hours During Climb by Altitude	A-63
Cumulative Occurrences of Incremental Vertical Maneuver Load Factor per 1000 Hours During Cruise by Altitude	A-64
Cumulative Occurrences of Incremental Vertical Maneuver Load Factor per 1000 Hours During Descent by Altitude	A-65
Cumulative Occurrences of Incremental Vertical Maneuver Load Factor per 1000 Hours During Approach by Altitude	A-66
Cumulative Occurrences of Incremental Vertical Maneuver Load Factor per 1000 Hours by Flight Phase	A-67
Cumulative Occurrences of Incremental Vertical Maneuver Load Factor per 1000 Hours, Combined Flight Phases	A-68
MANEUVER V-N DIAGRAM DATA	
Maneuver Load Factor and Coincident Speed vs V-n Diagram for Flaps Retracted	A-69
Maneuver Load Factor and Coincident Speed vs V-n Diagrams for Flaps Extended, Detents 8, 20, 30, and 45	A-70
COMBINED MANEUVER AND GUST VERTICAL LOAD FACTOR DATA	
Cumulative Occurrences of Incremental Vertical Load Factor per 1000 Hours by Flight Phase	A-71
Cumulative Occurrences of Incremental Vertical Load Factor per 1000 Hours, Combined Flight Phases	A-72
COMBINED MANEUVER AND GUST LATERAL LOAD FACTOR DATA	
Cumulative Occurrences of Lateral Load Factor per 1000 Hours by Flight Phase	A-73
Cumulative Occurrences of Lateral Load Factor per 1000 Hours, Combined Flight Phases	A-74

TABLE 7. STATISTICAL DATA FORMATS (Continued)

Data Description	Figure
FLAP USAGE DATA	
Cumulative Probability of Maximum Airspeed in Flap Detent During Departure	A-75
Relative Probability of Maximum Airspeed in Flap Detent During Departure	A-76
Cumulative Probability of Maximum Airspeed in Flap Detent During Approach	A-77
Relative Probability of Maximum Airspeed in Flap Detent During Approach	A-78
Percent of Time in Flap Detent During Departure	A-79
Percent of Time in Flap Detent During Approach	A-80
LANDING GEAR DATA	
Coincident Speed and Altitude Above Airport at Landing Gear Retraction	A-81
Coincident Speed and Altitude Above Airport at Landing Gear Extension	A-82
Cumulative Probability of Speed at Landing Gear Retraction and Extension	A-83
Cumulative Probability of Altitude Above Airport at Landing Gear Retraction and Extension	A-84
THRUST REVERSER DATA	
Cumulative Probability of Time With Thrust Reversers Deployed	A-85
Cumulative Probability of Speed at Thrust Reverser Deployment and Stowage	A-86
PROPULSION DATA	
Cumulative Probability of Percent of $N_1$ During Takeoff, at Thrust Reverser Deployment, and During Thrust Reverser Deployment	A-87

It should also be noted that the data presented in these figures are not always based on an identical number of flights or flight hours. For certain flights, some data frames and/or parameters exhibited random errors and were judged to be unacceptable for use. When this occurred, those questionable data were eliminated from the statistical database for any application, either directly or indirectly, of the other data measurements. Also, a number of plots (those based on 359 flights) are based on an earlier data set before all CRJ100 data became available. These plots were not rerun for this report. As a result, not all figures are based on data from identical numbers of flights, hours, or nautical miles.

## 5.1 AIRCRAFT USAGE DATA.

Figures A-1 through A-15 provide statistical data on the aircraft's operational usage. Information relating to wind speeds, ground and flight speeds, flight altitudes, aircraft attitude, and flight lengths based on normal everyday flight operations are presented. These data are primarily useful in defining typical flight profiles including speed, altitude, and the number of flights associated with each type profile. Unfortunately, gross weight data were not provided for the CRJ100 aircraft and aircraft gross weight usage statistics are, therefore, not presented in this report.

### 5.1.1 Altitude, Duration, and Speed Data.

Figure A-1 presents the flight duration in percent of flights where the flight duration is based on the time from liftoff to touchdown. Figure A-2 presents the maximum altitude attained during flight in terms of percent of flights.

Figure A-3 shows the maximum altitude attained during each flight plotted versus the duration of the flight. As would be expected, the data indicate that, as the flight length increases, the aircraft

consistently fly at the higher altitudes. The scatter plot also indicates that, regardless of flight length, the maximum altitude remains above 20,000 feet.

The cumulative probabilities of ground speed for taxi-in and taxi-out operations are presented in figure A-4. The taxi-in speed is somewhat higher than the taxi-out speed, which agrees with what has been observed with other aircraft models. This probably occurs because ground movement of inbound traffic to the terminal after landing is generally accomplished faster than movement from the terminal to the takeoff position. It should be noted for this report that the taxi-in phase of operation begins after the first turnoff from the active runway, as compared to previous UDRI reports that included the runway turnoff speeds as part of the taxi-in phase of operation. The higher taxi-in speeds, as observed in these earlier reports, probably occurred as the aircraft was exiting the runway during the turnoff.

Figure A-5 shows the relative and cumulative probabilities of wind speed parallel to the runway at the instant of touchdown. The wind speed parallel to the runway was determined by taking the cosine of the angle between the runway heading and the recorded wind direction, thus,  $windspeed_{Parallel} = windspeed_{Recorded} * \cos(\text{runwaydirection} - \text{winddirection})$ . Runway direction was determined by assuming that the calculated average magnetic heading of the aircraft on the runway after landing represented the direction of the runway. This introduces a small error, because the wind direction is measured from the geographical north, while the runway direction is expressed as the angular distance from the magnetic north.

Unfortunately, true heading was not an available parameter. From the figure, it can be seen that approximately 10 percent of the landings are conducted downwind, although downwind velocities do not exceed 7 knots. Sixty percent of landings are conducted in head winds between 0 and 10 knots. Thirty percent of landings are conducted in head winds exceeding 10 knots, with a maximum head wind of 42 knots. This high speed represents the wind parallel to the runway; thus, the actual wind speed may have been higher.

Figure A-6 shows the probability of crosswinds during landing. The wind speed across the runway was determined by taking the sine of the angle between the runway heading and the recorded wind direction. The figure shows that landings in crosswinds above 20 knots are very rare and amount to only 1.2 percent of the total landings. Crosswind limits are not always clearly specified by airworthiness authorities. Airport authorities may establish cross- and tailwind limits for noise abatement procedures. These limits generally are 25 knots crosswind and 5 knots tailwind. Crosswind limits are usually defined in airline operational flight procedures manuals, varying from 20-30 knots, depending on variables such as runway conditions, gustiness, or even pilot experience.

Figures A-7 and A-8 show the mean yaw angle and mean bank angle before touchdown versus the crosswind existing at touchdown, respectively. The crosswind at touchdown is assumed representative of the crosswinds existing during the final approach. The yaw angles in figure A-7 are not yaw angles in accordance with the conventional aeronautical definition, where yaw angle is defined as the angle between a line in the direction of flight in the air and the airplane heading. Instead, these angles represent what is known as crab angles, where crab angle is the angle between the aircraft track or flight line on the ground and the airplane heading. It is assumed

that the airplane is following its desired track during the final approach phase of flight and that this track coincides with the runway direction. The runway direction or track is obtained by assuming that the calculated average magnetic heading of the aircraft on the runway after landing represented the direction of the runway. The calculated difference in the aircraft heading prior to touchdown with the magnetic heading of the aircraft on the runway after landing was used to estimate the yaw (crab) angle. The mean yaw (crab) angle was determined by averaging the yaw (crab) angle measurements during the 10- to 3-second interval just prior to touchdown. The interval was terminated at -3 seconds prior to touchdown to ensure that data from touchdown were not included. The time increment from 10 to 3 seconds prior to touchdown is assumed to represent the final approach phase. Figures A-7 and A-8 show moderate linear correlation between mean yaw and mean bank angles and crosswind.

Figures A-9 and A-10 present the yaw angle and coincident crosswind at touchdown and the bank angle and coincident crosswind at touchdown, respectively. Figure A-9 shows no real correlation between yaw angle and crosswind at touchdown, while there is moderate correlation between the bank angle and crosswind at touchdown. During final approach in crosswind conditions, sideslip and accompanying bank into the wind can be used if it is desired to keep the nose of the airplane aligned with the runway. (i.e., maintain a heading identical to the course). The upwind wing is held low to counter the lateral drift, while opposite rudder is used to maintain the longitudinal alignment. However, this is not the most accepted crosswind landing technique used and, from a passenger comfort point of view, the crab technique is preferred. In the crab technique, the approach is flown into the wind (i.e., zero sideslip, zero rudder, and zero aileron) with the heading offset from the runway direction to account for drift and only applying rudder and aileron to lower the upwind wing and align the aircraft with the runway at the moment of touchdown. The similar correlations in figures A-7 and A-8 suggest that a combination of crab and sideslip may be used during final approach. The correlations in figures A-9 and A-10 suggest that the touchdown procedure is consistent with the preferred landing method where the airplane is aligned with the runway and bank angle is used to counteract the drift effects of the crosswind.

Figure A-11 presents the coincident parallel and crosswind components at landing.

Figure A-12 shows measured speeds plotted versus airspeed limits ( $V_{MO}$ ) as defined in the aircraft flight manual. Each plotted point represents the one airspeed per flight that occurred closest to or exceeded the speed limit at its coincident altitude regardless of flight phase. For example, in one flight, the maximum speed, with respect to the limit, might have been attained in the climb phase, while in another flight, the maximum speed may have occurred in a different phase. The plot indicates there were some flights that operate at speed values approaching or slightly exceeding the airspeed limits.

Figure A-13 shows the cumulative probabilities of calibrated airspeed at liftoff and at touchdown. The figure shows that the majority of takeoffs occur at speeds between 130 and 150 knots, while the touchdown speeds occur primarily between 115 and 135 knots. Comparison of the two figures also shows that the liftoff speeds for the CRJ100 are approximately 20 knots higher than the touchdown speeds. This speed difference is similar to that seen for the B-737-400 and

MD-82/83, but less than that for the B-767-200ER and A0320, which exhibited speed differences of 25-30 knots between liftoff and touchdown speeds [4-7].

### 5.1.2 Attitude and Rate Data.

Figure A-14 provides the cumulative probability of maximum pitch angle at liftoff and touchdown. There is little difference between the pitch angles at liftoff and touchdown. As in earlier reports, the pitch angle at liftoff was derived using the last pitch angle reading just before the squat switch indicated the aircraft had lifted off. Because the squat switch reading is not always an accurate indicator of liftoff, this criterion may result in pitch angles that exceed the clearance angle necessary to avoid a tail strike.

A recent study has shown that a criterion that is based on changes in radio altitude provides a better estimate of the instant of liftoff for the determination of pitch angle. Such a criterion uses an algorithm that identifies liftoff as the first reading in a series of increasing radio altitude values that are greater than a fixed level above the average radio altitude calculated during the takeoff roll. For the algorithm to be dependable the fixed level above the runway is sensitive to the aircraft type. Time restraints prevented the determination of the correct fixed radio altitude level to be used in the algorithm for this report.

Figure A-15 presents the cumulative probability of the maximum pitch angle during the departure and approach phases of flight. The data show that the pitch angle of the aircraft during departure varies between 11 and 20 degrees, while during its approach, the pitch angle varies between about 0 and 6 degrees. Chai and Mason attributed this difference to the fact that “with the flaps in the fully-deflected position, the critical angle of attack of the wing during landing (and approach) is smaller than during takeoff (and departure). Consequently, the pitch angle during landing is smaller than that during takeoff.”[8] Although the pitch angles for both departure and approach are slightly lower than those observed for the A-320 aircraft, for which identical data were reduced, the difference between the pitch angles for departure and approach is consistent with differences observed on the A-320 aircraft.

## 5.2 GROUND LOADS DATA.

Figures A-16 through A-31 provide statistical loads data based on the CRJ100's ground operations. The ground loads data include frequency and probability information on vertical, lateral, and longitudinal accelerations during takeoff, landing, taxi, and turning operations. These loads primarily affect the landing gear and landing gear backup structure and, to a lesser extent, the wing, fuselage, and empennage. (Statistical ground loads data for other aircraft models can be found in references 4-7.)

### 5.2.1 Lateral Load Factor Data.

Figure A-16 shows the maximum lateral load factor at touchdown and the coincident vertical load factor. Some of the flights did not experience an  $n_y$  peak associated with touchdown; therefore, no coincident  $n_z$  values were plotted for these flights.

Figure A-17 shows the cumulative occurrences of maximum lateral load factor that occur during ground turning operations, including the runway turnoff. The information is presented per 1000 flights for both pre- and postflight taxi and contains data for both left and right turns. The taxi-in load factor spectra are generally higher than the taxi-out spectra. This is consistent with data for the B-737-400, MD-82/83, and B-767-200 aircraft, as reported in references 4, 5, and 6. The higher taxi-in spectra are probably associated with the higher taxi-in speeds. Also, figure A-17 shows some differences between the total number of left and right turns. Comparison of the ground turning lateral load factor spectra of the B-737-400, MD-82/83, B-767-200ER, A-320, and B-747-400 also shows such differences.

Figure A-18 presents the cumulative probability of maximum lateral load factor at touchdown.

Figures A-19 and A-20 present scatter plots of the maximum lateral load factor encountered during ground turns during taxi-out and taxi-in, respectively. Negative longitudinal load factors appear to occur slightly more frequently and the magnitudes are larger during taxi-in turns than during taxi-out turns.

Figures A-21 and A-22 contain scatter plots showing the maximum lateral load factor and coincident yaw angle and bank angle at touchdown, respectively. As previously mentioned, the yaw angles are estimated values and represent what are generally known as crab angles. A full discussion of the estimation procedure can be found in section 5.3.1. Figure A-21 shows little correlation between lateral load factor and yaw angle. On the other hand, figure A-22 shows good correlation between lateral load factor and bank angle. Review of the results from figures A-21 and A-22, in conjunction with the results from figure A-10, suggest that asymmetric landings involving bank angle are a normal part of operational experience and are affecting the input of side loads to the gear. Figures A-23 and A-24 show the maximum lateral load factor at touchdown correlated with the wind component parallel and across the runway, respectively. From the scatter plot, it is evident that no meaningful correlation exists between the wind components at touchdown and the aircraft lateral load factor experienced at touchdown.

### 5.2.2 Longitudinal Load Factor Data.

Figure A-25 presents the cumulative occurrences of longitudinal load factor during pre- and postflight taxi operations per 1000 flights. The occurrences of longitudinal load factor during taxi primarily occur due to braking and throttle changes. The magnitude of longitudinal load factors observed during taxi varies between -0.47 and +0.31 g. Taxi-out load factors are skewed to the positive values of longitudinal acceleration indicating a major influence of thrust inputs, while the taxi-in load factors are skewed to the negative side indicating the influence of braking actions.

Figure A-26 shows the cumulative frequency of the maximum and minimum longitudinal load factor measured at touchdown and during the landing rollout with and without thrust reverser deployment. The maximum negative value of the longitudinal load factor observed is identical for the landing roll with or without thrust reverser. The occurrence of positive longitudinal load factors, even though very small, probably occurs due to the variations in retardation forces caused by the thrust reversers, hydraulic brakes, and rolling friction.

### 5.2.3 Vertical Load Factor Data.

Figure A-27 presents cumulative occurrences of incremental vertical load factor per 1000 flights for the taxi-in and taxi-out phases of ground operations. The data show that the distribution of vertical load factor during taxi-in is slightly higher than for taxi-out. This slight difference was also observed on the B-737-400, MD-82/83, and B-767 aircraft [4-6] and is probably due to the slightly higher taxi-in speeds shown in figure A-4.

Figure A-28 presents the cumulative occurrences of positive and negative incremental vertical load factors per 1000 flights that occurred during the takeoff roll. While the magnitudes of load factor appear to be consistent with what one would expect during the takeoff roll, these values are primarily a function of the condition or roughness of the runway.

Figure A-29 presents the cumulative occurrences of the minimum and maximum incremental vertical load factor per 1000 flights associated with touchdown and deployment of the ground spoilers. This figure shows that approximately the same minimum and maximum load factor peaks are attributable to each event. These identical readings probably occur because the sampling rate for each event indicator is only once per second and deployment of the ground spoilers occurs very quickly after touchdown. Thus, when this occurred, it was impossible to determine which event actually caused the minimum and maximum load factor peaks. So, unless the peaks were separated by several seconds, the same minimum or maximum peak was probably identified and assigned as having occurred both at touchdown and during deployment of the spoilers.

Figure A-30 presents the cumulative occurrences of incremental vertical load factor per 1000 flights during the landing roll for operations with and without thrust reversers. These curves may also include the effects of ground spoiler usage on vertical load factor because the spoilers are normally used during the landing rollout concurrently with the thrust reversers. The spectra are practically identical regardless of thrust reverser position. This is a major difference from what was seen on previous aircraft models such as the B-737-400, MD-82.83, B-767-200ER, and A-320. For those aircraft, the vertical spectrum for the thrust reversers in operation was considerably lower than the spectrum without thrust reversers.

Figure A-31 is a scatter plot that shows the maximum incremental vertical load factor versus the coincident calibrated airspeed at touchdown. The magnitude of the vertical load factor does not appear to be related to the airspeed at touchdown.

### 5.3 FLIGHT LOADS DATA.

Flight loads data are presented as cumulative occurrences per 1000 hours. When presented by phase of flight, the cumulative occurrences per 1000 hours are based on per 1000 hours in the particular phase. In contrast, the data shown for the total cumulative occurrences are based on per 1000 hours of the total number of hours.

The gust loads data are presented in the form of incremental vertical load factors, derived gust velocity ( $U_{de}$ ), and continuous gust intensity ( $U_{\sigma}$ ). Gust vertical factor data are plotted as

cumulative occurrences per 1000 hours. The derived gust velocity and continuous gust intensity are computed values and plotted as occurrences per nautical mile by altitude and flap position.

Maneuver loads data are also presented as cumulative occurrences of incremental load factor per 1000 hours by phase of flight and altitude.

This section also presents the combined total vertical and lateral load factor occurrences due to the maneuver and gust environment presented per 1000 hours by phase of flight and for vertical load factor for all flight phases combined. V-n diagrams showing the coincident gust and maneuver vertical load factor versus speed for the flaps retracted and extended conditions are presented. Cumulative frequency of maximum lateral load factor for the combined phases is presented.

### 5.3.1 Gust Vertical Load Factor Data.

Figure A-32 shows the cumulative occurrences of incremental vertical gust load factor per 1000 hours by phase of flight, and figure A-33 shows the cumulative occurrences of incremental vertical gust load factor for all the airborne phases combined per 1000 hours.

### 5.3.2 Derived Gust Velocity Data.

The magnitudes for the gust velocities were derived from the measured accelerations in accordance with the procedures presented in section 4.2.4. The procedure requires gross weight as input. Unfortunately, gross weight was not a provided parameter and estimated values had to be used. Since fuel flow measurements were available, the gross weights used were estimated by taking an average takeoff gross weight of 44,360 lbs and adjusting this weight for fuel used during the flight. Figures A-34 through A-38 present scatter plots of the derived vertical gust velocities and the associated incremental vertical acceleration for 50-knot airspeed increments from 100 to 350 knots indicated airspeed. The slope of the data points provides an indication of the aircraft acceleration response to gust inputs. Figures A-39 through A-44 present similar data for the lateral case. It is noted that the slope of the scatter points for the lateral case is less steep than those for the vertical gust inputs. This indicates that the acceleration response to a given gust input is far less in the lateral plane than in the vertical plane. Figures A-45 and A-46 present the cumulative frequencies of derived vertical gust velocities and lateral gust velocities, respectively, for the climb, cruise, and descent phases of flight. Comparison of the frequency distributions in figures A-45 and A-46 shows that the lateral gust velocity frequency distributions are higher than the vertical velocities frequency distributions by a considerable amount. On the other hand, when comparing the vertical acceleration frequencies of figure A-32 and the lateral accelerations frequencies of figure A-73, it is seen that the vertical acceleration cumulative frequency plots are considerably higher than the lateral acceleration cumulative frequency plots. The primary reason for this reversal of frequency plots is the fact that the lateral gust response factor is much lower in the lateral direction than in the vertical direction, as discussed previously. Since the gust velocity is a derived value using the measured acceleration and the gust response factor, this means that the derived lateral gust velocity will be higher than the derived vertical gust velocity for identical acceleration magnitudes by the ratio of the lateral to vertical gust response factors. In the field of atmospheric turbulence as it relates to aircraft design, a basic assumption has been that atmospheric turbulence is isotropic, i.e., the frequency of turbulence intensities is the same for the three components of turbulence—vertical, lateral, and longitudinal.

References 9 to 15 present the results of a comprehensive program to measure gust velocity distributions. The results indicate that the turbulence was not entirely isotropic and that the lateral component tended to be somewhat more severe than the vertical component, with the difference becoming more pronounced as the gust velocity increased. Although the direct gust velocity measurements presented in references 9 through 15 showed the lateral gust velocity cumulative frequencies to be higher than the vertical gust velocity cumulative frequencies, this difference was much smaller than the difference shown in the data of this report. Unfortunately, the gust velocities presented in this report are fictitious gust velocities derived from measured accelerations, whereas the gust velocities of references 9 through 15 represent actual measured gust velocities; thus no direct comparisons can be made between the two. References 16 and 17 also include some vertical versus lateral gust frequency comparisons. These comparisons also show lateral gust frequencies somewhat higher than the vertical frequencies.

In contrast to the comparisons of measured gust velocities in references 9 through 15, reference 18 includes a comparison of the cumulative frequencies of lateral- and vertical-derived gust velocities. The comparisons in reference 18 are consistent with the comparisons shown in this report in that the lateral-derived gust frequency distributions are much higher than the vertical-derived gust frequency distributions.

Since the gust velocity distributions of references 9 through 17 are based on directly measured gusts, it may be assumed that they are more representative of the actual turbulence characteristics than the derived gust velocities presented in this report and in reference 18. If this is so, this indicates that either the lateral or the vertical gust response factor, or both, as used in the derivation of gust velocities, do not correctly describe the real airplane response to gust inputs. This suggests that the vertical- and lateral-derived gust design requirements are inconsistent and that the lateral gust requirement should be higher to obtain strength levels for lateral gust equivalent to strength levels for vertical gust. In figures A-47 and A-48, derived gust velocity ( $U_{de}$ ) is plotted as cumulative occurrences per nautical mile for altitudes above the airport; in figures A-49 through A-55,  $U_{de}$  is plotted as cumulative occurrences per nautical mile for pressure altitudes from sea level to 39,500 feet. In all figures, the gust velocity distributions derived from the measured CRJ100 gust accelerations are compared to derived gust velocity distributions used in NACA TR-4332 [7] to define a statistical description of root-mean-square gust velocity distributions for use in the power spectral density approach to gust load calculations.

The spectra for the derived gust velocities at altitudes from 0 to 1500 feet above the airport, as shown in figures A-47 and A-48, are nearly identical to the spectra shown for pressure altitudes from 0 to 1500 feet, as shown in figures A-49 and A-50. This suggests that the CRJ100 operations evaluated for this report did not include many, if any, high-altitude airports.

Figures A-56 and A-57 present derived gust velocity ( $U_{de}$ ) per nautical mile for the flaps extended and retracted conditions, respectively.

### 5.3.3 Continuous Gust Intensity Data.

The magnitudes of the continuous gust intensities ( $U_{\sigma}$ ) were derived from the measured accelerations in accordance with the procedures presented in section 4.2.5. The cumulative occurrences of

continuous gust intensity per nautical mile for the flaps extended and retracted conditions are presented in figures A-58 and A-59, respectively.

#### 5.3.4 Gust V-n Diagram Data.

For illustration purposes, coincident speed and gust accelerations are displayed on representative V-n diagrams for the flaps retracted and extended configurations. Since V-n diagrams are for illustration purposes only and are a function of altitude and gross weight, a minimum flying gross weight of 26,958 pounds at sea level was used.

Figures A-60 and A-61 show the coincident gust acceleration and airspeed measurements plotted on the V-n diagrams for the flaps retracted and extended configurations, respectively. All flap detent positions for which data were available (8, 20, 30, and 45) are shown in order to provide a range of flap extension conditions. Figure A-61 shows no gust acceleration points outside the V-n diagrams. These results deviate from those observed on other aircraft [4-7] with the flaps extended, where accelerations outside the V-n diagram did occur. However, one must keep in mind that the V-n diagrams shown here are representative of only one gross weight and altitude condition. If the measured gust acceleration data were plotted against the V-n diagram for the actual gross weight and altitude conditions that existed at the time the acceleration was measured, the data might fall outside the V-n diagram. Conversely, if a different gross weight had been used for the other aircraft [4-6], the acceleration points might have fallen within the V-n diagram. Clearly, since the V-n diagrams are for illustration only and represent a single gross weight-altitude condition, no firm conclusion should be drawn if points fall within or outside the diagrams.

#### 5.3.5 Maneuver Vertical Load Factor Data.

Figures A-62 through A-66 present the cumulative occurrences of incremental maneuver load factor per 1000 hours by altitude for each of the airborne flight phases, i.e., departure, climb, cruise, descent, and approach, respectively.

Figure A-67 shows the total cumulative occurrences of incremental maneuver load factor per 1000 hours for each phase of flight, regardless of altitude. The figure also shows the cumulative occurrences of the maximum maneuver load factor associated with liftoff. Clearly, the liftoff load factors account for most, if not all, load factors above 0.2 g in the departure phase. The maximum incremental vertical maneuver load factor encountered by the CRJ100 was 0.4 g and occurred during the departure, cruise, and descent phases of flight. Figure A-68 contains the total cumulative occurrences of incremental maneuver load factor per 1000 hours for all flight phases combined.

#### 5.3.6 Maneuver V-n Diagram Data.

As with the V-n diagram for gust loads, a minimum flying gross weight of 26,958 pounds at sea level was used to calculate representative maneuver V-n diagrams.

Figures A-69 and A-70 show the maneuver V-n diagrams with flaps retracted and extended with the coincident acceleration and speed measurements. All flap detent positions for which data

were available (8, 20, 30, and 45) are shown in figure A-70 to provide a range of flap extension conditions. As for the gust cases, figure A-70 shows that, for the flaps extended cases, no maneuver acceleration points occur at speeds outside the maneuver V-n diagram. Again, these results are opposite to those observed on other aircraft [4-7] with the flaps extended. As pointed out in section 5.3.4, the V-n diagrams are for illustration only and whether points fall within or outside the V-n diagram is dependent on the altitude and gross weight selected for the V-n diagram.

#### 5.3.7 Combined Maneuver and Gust Vertical Load Factor Data.

Figure A-71 shows the cumulative occurrences of the combined maneuver and gust incremental vertical load factor per 1000 hours by phases of flight, and figure A-72 shows the incremental vertical load factor occurrences for all flight phases combined. The curves in figure A-71 are based on a frequency per 1000 hours of flight in the specific phase of flight. The curve in figure A-72 is based on a frequency per 1000 hours of total flight. Comparison of the spectra in figures A-71 and A-72 with similar data for other aircraft [4-7] show that the load factor spectra for the CRJ100 are very close to those for the B-737-400, MD-82/83, A-320, and B-767-200ER. This is in contrast to a comparison with the BE-1900D where significant differences were observed.

#### 5.3.8 Combined Maneuver and Gust Lateral Load Factor Data.

Figure 73 presents the cumulative occurrences of lateral load factor per 1000 hours by phase of flight. Figure A-74 presents the cumulative occurrences per 1000 hours for all phases combined. The curves in figure A-73 are based on a frequency per 1000 hours of flight in the specific phase of flight. The curve in figure A-74 is based on a frequency per 1000 hours of total flight. Maximum lateral load factor values between approximately -0.22 and +0.20 g were observed during flight operations of the CRJ100.

### 5.4 SYSTEMS OPERATIONAL DATA.

This section contains operational usage data for the flaps, landing gear, thrust reversers, and the propulsion system. Although control surface position information was available for the aileron, rudder, and elevator systems, it was not processed because the sampling rates were deemed to be too slow to provide reliable statistical usage information for these components.

#### 5.4.1 Flap Usage Data.

Flap usage data showing airspeed and percent of time spent are presented by flap detent and phase of flight. These data can be used to characterize the sources of repeated loads on the flaps, backup structure, and other flap components. The CRJ100 flap operational speed limits for each detent setting were listed in table 6.

Figures A-75 and A-76 present the cumulative and relative probability of the maximum airspeed encountered in various flap detents during the departure phase of flight, respectively. Figures A-77 and A-78 present similar probability data for the approach phase of flight. Figure A-77 shows that the most probable speed at which the flaps are first deployed during the approach phase of flight for detent 8 occurs at above 200 knots, for detent 20 between about 165 and 190 knots, for

detent 30 between about 155 and 175 knots, and for detent 45, the speeds vary between about 145 and 160 knots.

Figures A-79 and A-80 present the percent of time spent in each flap detent setting during the departure and approach phases of flight, respectively. Flap detent 8 is the most frequently-used setting during the departure phase (90%); flap detents 8 (35%), 20 (25%), and 45 (32%) are the most often used settings during the approach phase.

#### 5.4.2 Landing Gear Data.

Statistical data showing the speeds, altitudes, and vertical load factor when the landing gear begins to be retracted or extended are shown in figures A-81 through A-82. This information characterizes the operational usage of the landing gear for the airline and also provides data for the aircraft manufacturer that can be used to assess the loading conditions for the landing gear and backup structure.

Figures A-81 and A-82 contain scatter plots showing the coincident speed and altitude above the airport at the start of gear retraction and extension. Figure A-82 shows that gear retraction is initiated at altitudes below 100 feet; figure A-81 shows a few gear extensions above 5000 feet, with two extensions above 7000 feet.

Figures A-83 and A-84 contain the same data points used to generate the scatter plots shown in figures A-81 and A-82 but are plotted here as the probability of speed and altitude above the airport at the beginning of landing gear extension and retraction.

#### 5.4.3 Thrust Reverser Data.

The times and speeds associated with thrust reverser ground operations were derived from the measured data. Figure A-85 presents the cumulative probability of time during which the thrust reversers are deployed. The data show that, for 90 percent of the flights, the thrust reversers are deployed for less than 30 seconds. Figure A-86 presents the cumulative probability of the speed at the time the thrust reversers were deployed and stowed. Most thrust reverser deployment cycles begin at speeds between 95 and 120 knots and are stowed at speeds between 20 and 60 knots.

#### 5.4.4 Propulsion Data.

Figure A-87 presents the cumulative probability of the maximum engine fan speed ( $N_1$ ) during takeoff, at the instant of thrust reverser deployment during the landing roll, and during the time that the thrust reverser is deployed. Fan speed values for takeoff range between 84% and 91%. The fan speeds at thrust reverser deployment are below 30%, while the fan speeds used during the time that the thrust reversers are deployed ranges from a low of 26 percent to a maximum of 85 percent.

### 6. CONCLUSIONS.

Comparison of the flight loads data in this report with data available for the BE-1900D, a commuter-type aircraft, shows major differences for in-flight operations. However, flight load

comparisons of the statistical data presented in this report with similar data available for the B-737-400, MD-82/83, A-320, and B-767-200ER have shown that the operational airborne usage of the CRJ100 aircraft obtained from one specific carrier is very similar to that of these larger transports. This suggests that operational data from these larger aircraft may possibly be used for application to the CRJ100 if such data is not directly available for the CRJ100. It also indicates that the data from smaller commuter-type aircraft should not necessarily be considered representative of operational data of the CRJ100-type aircraft. It must be kept in mind that these conclusions are based on the data from a single carrier. It is conceivable that the operational procedures used on the CRJ100 are influenced by whether a carrier is substituting larger MD-80- and B-737-type aircraft with CRJ100s or replacing smaller aircraft, such as the BE-1900D or HS748, with CRJ100 aircraft.

In response to increasing interest in operational conditions during landing touchdown, this report includes additional touchdown operational data not previously available or processed for inclusion in earlier reports on other aircraft. During final approach in crosswind conditions, sideslip and accompanying bank into the wind can be used if it is desired to keep the nose of the airplane aligned with the runway (i.e., maintain a heading identical to the course.) The upwind wing is held low to counter the lateral drift, while the opposite rudder is used to maintain the longitudinal alignment. However, this is not the most accepted crosswind landing technique used. The preferred method is the crab technique, where the approach is flown into the wind (i.e., zero sideslip, zero rudder, and zero aileron) with the heading offset from the runway direction to account for drift and only applying rudder and aileron to align the aircraft with the runway at the moment of touchdown. The data in this report suggest that a combination of sideslip and crab is used during final approach, but that at the flare, the airplane is aligned with the runway using bank angle to counteract the drift effects of the crosswind.

The lateral load factors at touchdown are well correlated with bank angle. The relationship between yaw angle and lateral load factor appears to be rather minimal. Lateral load factor inputs appear to be unrelated to either parallel or crosswinds. It is clear that asymmetric landings involving bank angle are quite common during normal flight operations and that bank angle is the primary cause of lateral load inputs during landings.

In response to an interest expressed in additional derived gust velocity information, this report was expanded to include various comparisons of vertical- and lateral-derived gust velocities. The derived lateral gust velocity frequency distributions were found to be considerably higher than those derived for the vertical gust velocities. In the field of atmospheric turbulence as it relates to aircraft design, a basic assumption has been that atmospheric turbulence is isotropic, i.e., the frequency of turbulence intensities is the same for the three components of turbulence—vertical, lateral, and longitudinal. While actual gust velocity measurements have indicated that the turbulence is not entirely isotropic and that the lateral component tends to be somewhat more severe than the vertical, this difference was much smaller than the difference shown in the data of this report. Comparisons of derived vertical and lateral gust velocities presented in this report are more consistent with the comparisons of derived vertical and lateral gust distributions shown in reference 18.

Gust velocity distributions based on directly measured gusts may be assumed to be more representative of the actual turbulence characteristics than the derived gust velocities presented in this report and in reference 18. If this is so, this indicates that either the lateral or the vertical

gust response factor, or both, as used in the derivation of gust velocities, do not correctly express the airplane response to gust inputs. Since the derived gust velocities represent fictitious rather than true gust velocities, they can still be used for design requirements. However, to obtain strength levels for lateral gust equivalent to strength levels for vertical gust, the design gusts for the lateral case must be correspondingly higher than for the vertical case. Federal Aviation Regulations 25.341 requires identical derived gust velocities for the vertical and lateral gust inputs resulting in inconsistent strength levels. The conclusions of the lateral versus vertical gust comparison in this report suggest that further study of lateral gust response and gust design criteria is needed.

## 7. REFERENCES.

1. de Jonge, B., "Reduction of Incremental Load Factor Acceleration Data to Gust Statistics," FAA Report DOT/FAA/CT-94/57, August 1994.
2. Tipps, Daniel O., John W. Rustenburg, and Donald A. Skinn, "Study of Side Load Factor Statistics from Commercial Aircraft Ground Operations," University of Dayton Research Institute Report UDR-TR-2001-00005, January 2001.
3. Rustenburg, John W., Donald A. Skinn, and Daniel O. Tipps, "An Evaluation of Methods to Separate Maneuver and Gust Load Factors from Measured Acceleration Time Histories," FAA Report DOT/FAA/AR-99/14, April 1999.
4. "Flight Loads Data for a Boeing 737-400 in Commercial Operation," FAA Report DOT/FAA/AR-98/28, August 1998.
5. "Flight Loads Data for a MD-82/83 in Commercial Operation," FAA Report DOT/FAA/AR-98/65, February 1999.
6. "Statistical Loads Data for B-767-200 Aircraft in Commercial Operation," FAA Report DOT/FAA/AR-00/10, March 2000.
7. "Statistical Loads Data for A-320 Aircraft in Commercial Operation," UDRI Report UDR-TR-2001-00080.
8. Chai, Sonny T. and William H. Mason, "Landing Gear Integration in Aircraft Conceptual Design," Virginia Polytechnic Institute and State University Report MAD 96-09-01, September 1996 (rev. March 1997).
9. Press, Harry and Roy Steiner, "An Approach to the Problem of Estimating Severe and Repeated Gust Loads for Missile Operations," National Advisory Committee for Aeronautics Technical Note 4332, Langley Aeronautical Laboratory, Langley Field, VA, September 1958.
10. Crooks, Walter M., Frederic M. Hoblit, David T. Prophet, et al., "Project Hicat, An Investigation of High Altitude Clear Air Turbulence," Air Force Flight Dynamics

- Laboratory, Air Force Systems Command, Wright-Patterson Air Force Base, Ohio, Technical Report AFFDL-TR-67-123, November 1967.
11. Crooks, Walter M., Frederic M. Hoblit, Finis A. Mitchell, et al., "Project Hicat High Altitude Clear Air Turbulence Measurements and Meteorological Correlations," Air Force Flight Dynamics Laboratory, Air Force Systems Command, Wright-Patterson Air Force Base, Ohio, Technical Report AFFDL-TR-68-127, November 1968.
  12. Gunter, D.E., G.W. Jones, and K.R. Monson, "Low Altitude Atmospheric Turbulence, Lo-Locat, Phases I & II," Deputy for Engineering, Aeronautical Systems Division, Air Force Systems Command, Wright-Patterson Air Force Base, Ohio, Technical Report ASD-TR-69-12, February 1969.
  13. Jones, J.W., R.H. Mielke, and G.W. Jones, "Low Altitude Atmospheric Turbulence, Lo-Locat, Phase III," Air Force Flight Dynamics Laboratory, Air Force Systems Command, Wright-Patterson Air Force Base, Ohio, Technical Report AFFDL-TR-70-10, November 1970.
  14. Ryan, J.P., A.P. Berens, A.C. Robertson, R.J. Dominic, and K.C. Rolle, "Medium Altitude Critical Atmospheric Turbulence (Medcat) Data Processing and Analysis," Air Force Flight Dynamics Laboratory, Air Force Systems Command, Wright-Patterson Air Force Base, Ohio, Technical Report AFFDL-TR-71-82, July 1971.
  15. McCloskey, John W., James K. Luers, John P. Ryan, and Nicholas A. Engler, "Statistical Analysis of Lo-Locat Turbulence Data for use in the Development of Revised Gust Criteria," Air Force Flight Dynamics Laboratory, Air Force Systems Command, Wright-Patterson Air Force Base, Ohio, Technical Report AFFDL-TR-71-29, April 1971.
  16. Rustenburg, John W., "Development of Generalized Gust Exceedance Curves for Low Altitude Contour Flight," Directorate of Flight Systems Engineering, Aeronautical Systems Division, Air Force Systems Command, Wright-Patterson Air Force Base, Ohio, Technical Report ASD-TR-88-5001, May 1988.
  17. Rustenburg, John W., "Handbook of Continuous Atmospheric Turbulence Descriptions," Directorate of Flight Systems Engineering, Aeronautical Systems Division, Air Force Systems Command, Wright-Patterson Air Force Base, Ohio, Technical Report ASD-TR-91-5014, November 1991.
  18. Van Gelder, P.A., "Derivation of Lateral and Vertical Gust Statistics From In-Flight Measurements," National Aerospace Laboratory Technical Publication NLR TP 97036L, Presented at 38<sup>th</sup> AIAA/ASME/ASCE/AHS/ASC Structural Dynamics and Material Conference, Kissimmee, Florida, April 7-10, 1997.

# APPENDIX A—DATA PRESENTATION

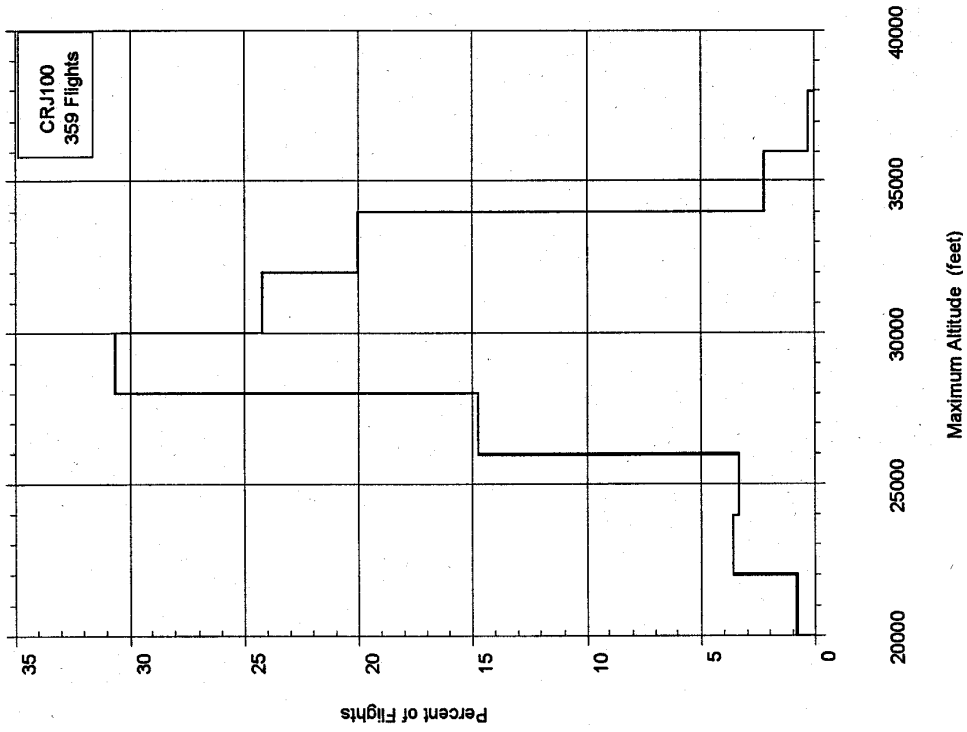


FIGURE A-1. PERCENT OF FLIGHTS VS  
FLIGHT DURATION

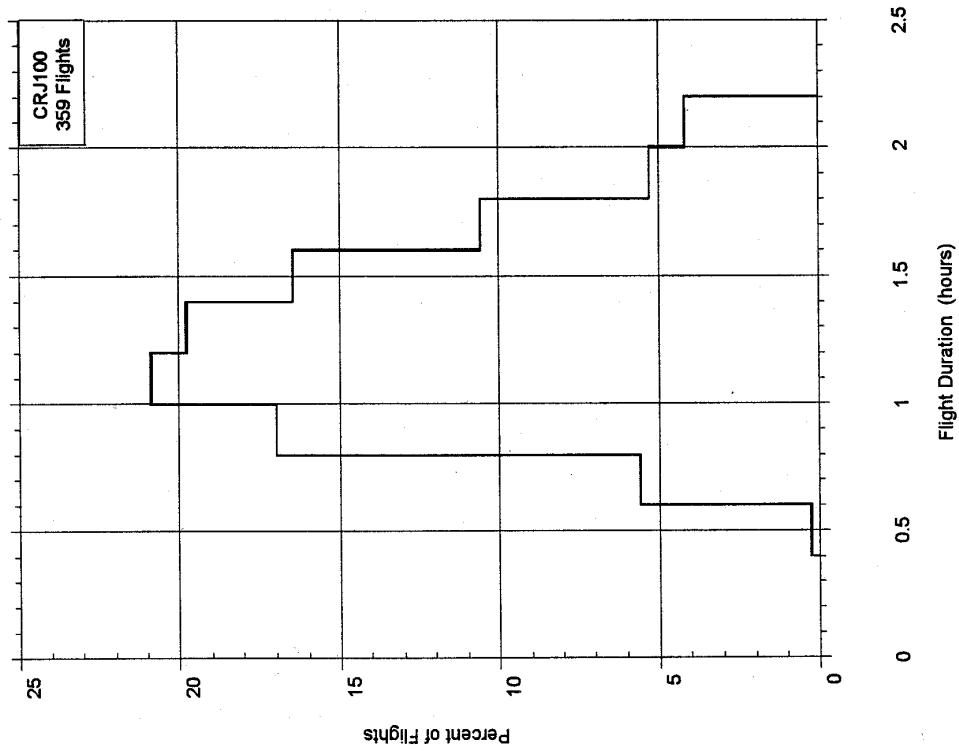


FIGURE A-2. PERCENT OF FLIGHTS VS  
MAXIMUM FLIGHT ALTITUDE

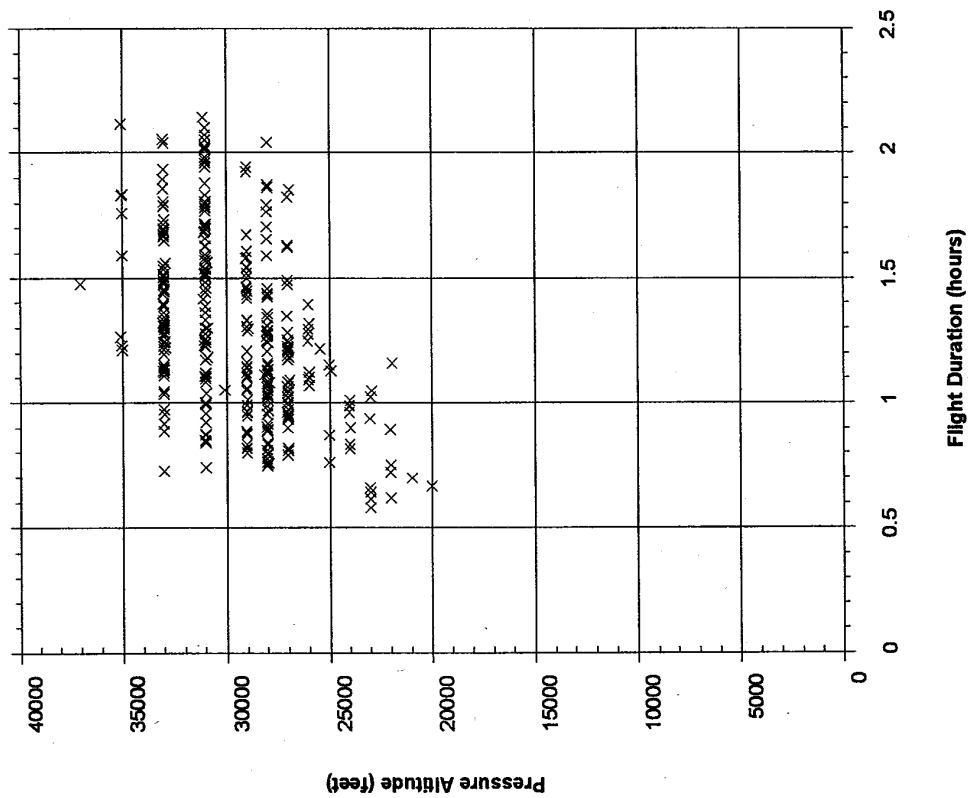


FIGURE A-3. CORRELATION OF MAXIMUM ALTITUDE AND FLIGHT DURATION

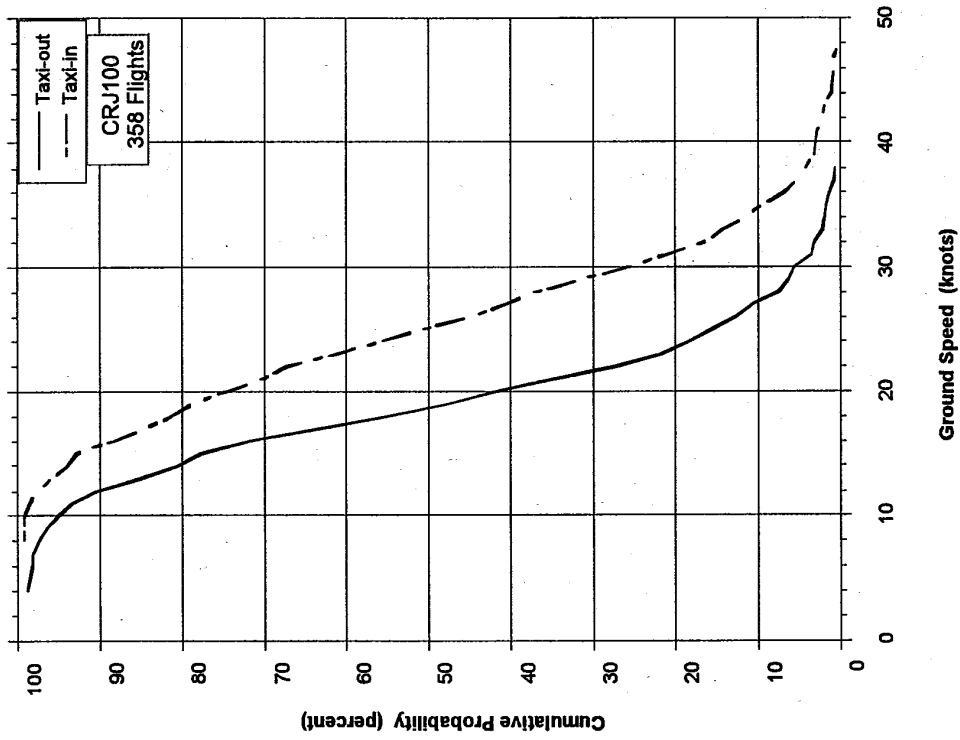


FIGURE A-4. CUMULATIVE PROBABILITY OF MAXIMUM GROUND SPEED DURING TAXI

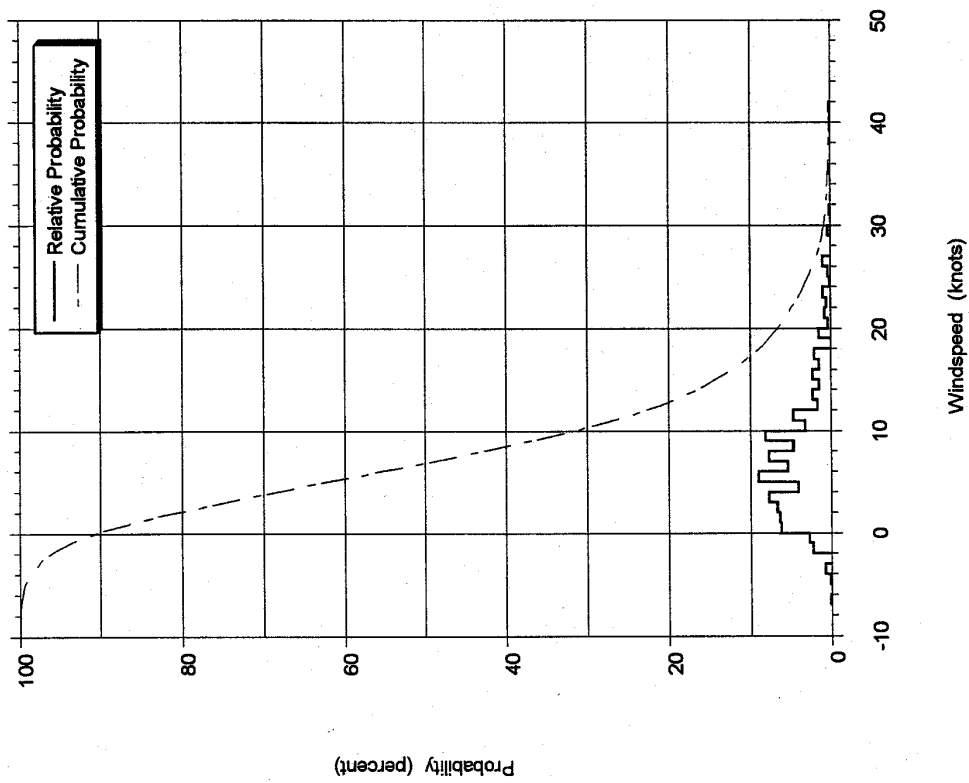


FIGURE A-5. PROBABILITIES OF WIND SPEED  
PARALLEL TO RUNWAY AT TOUCHDOWN

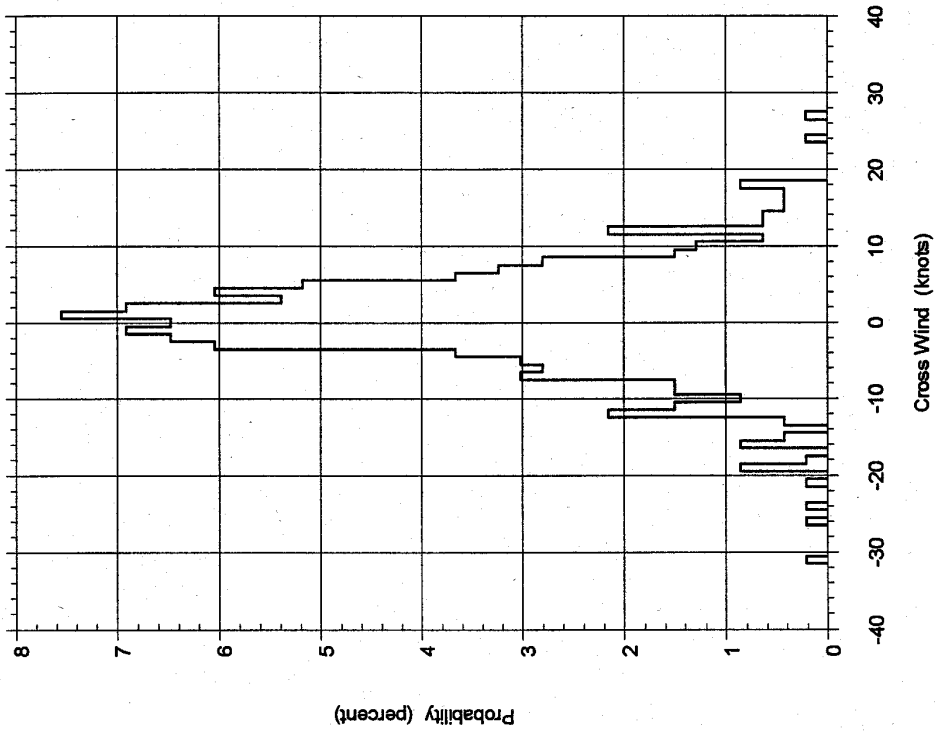


FIGURE A-6. RELATIVE PROBABILITY OF WIND  
SPEED ACROSS RUNWAY AT TOUCHDOWN

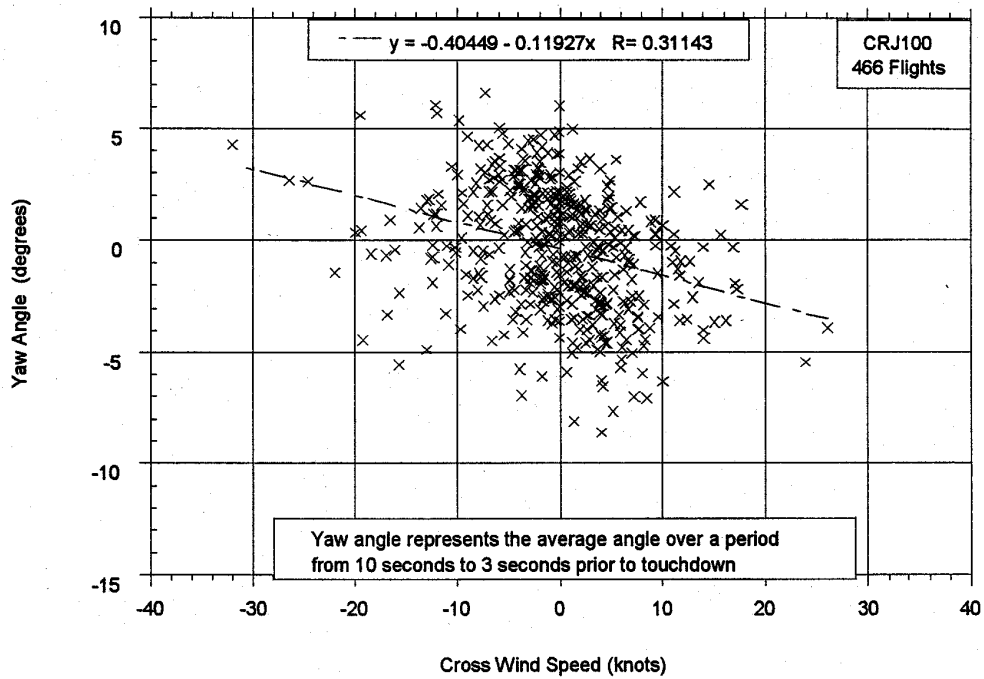


FIGURE A-7. MEAN YAW ANGLE BEFORE TOUCHDOWN VS CROSSWIND AT TOUCHDOWN

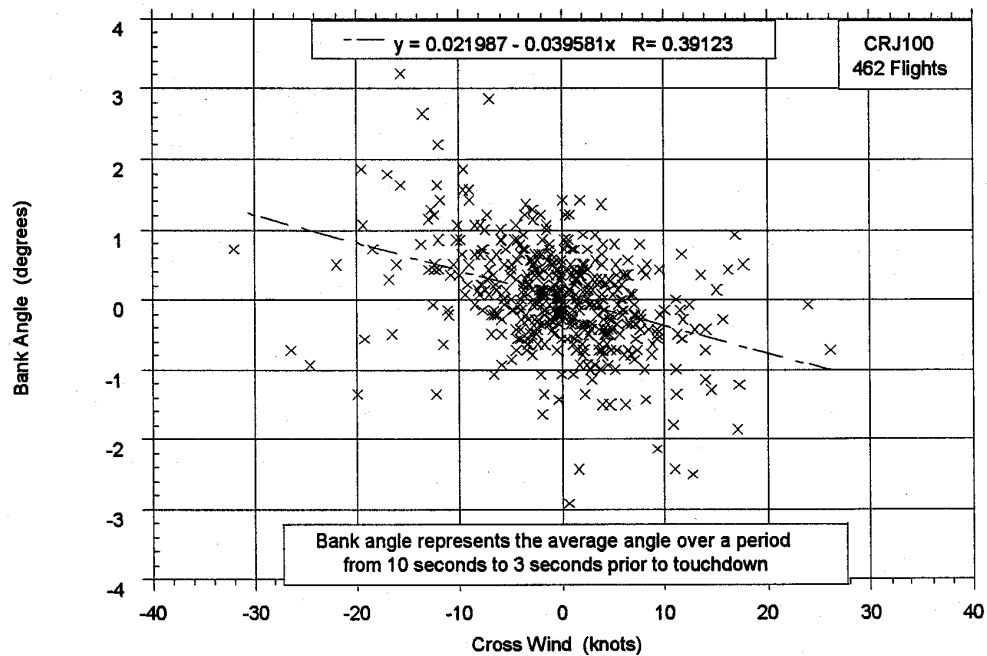


FIGURE A-8. MEAN BANK ANGLE BEFORE TOUCHDOWN VS CROSSWIND AT TOUCHDOWN

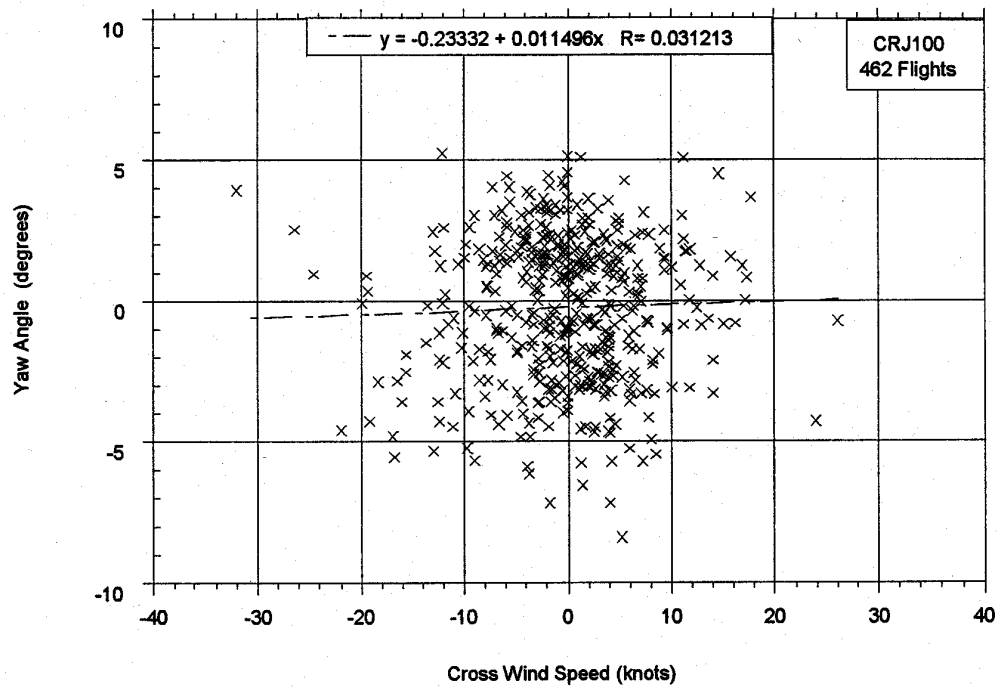


FIGURE A-9. YAW ANGLE VS CROSSWIND AT TOUCHDOWN

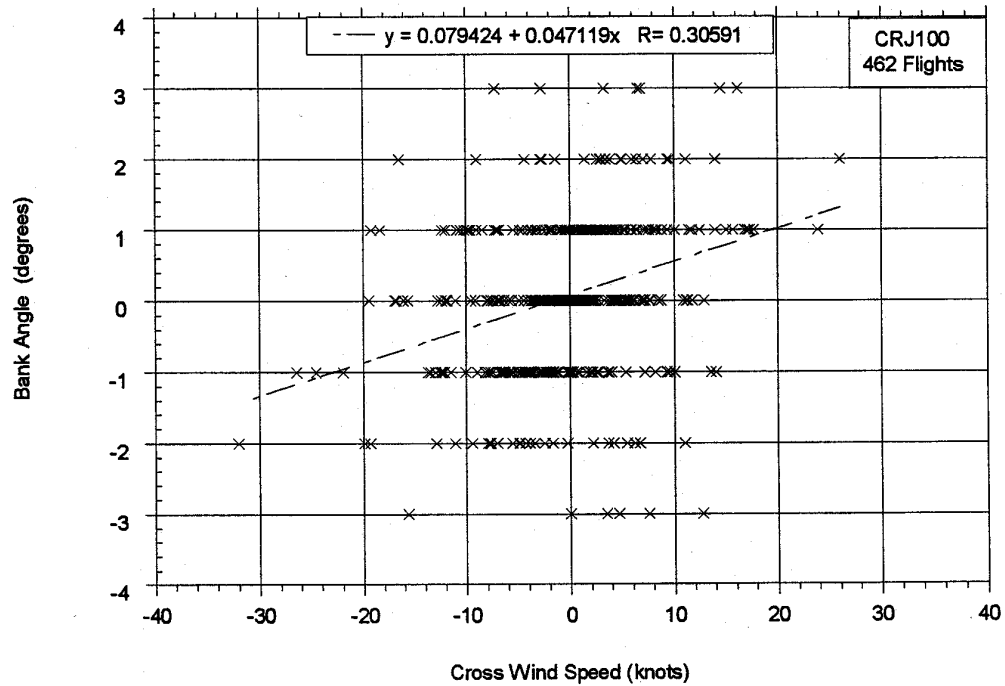


FIGURE A-10. BANK ANGLE VS CROSSWIND AT TOUCHDOWN

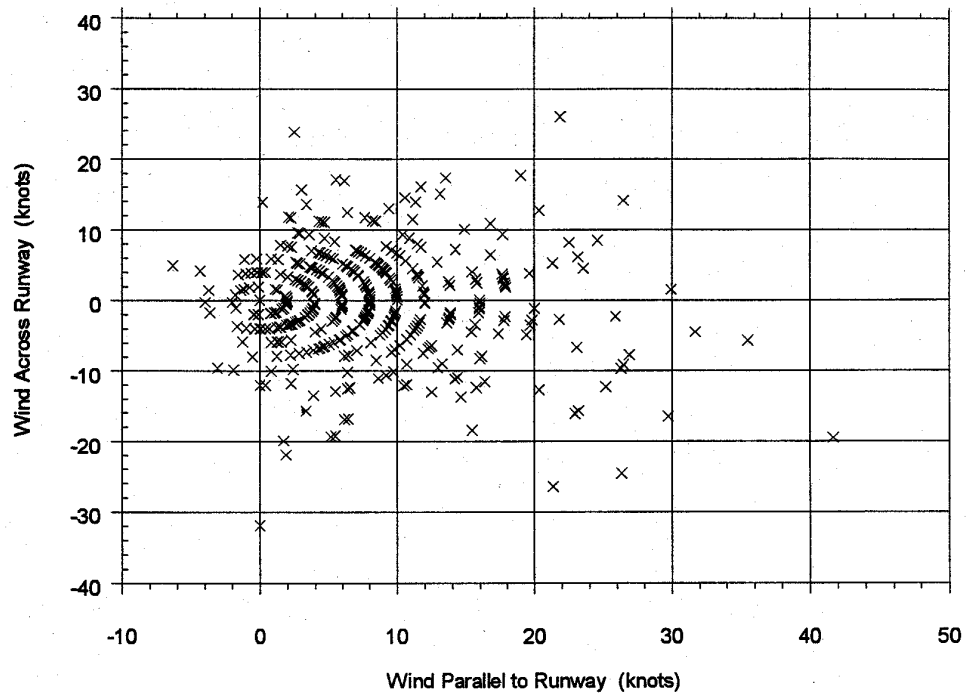


FIGURE A-11. COINCIDENT PARALLEL AND CROSSWIND SPEEDS AT TOUCHDOWN

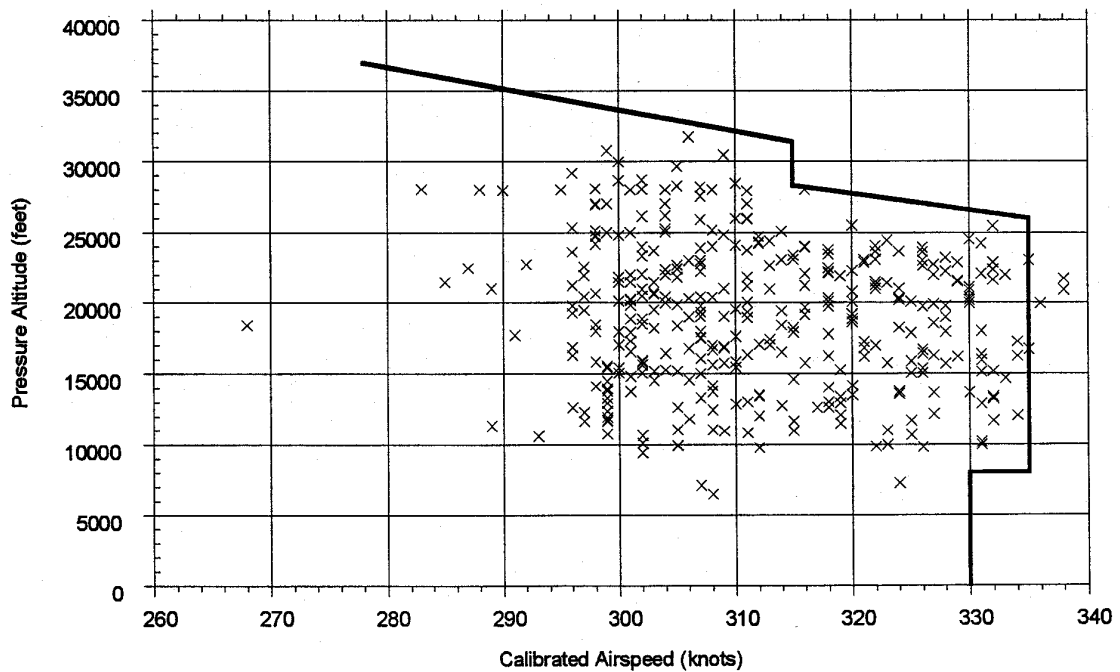


FIGURE A-12. MAXIMUM CALIBRATED AIRSPEED AND COINCIDENT ALTITUDE, ALL FLIGHT PHASES

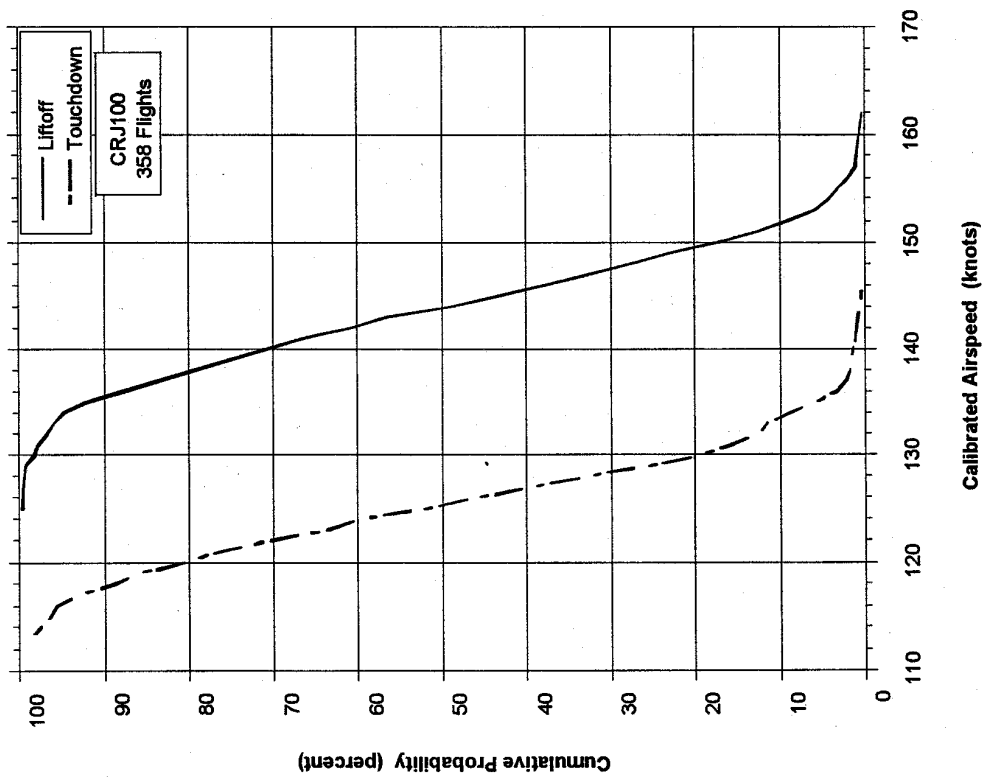


FIGURE A-13. CUMULATIVE PROBABILITY OF AIRSPEED AT LIFTOFF AND TOUCHDOWN

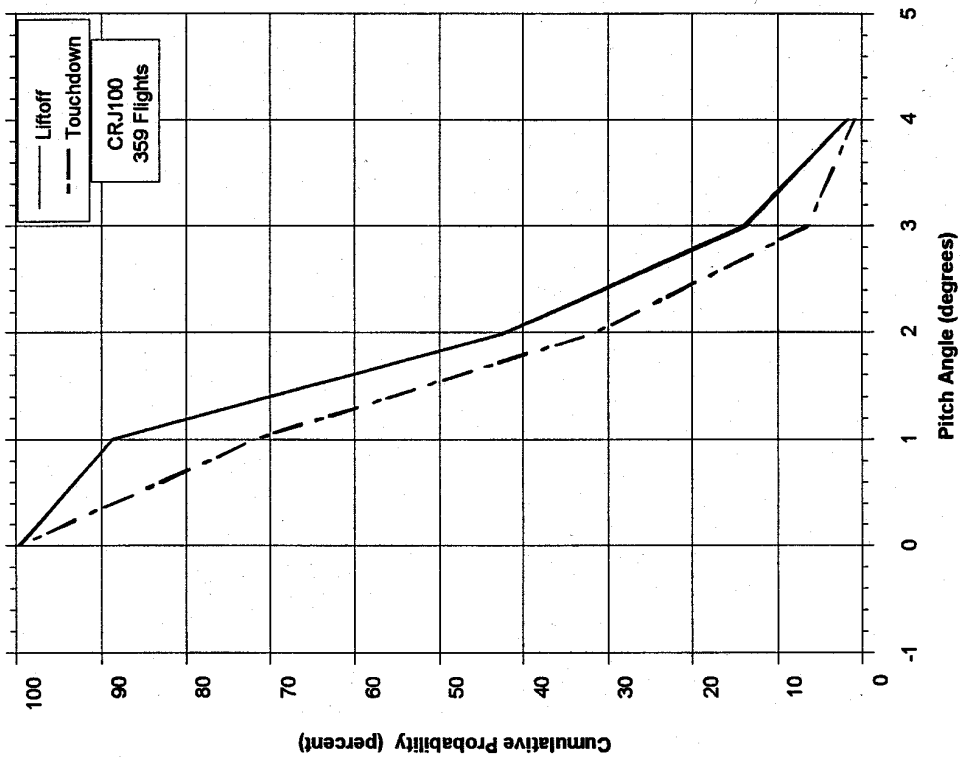


FIGURE A-14. CUMULATIVE PROBABILITY OF PITCH ANGLE AT LIFTOFF AND TOUCHDOWN

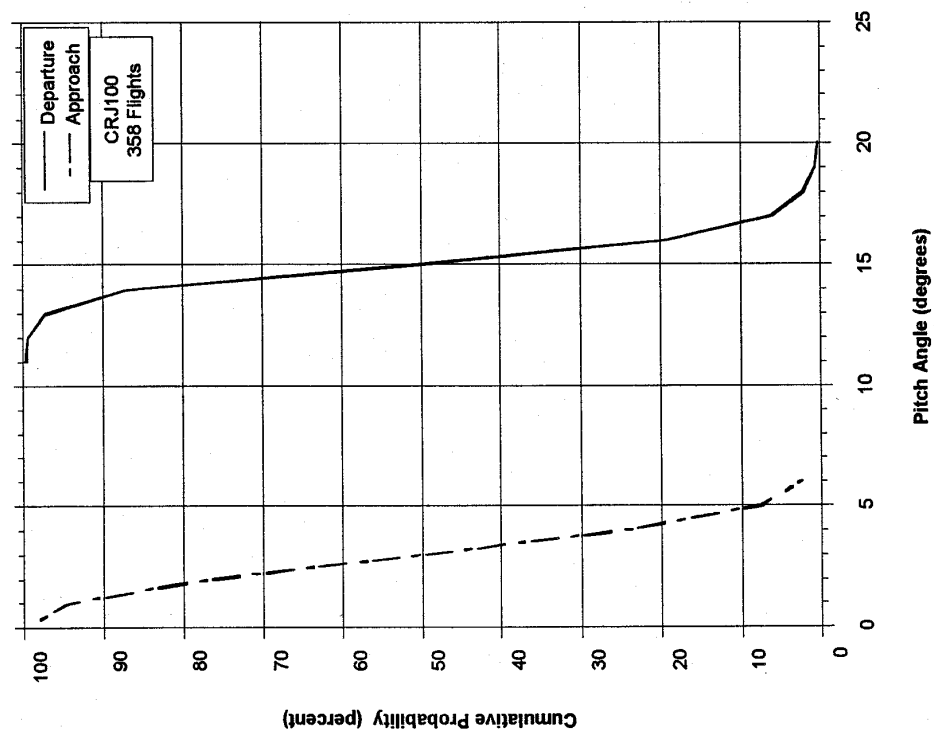


FIGURE A-15. CUMULATIVE PROBABILITY OF MAXIMUM PITCH ANGLE DURING DEPARTURE AND APPROACH

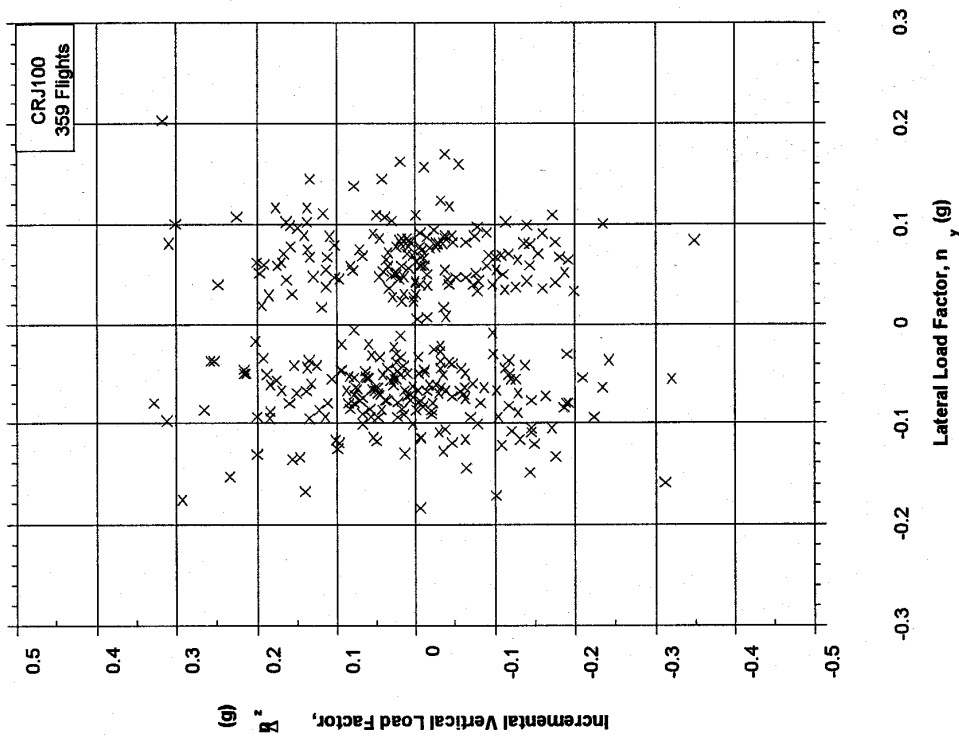


FIGURE A-16. MAXIMUM LATERAL LOAD FACTOR AND COINCIDENT INCREMENTAL VERTICAL LOAD FACTOR AT TOUCHDOWN

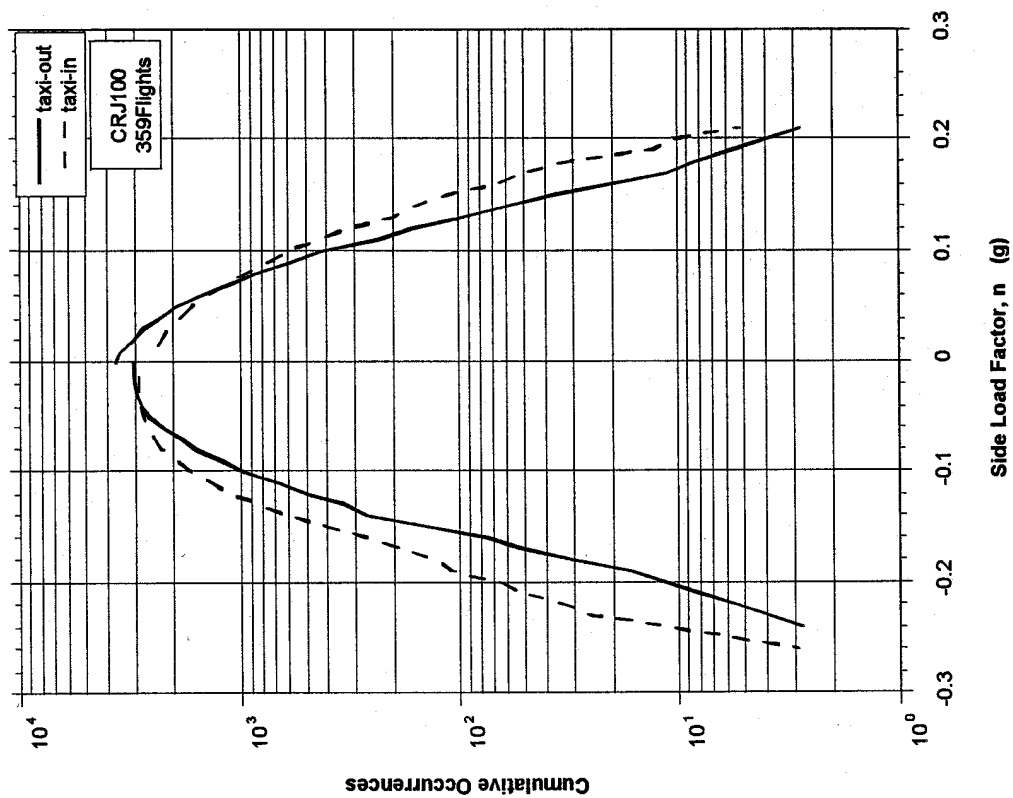


FIGURE A-17. CUMULATIVE FREQUENCY OF  
MAXIMUM LATERAL LOAD FACTOR DURING  
GROUND TURNS

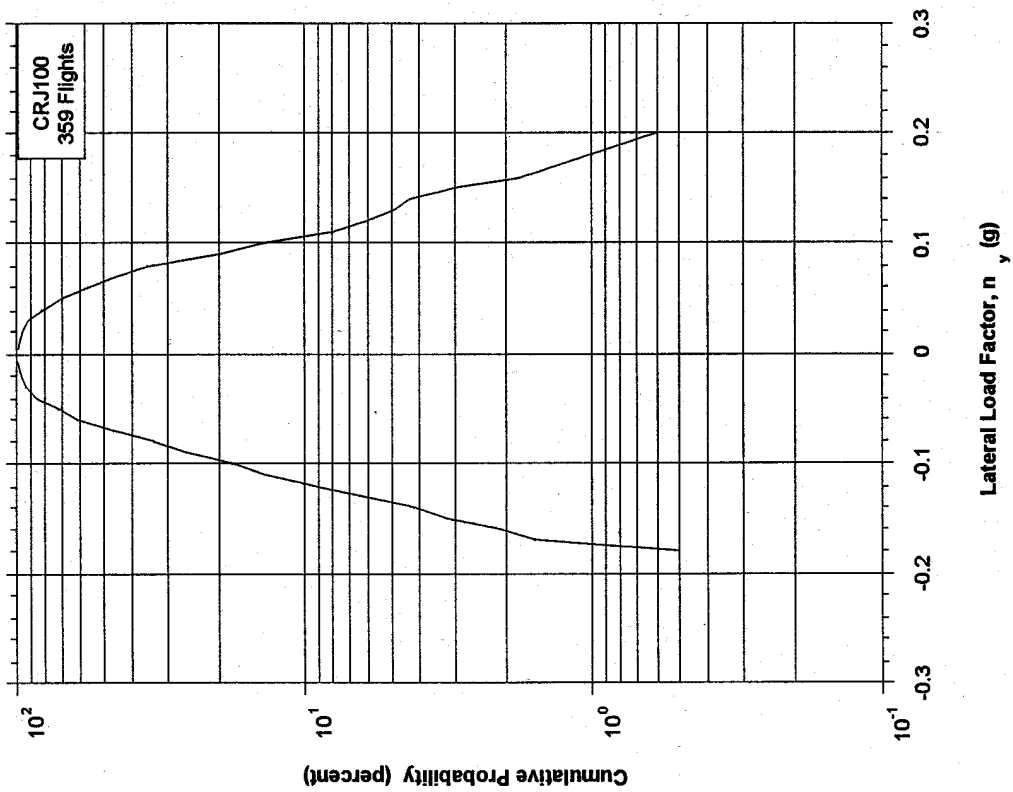


FIGURE A-18. CUMULATIVE FREQUENCY OF  
MAXIMUM LATERAL LOAD FACTOR AT  
TOUCHDOWN

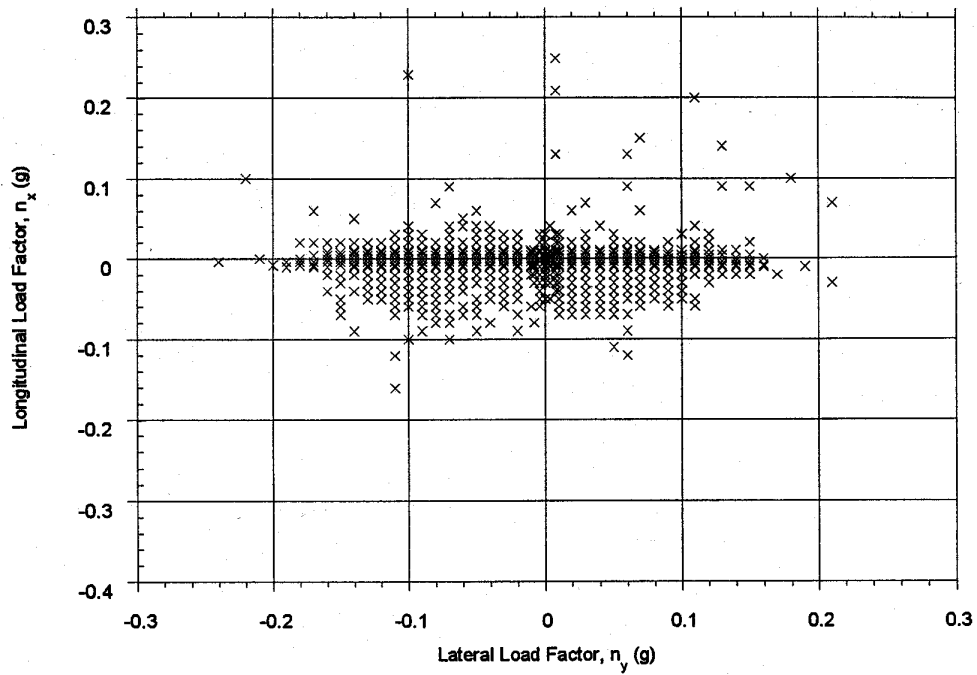


FIGURE A-19. MAXIMUM LATERAL LOAD FACTOR AND COINCIDENT LONGITUDINAL LOAD FACTOR DURING GROUND TURNS, TAXI-OUT

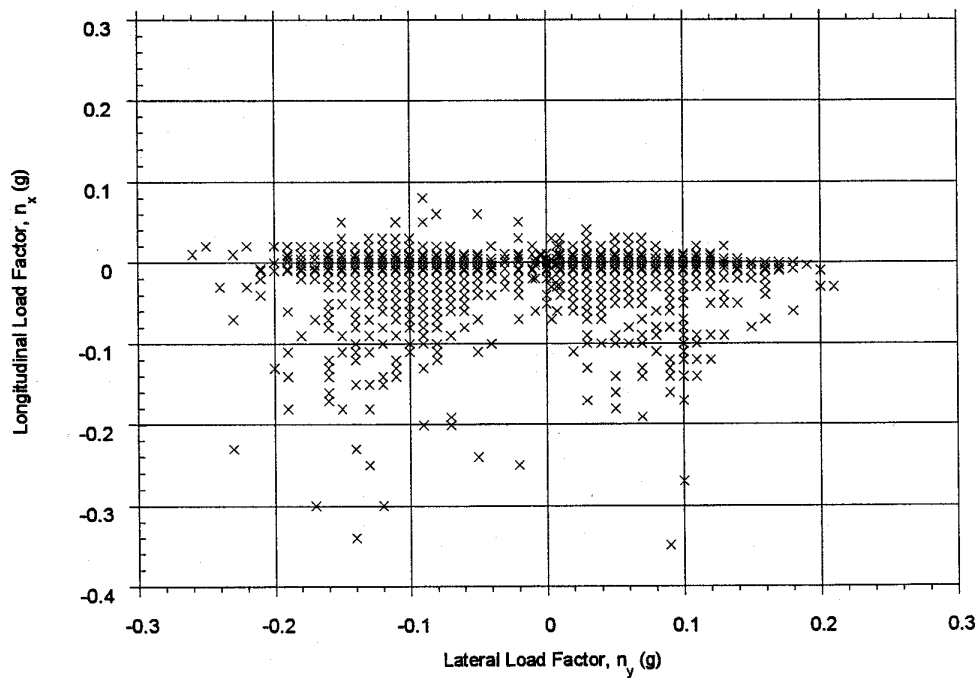


FIGURE A-20. MAXIMUM LATERAL LOAD FACTOR AND COINCIDENT LONGITUDINAL LOAD FACTOR DURING GROUND TURNS, TAXI-IN

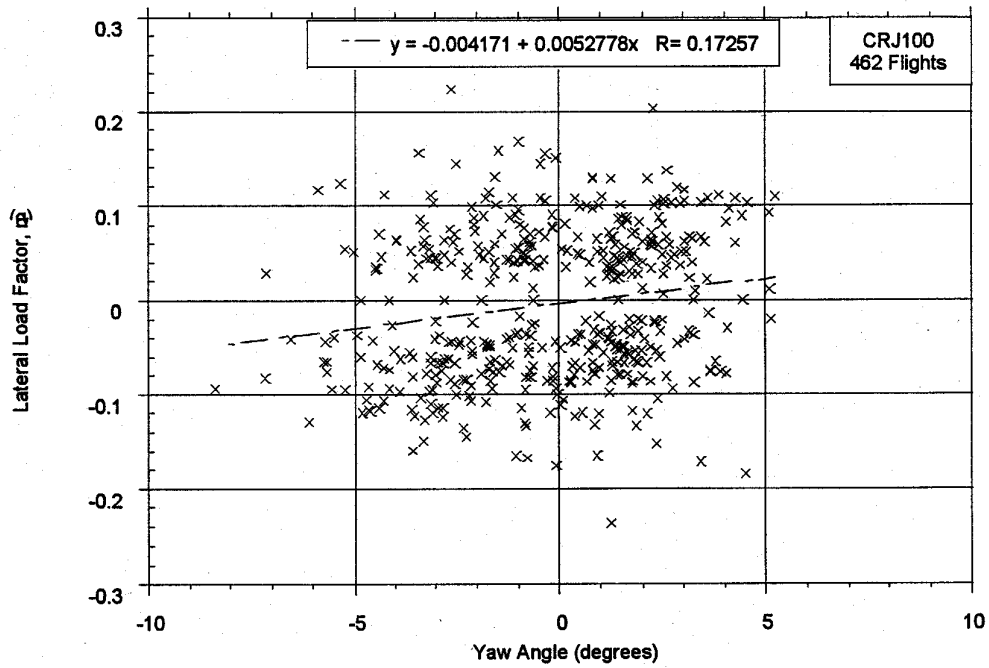


FIGURE A-21. MAXIMUM LATERAL LOAD FACTOR AND COINCIDENT YAW ANGLE AT TOUCHDOWN

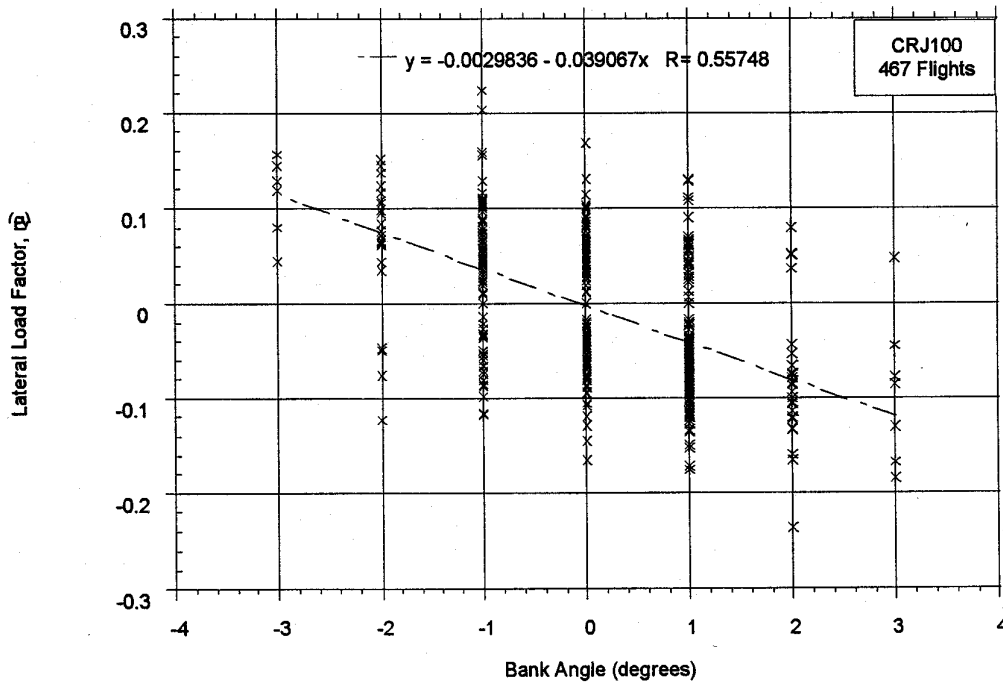


FIGURE A-22. MAXIMUM LATERAL LOAD FACTOR AND COINCIDENT BANK ANGLE AT TOUCHDOWN

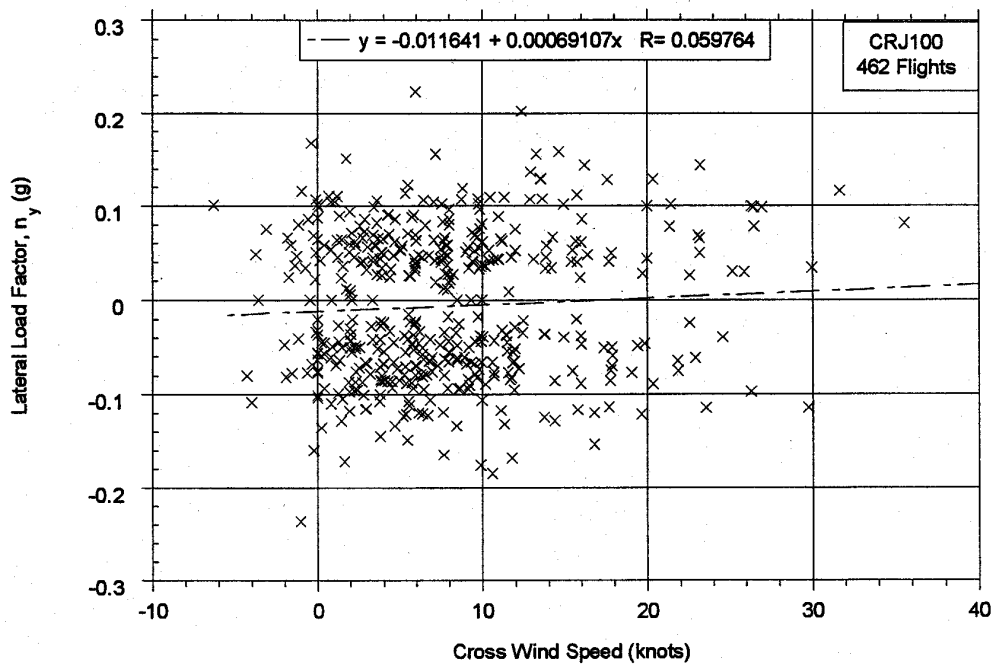


FIGURE A-23. MAXIMUM LATERAL LOAD FACTOR VS PARALLEL WIND SPEED AT TOUCHDOWN

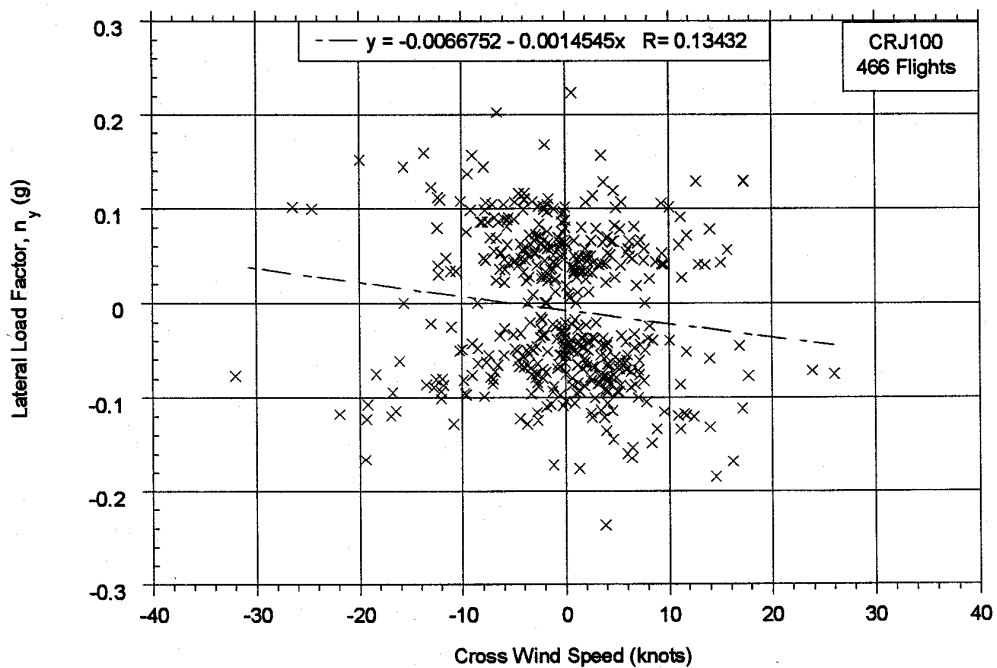


FIGURE A-24. MAXIMUM LATERAL LOAD FACTOR VS CROSSWIND SPEED AT TOUCHDOWN

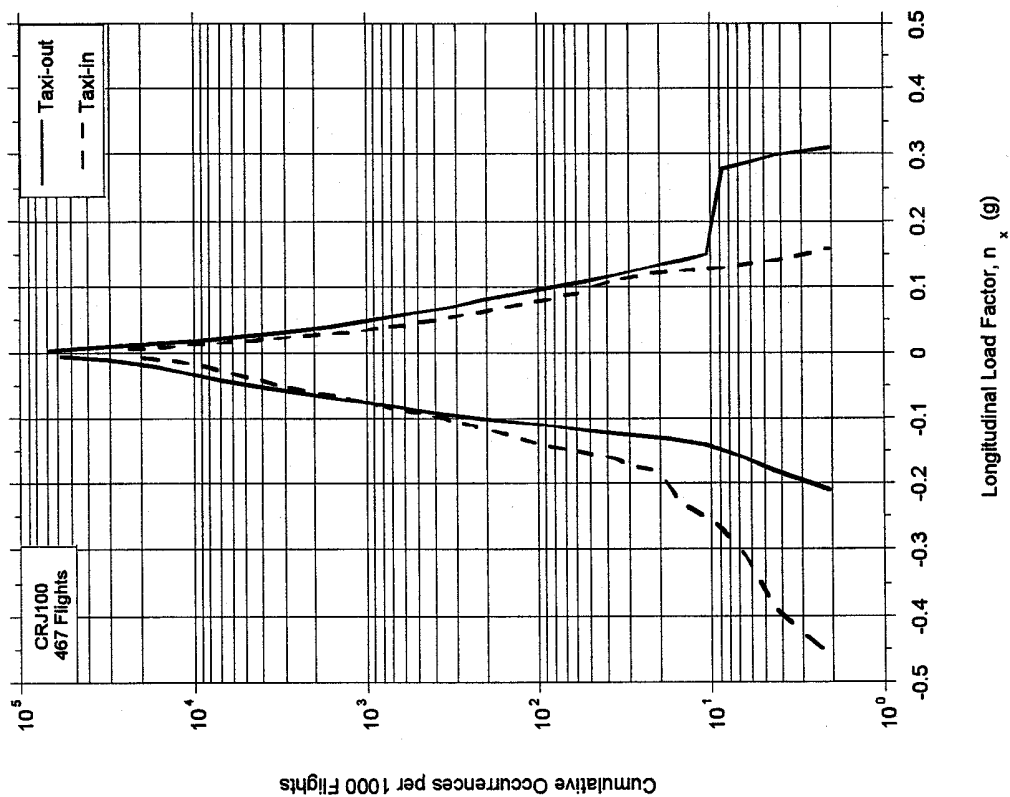


FIGURE A-25. CUMULATIVE FREQUENCY OF  
LONGITUDINAL LOAD FACTOR DURING TAXI  
OPERATIONS

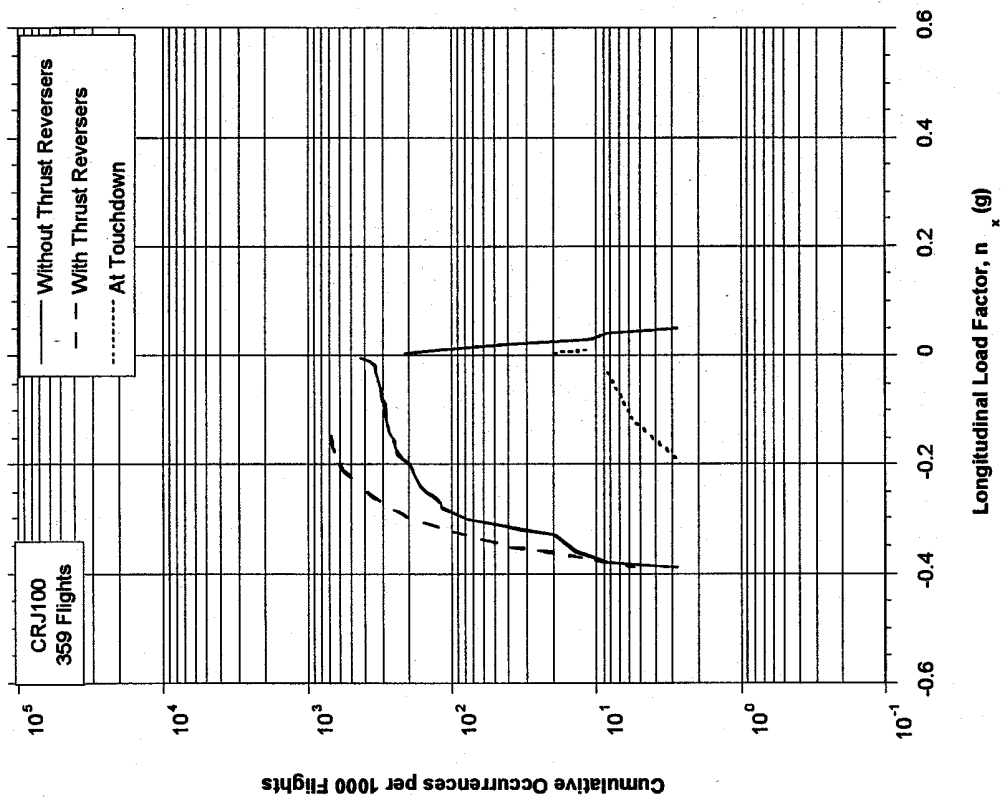


FIGURE A-26. CUMULATIVE FREQUENCY OF  
LONGITUDINAL LOAD FACTOR AT TOUCHDOWN  
AND DURING LANDING ROLL

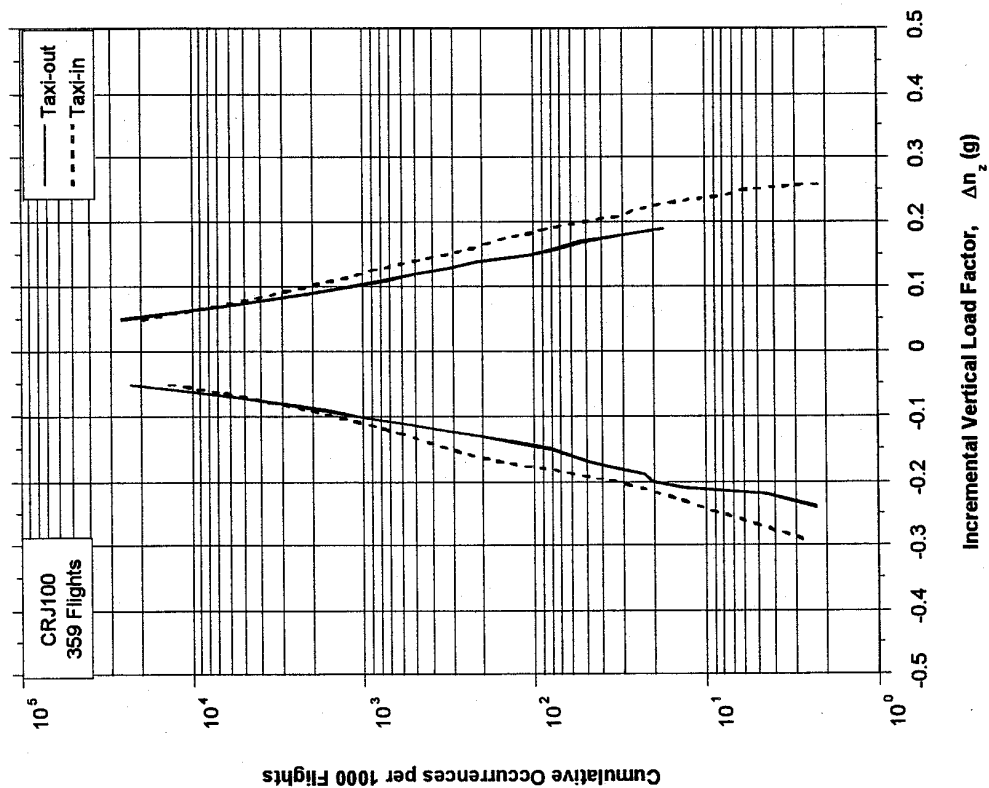


FIGURE A-27. CUMULATIVE FREQUENCY OF INCREMENTAL VERTICAL LOAD FACTOR DURING TAXI OPERATIONS

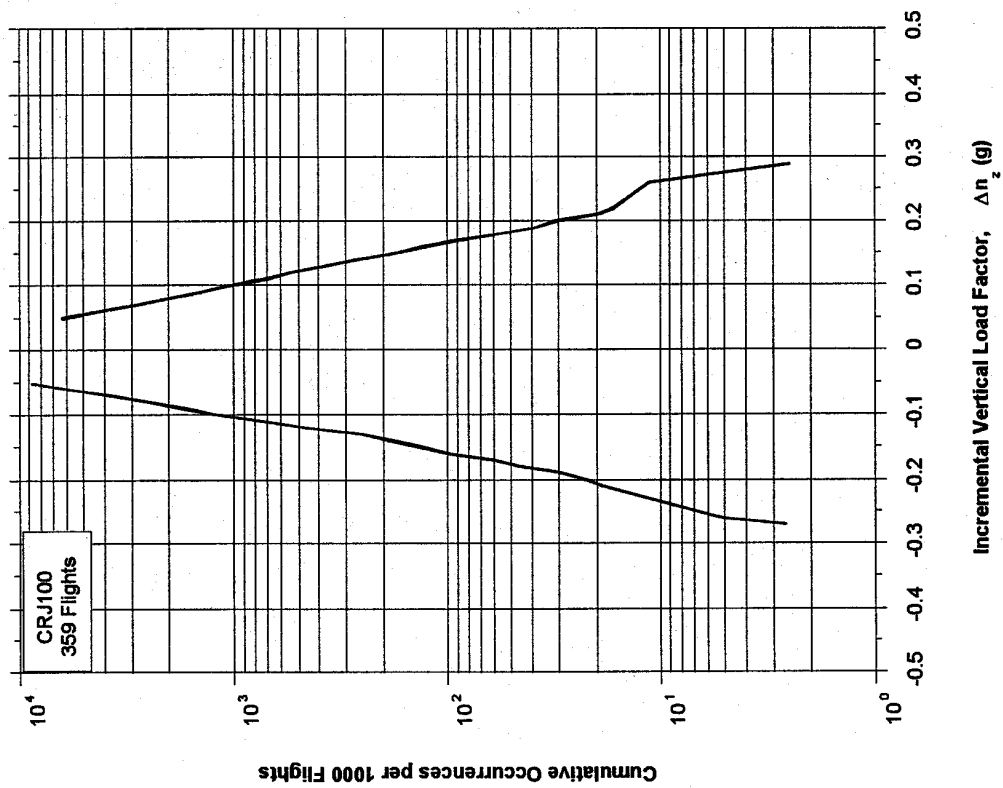


FIGURE A-28. CUMULATIVE FREQUENCY OF INCREMENTAL VERTICAL LOAD FACTOR DURING TAKEOFF ROLL

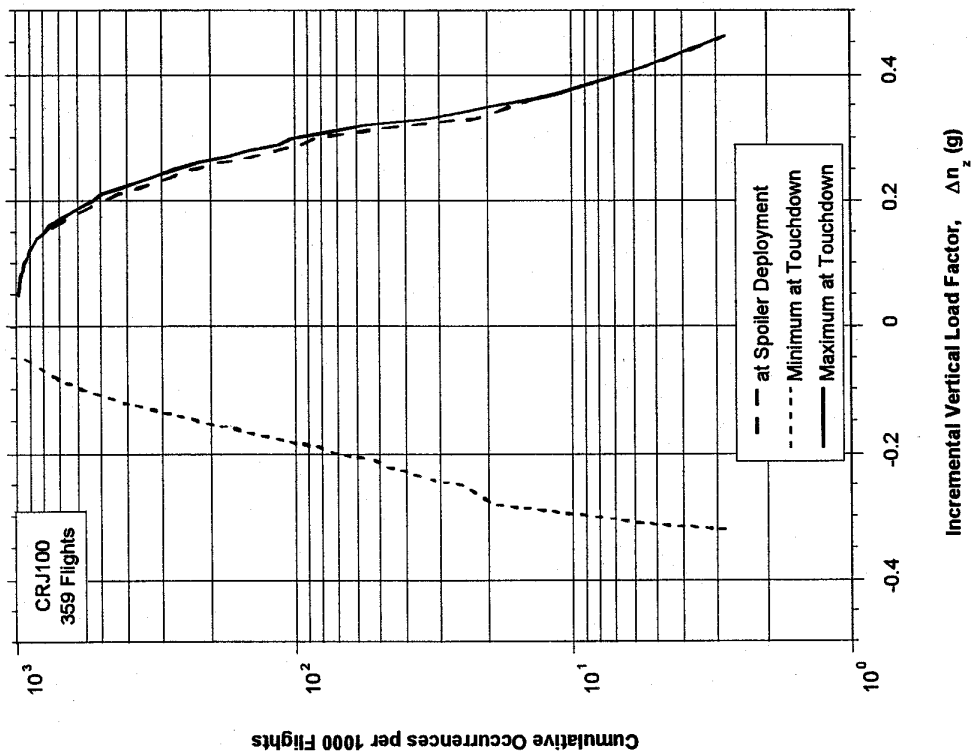


FIGURE A-29. CUMULATIVE FREQUENCY OF INCREMENTAL VERTICAL LOAD FACTOR AT SPOILER DEPLOYMENT AND AT TOUCHDOWN

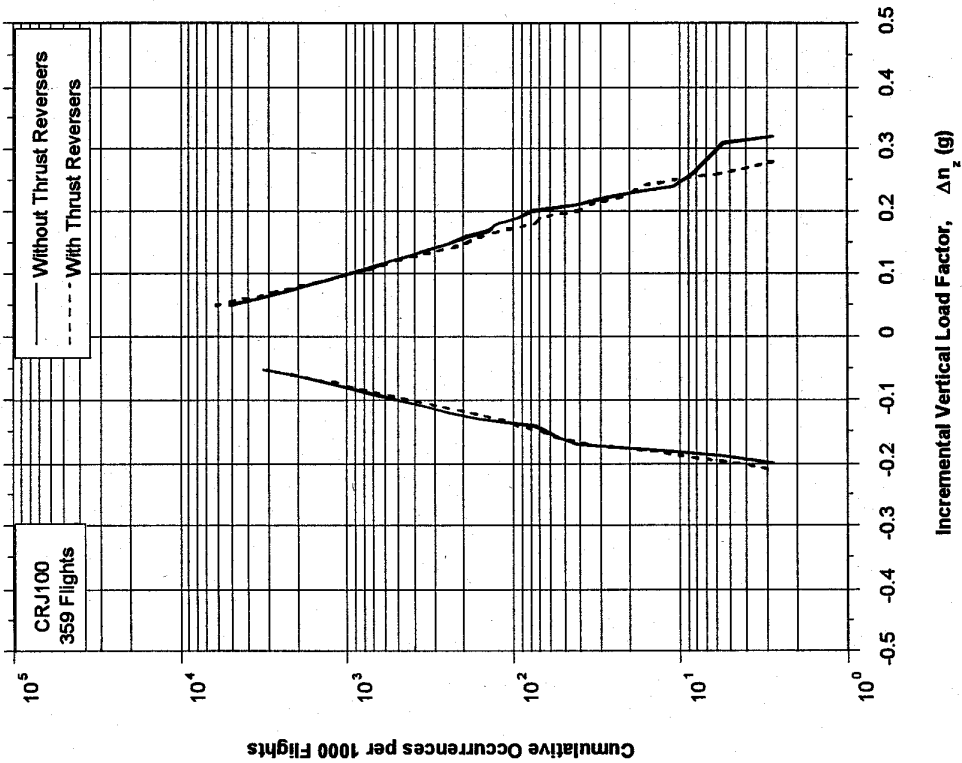


FIGURE A-30. CUMULATIVE FREQUENCY OF INCREMENTAL VERTICAL LOAD FACTOR DURING LANDING ROLL

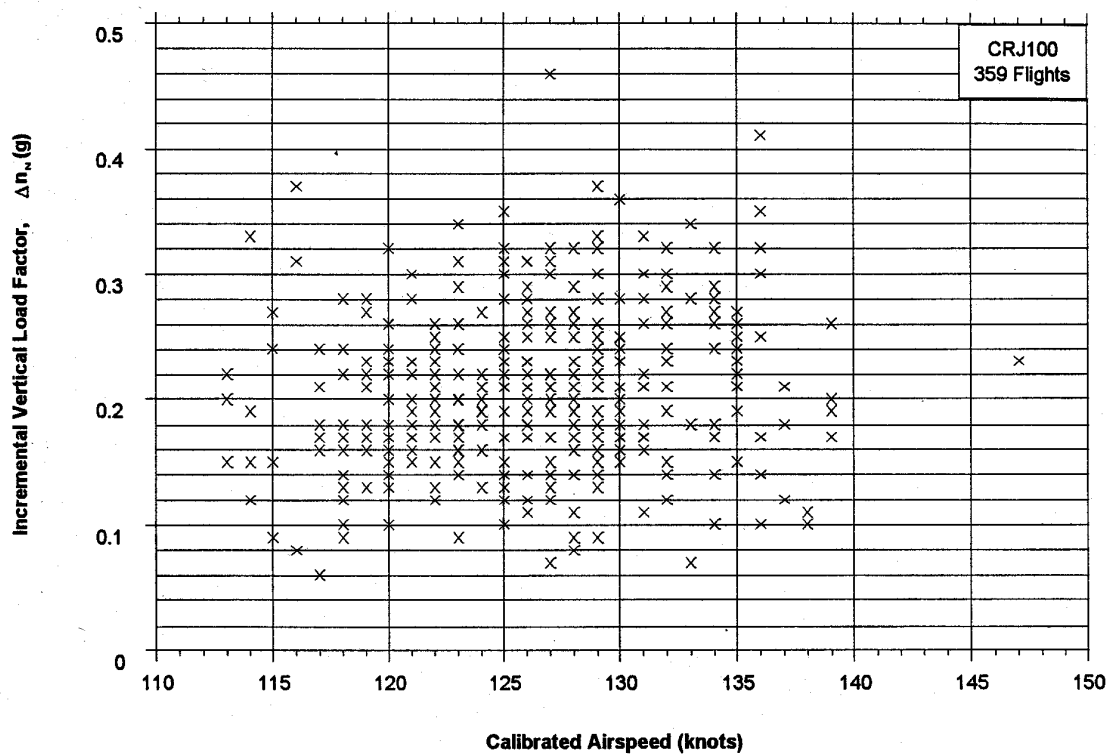


FIGURE A-31. MAXIMUM INCREMENTAL VERTICAL LOAD FACTOR VS COINCIDENT AIRSPEED AT TOUCHDOWN

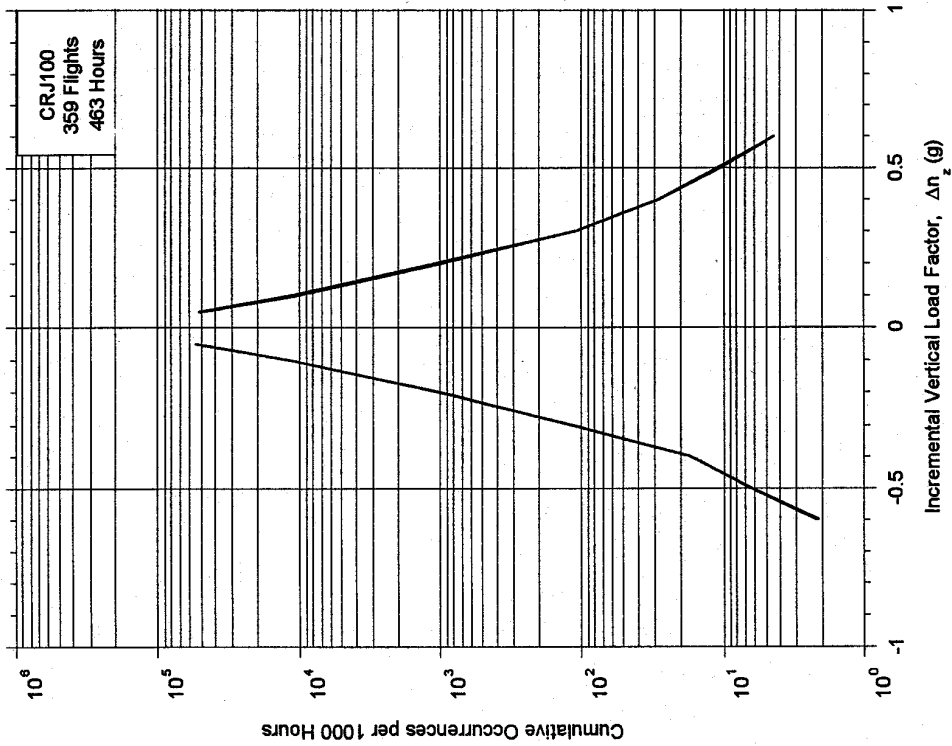


FIGURE A-32. CUMULATIVE OCCURRENCES OF INCREMENTAL VERTICAL GUST LOAD FACTOR PER 1000 HOURS, COMBINED FLIGHT PHASES

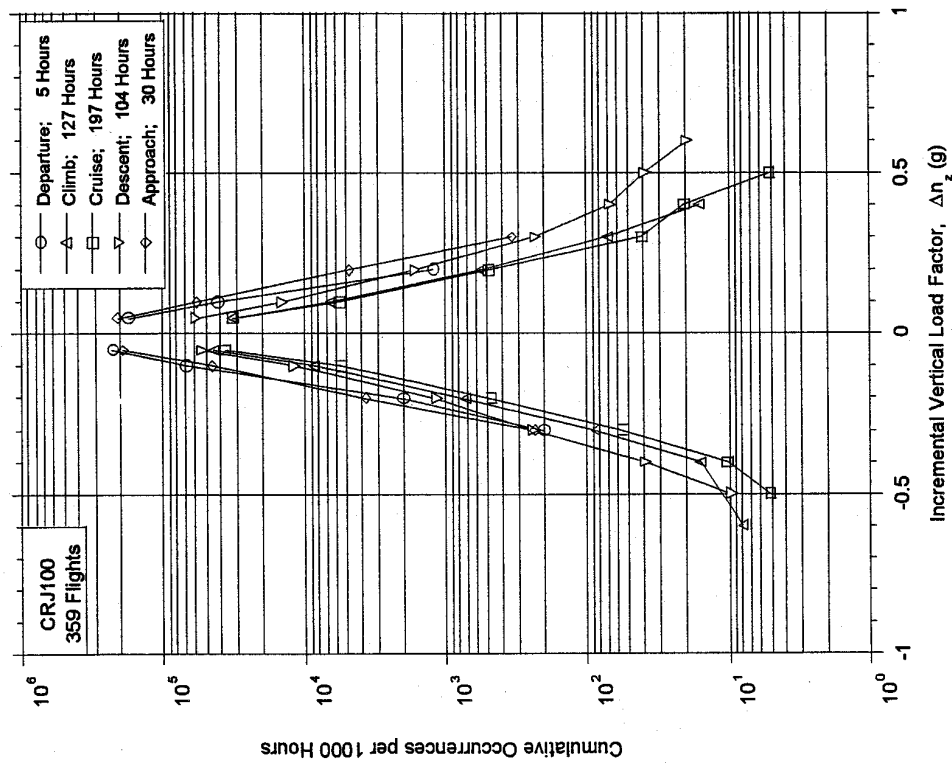


FIGURE A-33. CUMULATIVE OCCURRENCES OF INCREMENTAL VERTICAL GUST LOAD FACTOR PER 1000 HOURS, COMBINED FLIGHT PHASES

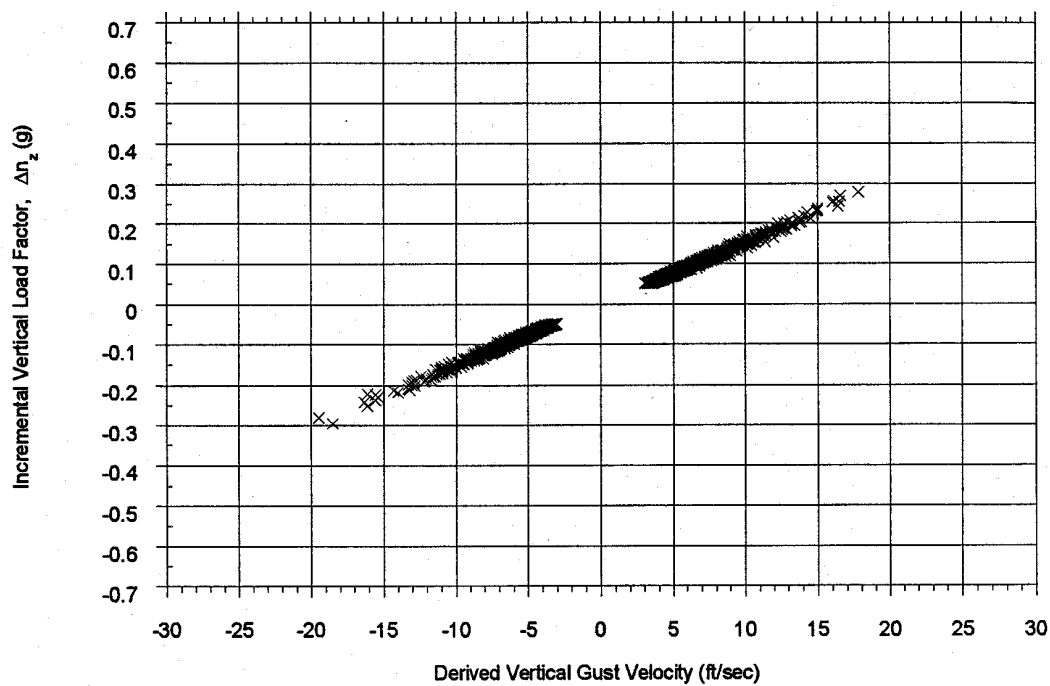


FIGURE A-34. INCREMENTAL VERTICAL LOAD FACTOR VS DERIVED VERTICAL GUST VELOCITY FOR 100-150 KIAS

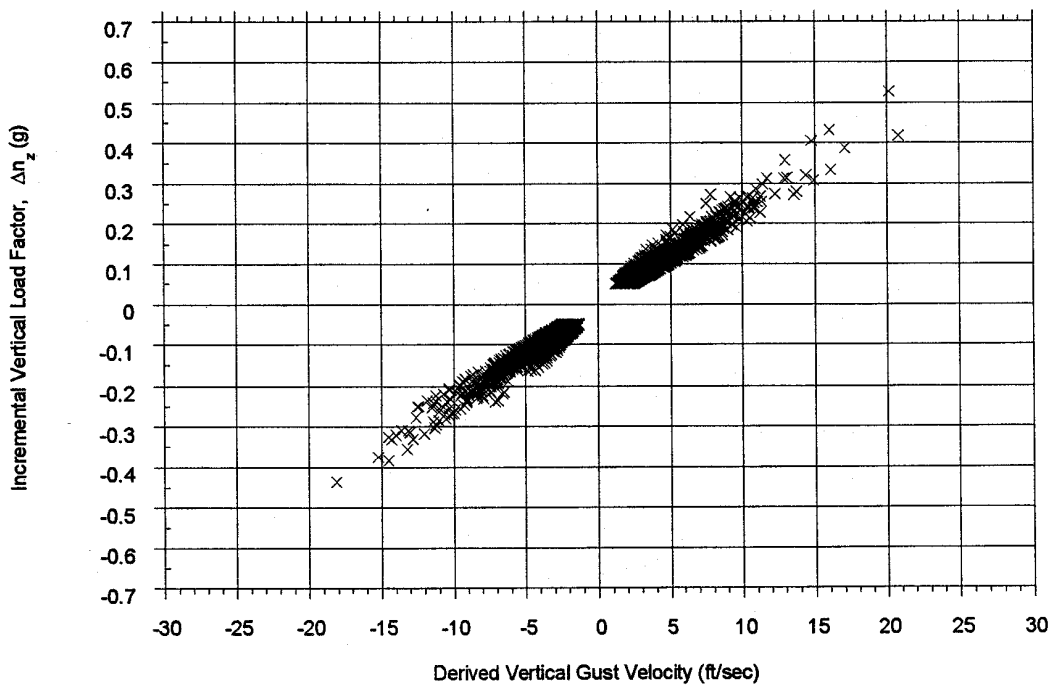


FIGURE A-35. INCREMENTAL VERTICAL LOAD FACTOR VS DERIVED VERTICAL GUST VELOCITY FOR 150-200 KIAS

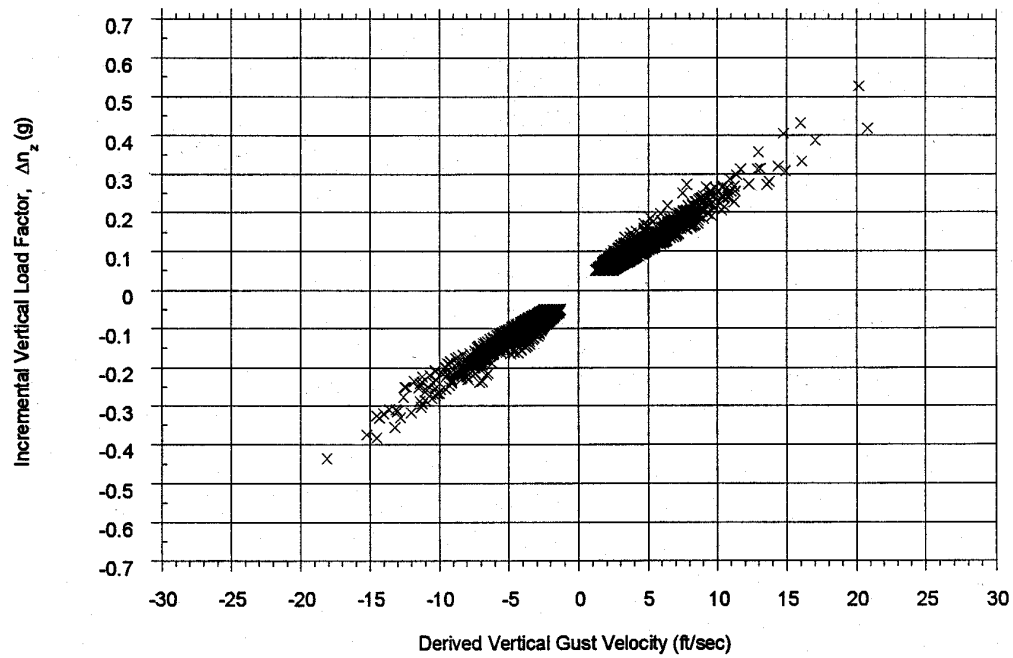


FIGURE A-36. INCREMENTAL VERTICAL LOAD FACTOR VS DERIVED VERTICAL GUST VELOCITY FOR 200-250 KIAS

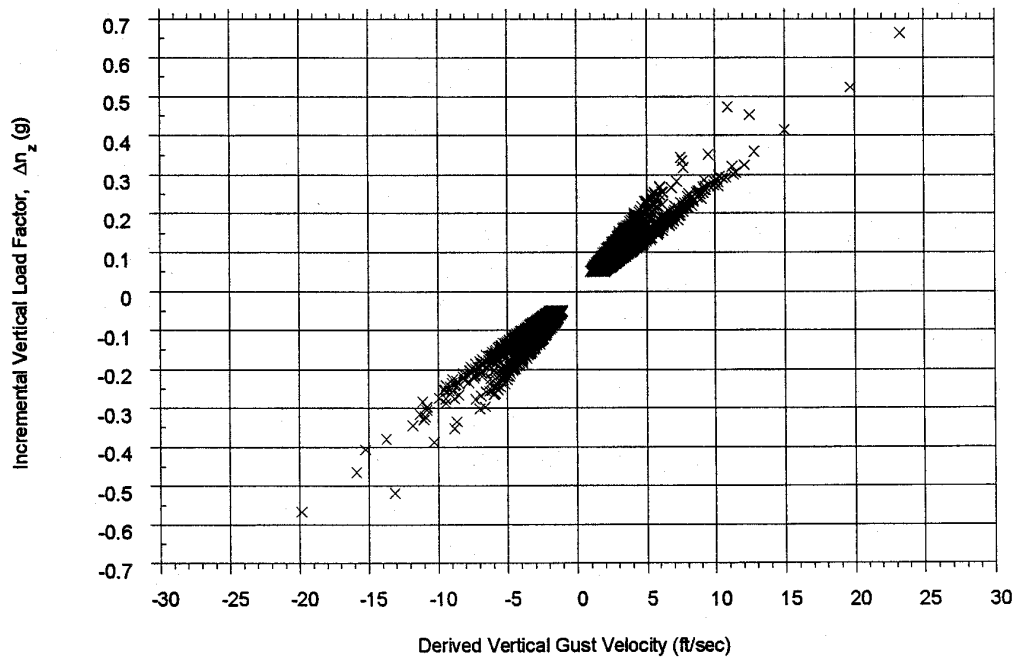


FIGURE A-37. INCREMENTAL VERTICAL LOAD FACTOR VS DERIVED VERTICAL GUST VELOCITY FOR 250-300 KIAS

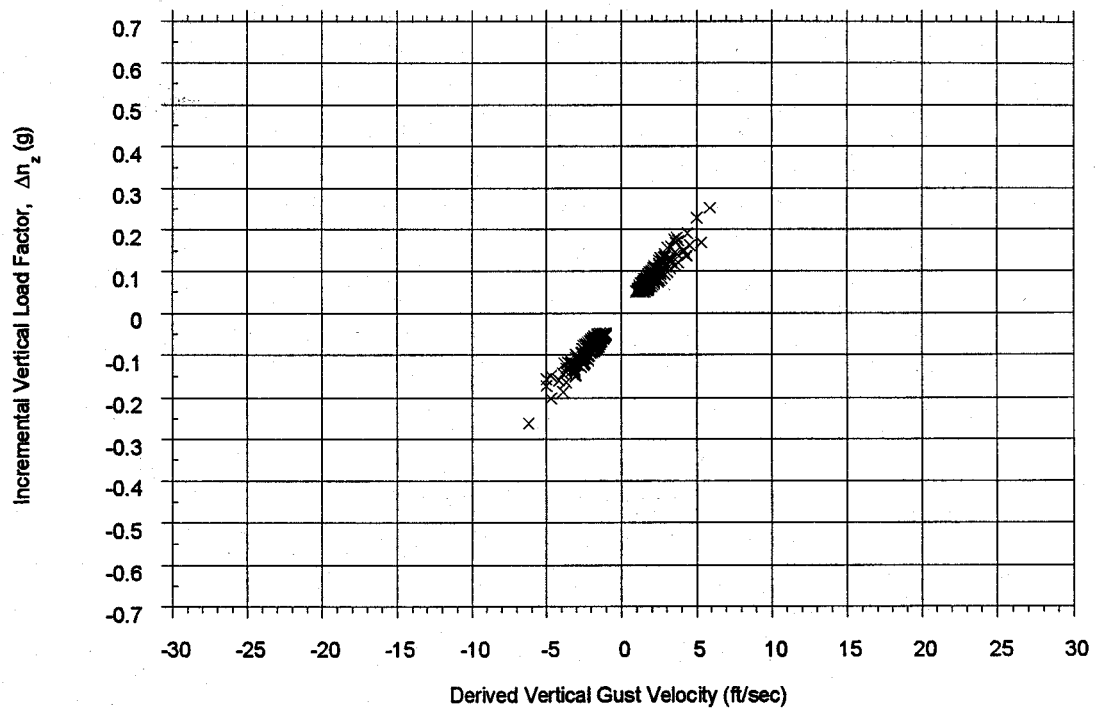


FIGURE A-38. INCREMENTAL VERTICAL LOAD FACTOR VS DERIVED VERTICAL GUST VELOCITY FOR 300-350 KIAS

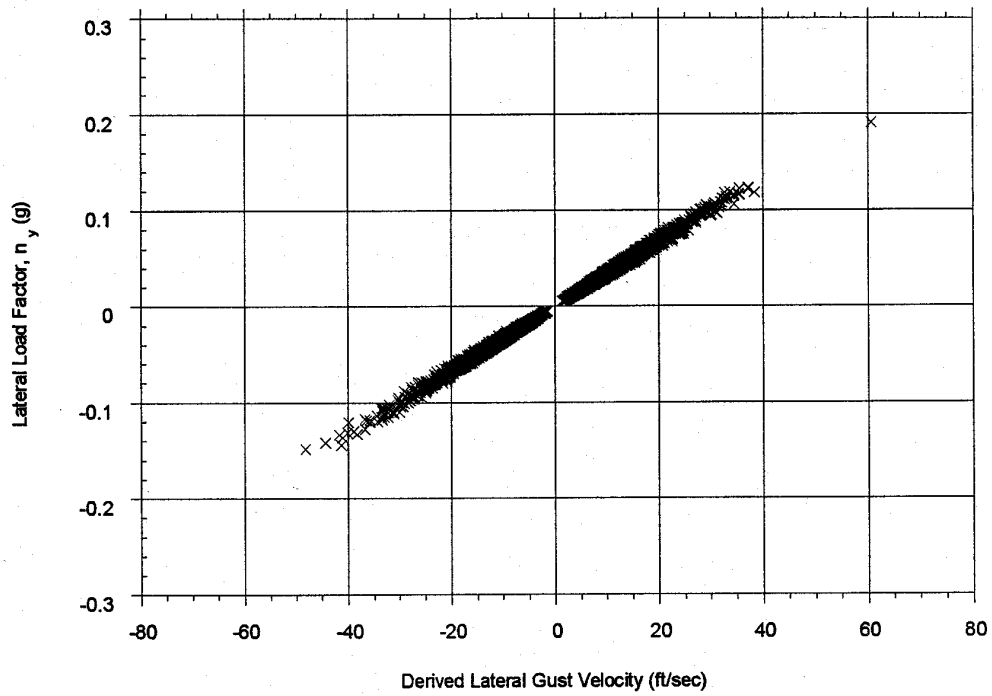


FIGURE A-39. LATERAL LOAD FACTOR VS DERIVED LATERAL GUST VELOCITY FOR 100-150 KIAS

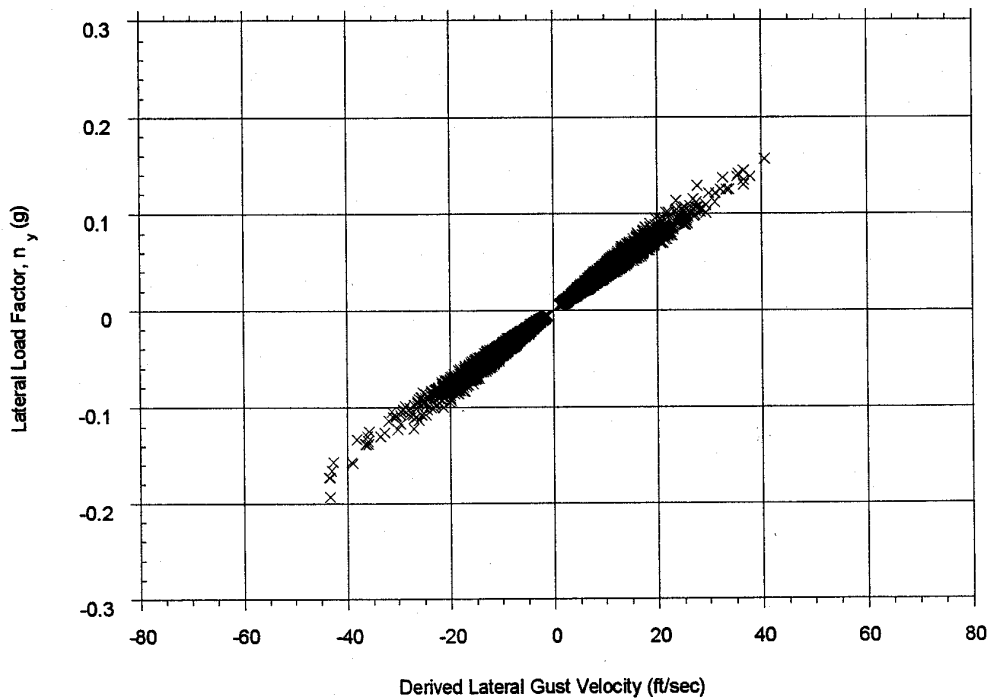


FIGURE A-40. LATERAL LOAD FACTOR VS DERIVED LATERAL GUST VELOCITY FOR 150-200 KIAS

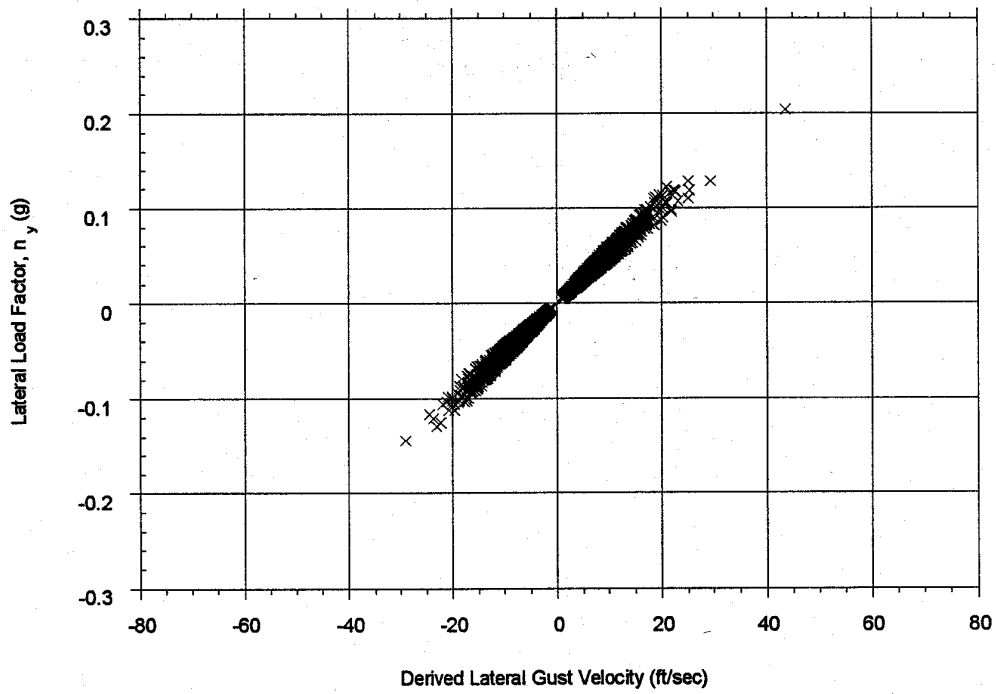


FIGURE A-41. LATERAL LOAD FACTOR VS DERIVED LATERAL GUST VELOCITY FOR 200-250 KIAS

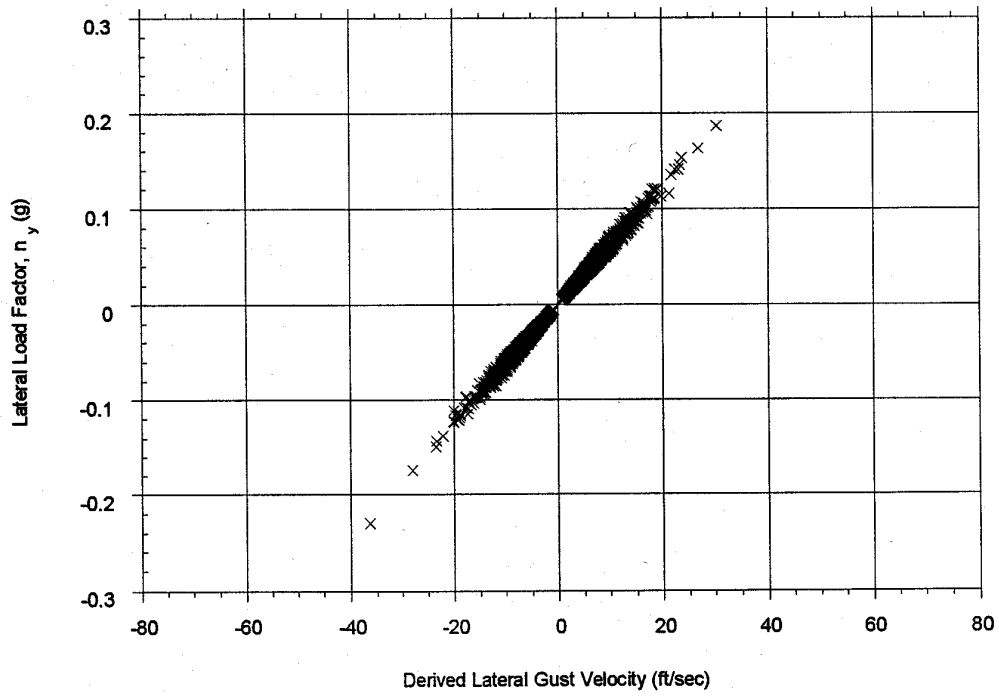


FIGURE A-42. LATERAL LOAD FACTOR VS DERIVED LATERAL GUST VELOCITY FOR 250-300 KIAS

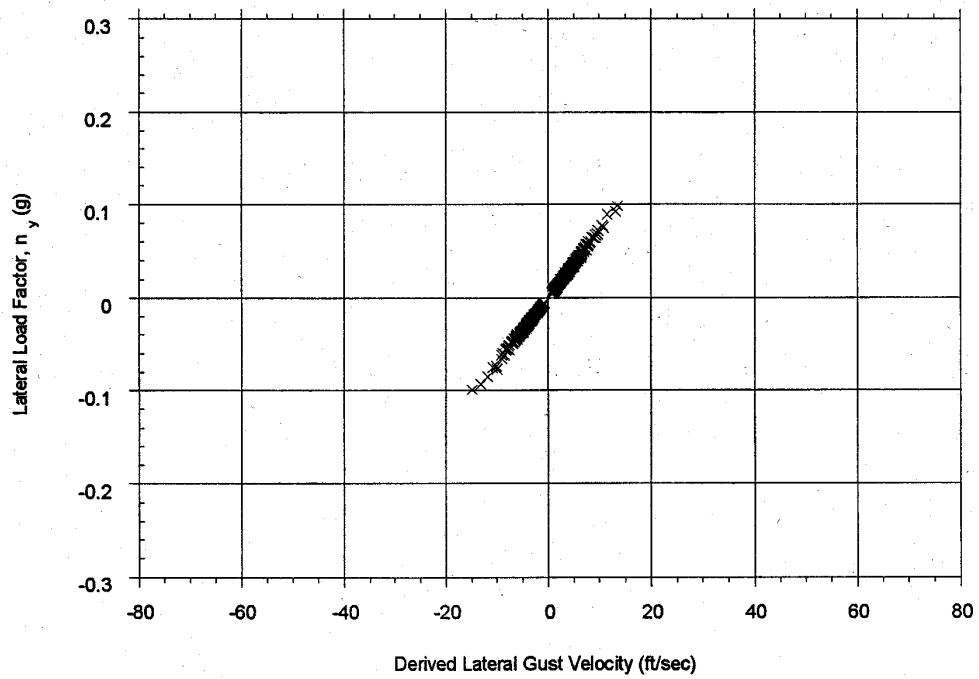


FIGURE A-43. LATERAL LOAD FACTOR VS DERIVED LATERAL GUST VELOCITY FOR 300-350 KIAS

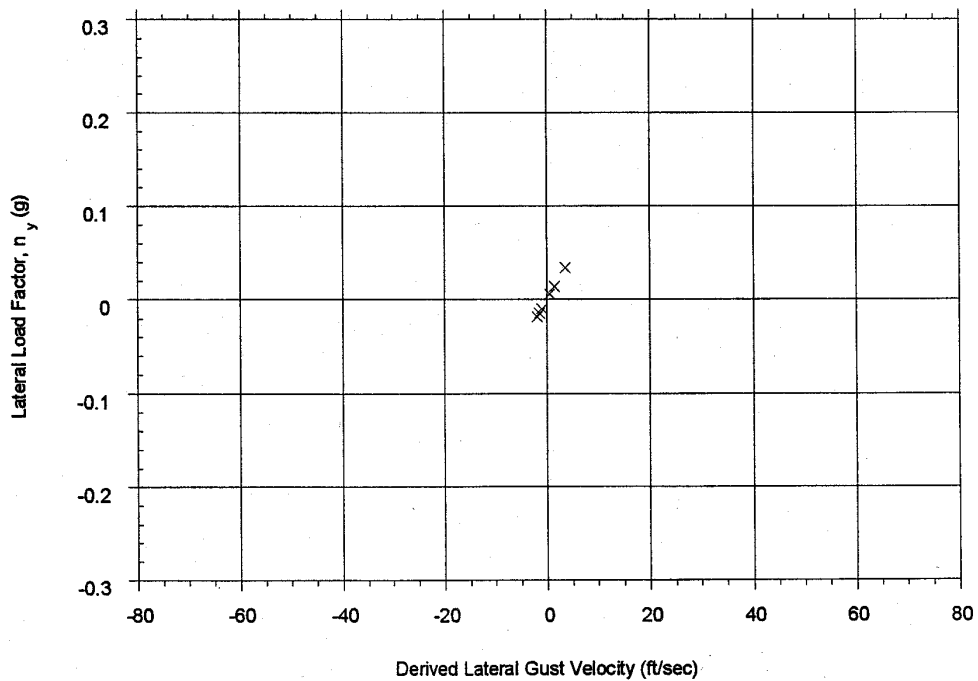


FIGURE A-44. LATERAL LOAD FACTOR VS DERIVED LATERAL GUST VELOCITY FOR 400-450 KIAS

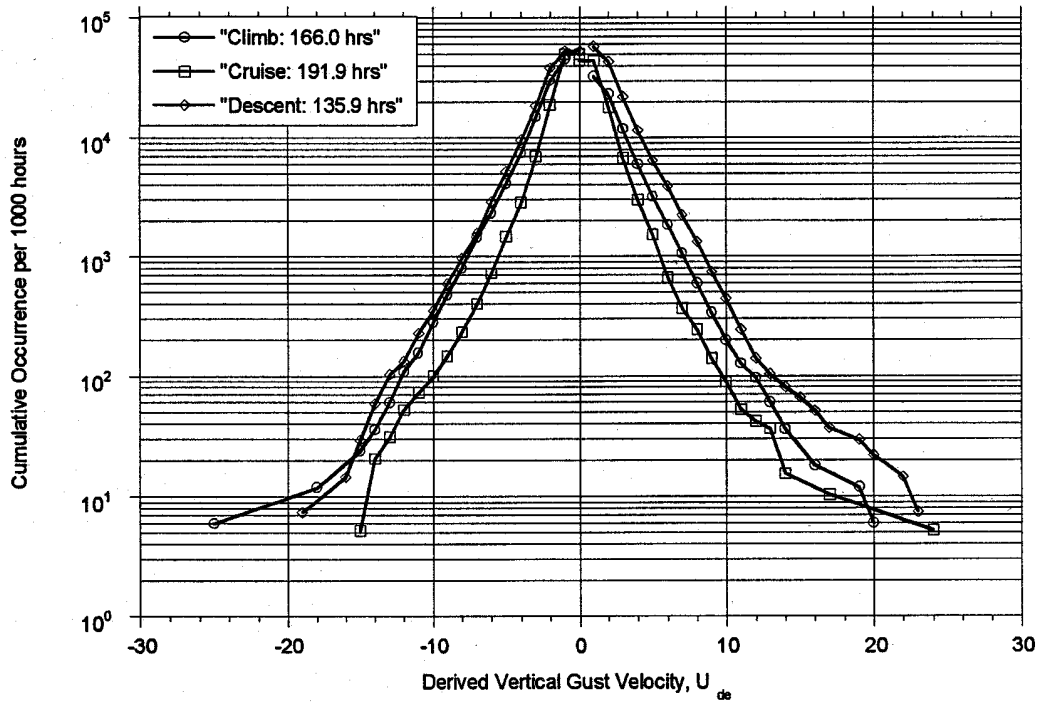


FIGURE A-45. CUMULATIVE OCCURRENCES OF DERIVED VERTICAL GUST VELOCITY PER 1000 HOURS—CLIMB, CRUISE, AND DESCENT PHASES

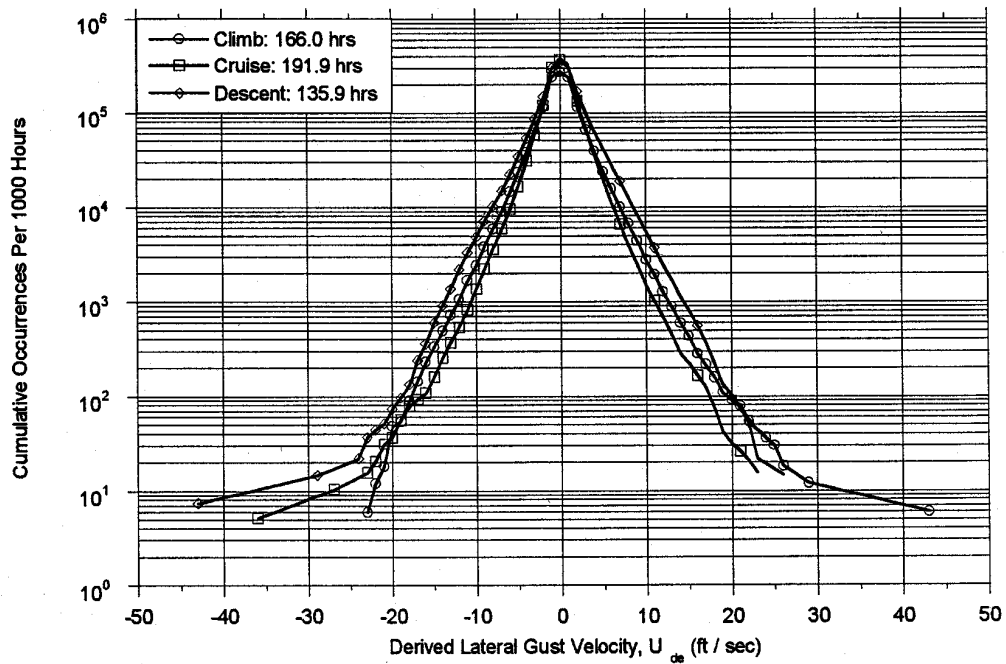


FIGURE A-46. CUMULATIVE OCCURRENCES OF DERIVED LATERAL GUST VELOCITY PER 1000 HOURS—CLIMB, CRUISE, AND DESCENT PHASES

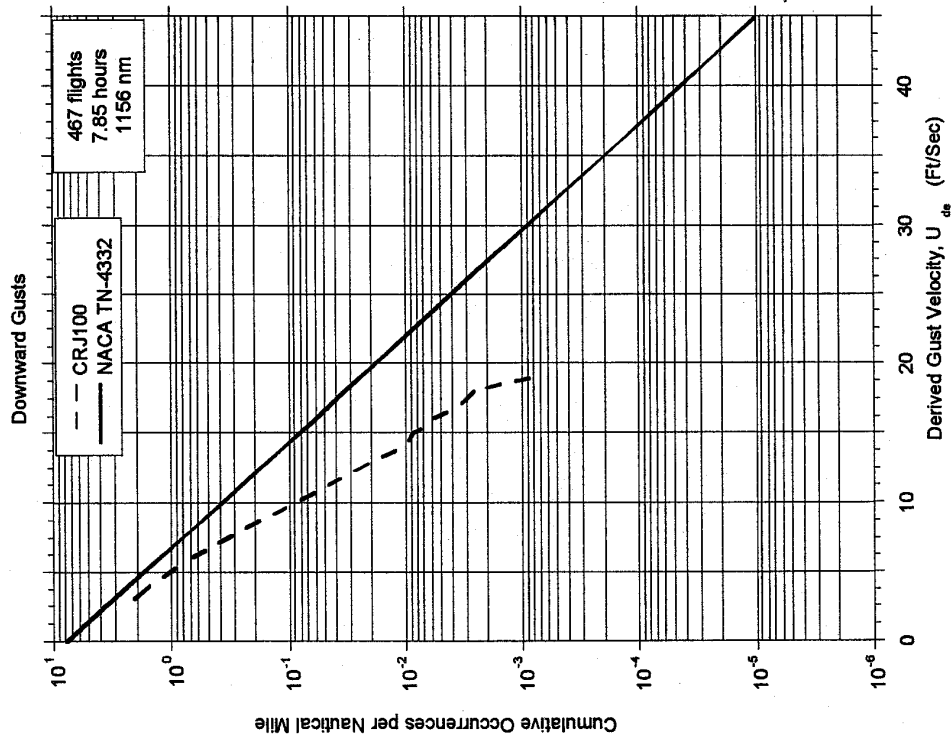
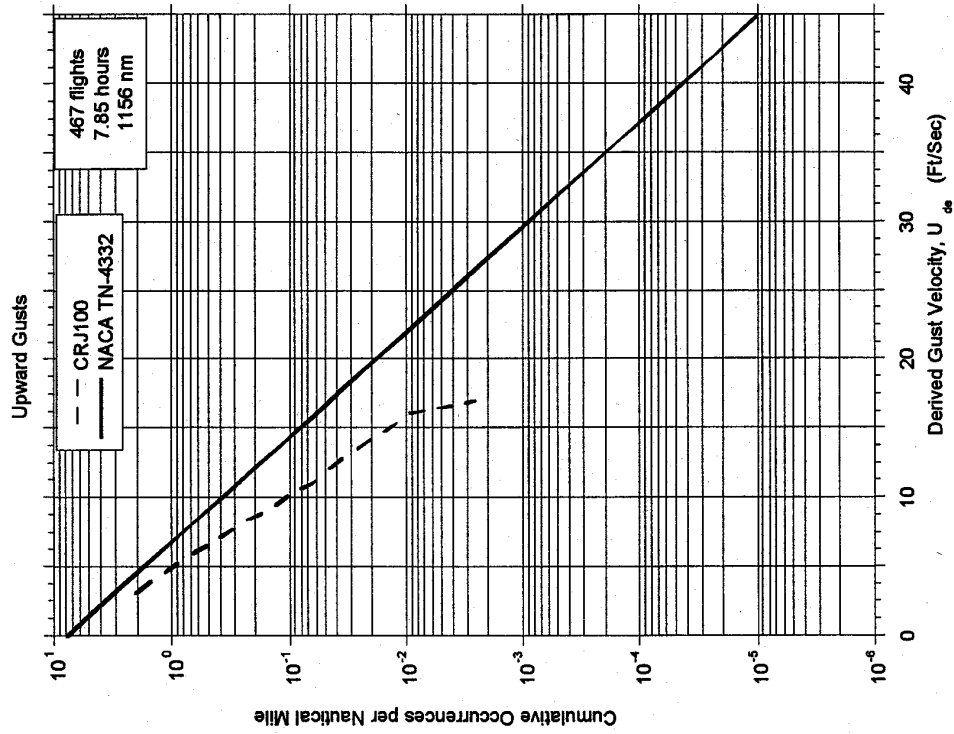


FIGURE A-47. CUMULATIVE OCCURRENCES OF DERIVED GUST VELOCITY PER NAUTICAL MILE,  
<500 FEET ABOVE AIRPORT

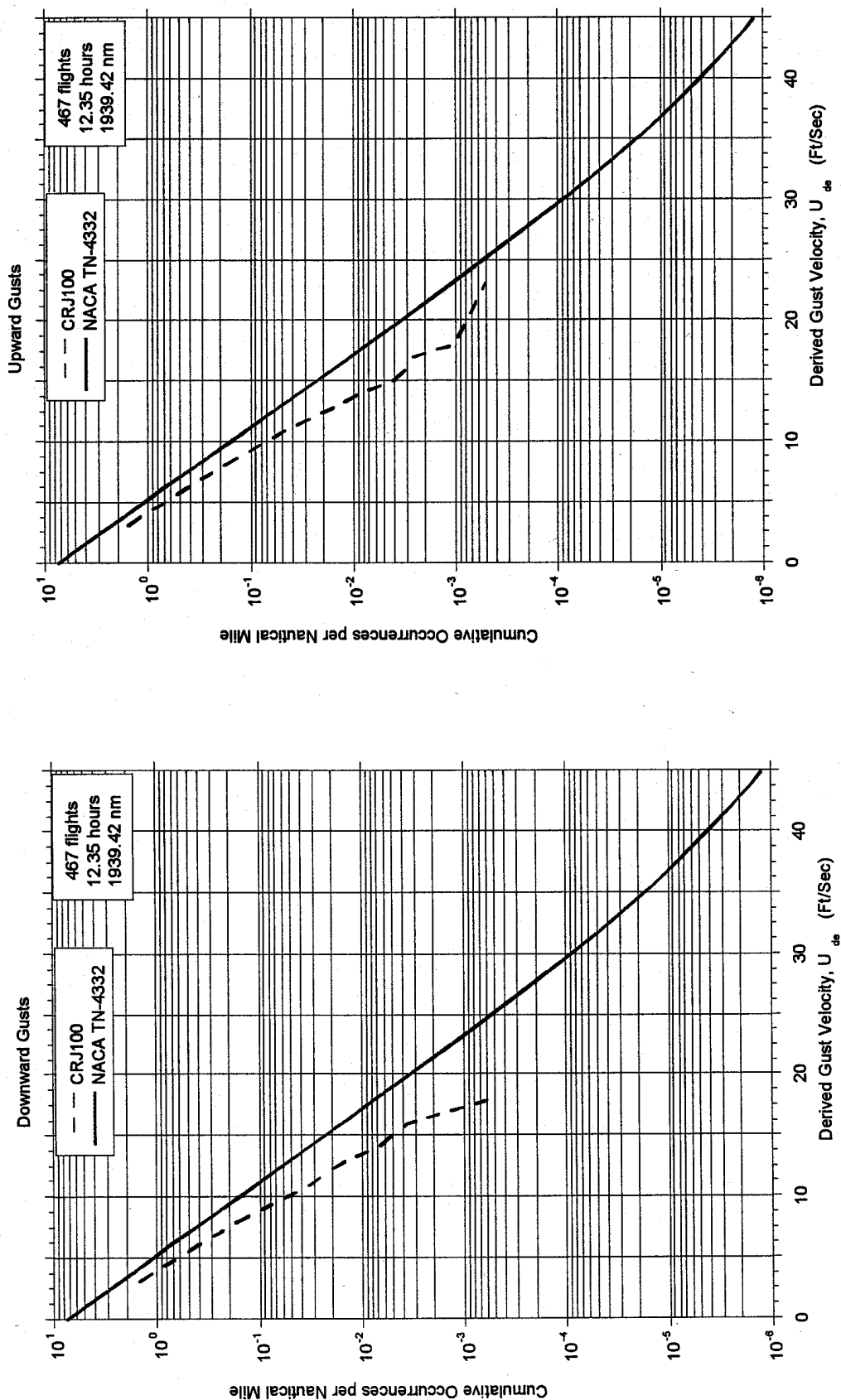


FIGURE A-48. CUMULATIVE OCCURRENCES OF DERIVED GUST VELOCITY PER NAUTICAL MILE,  
500-1500 FEET ABOVE AIRPORT

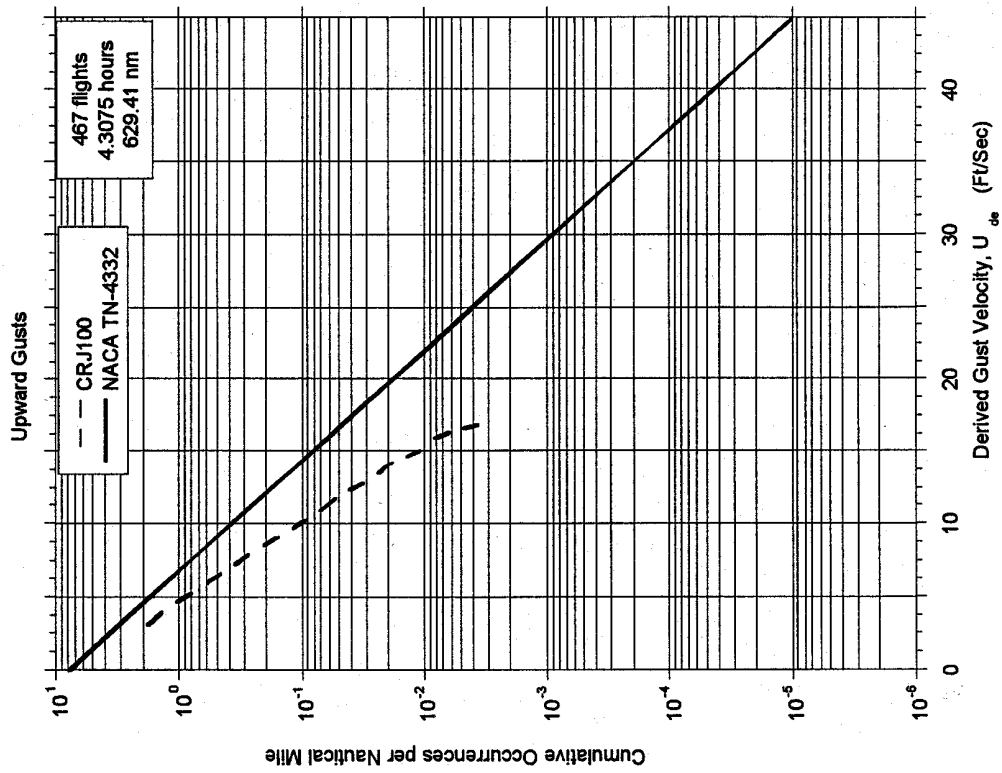
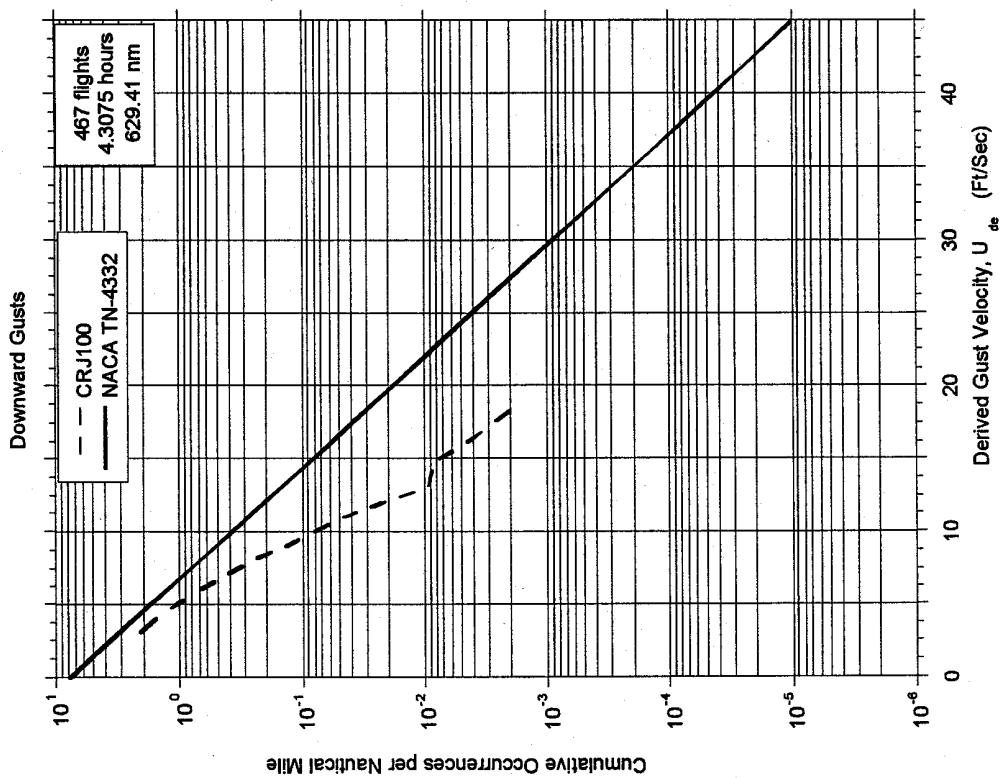


FIGURE A-49. CUMULATIVE OCCURRENCES OF DERIVED GUST VELOCITY PER NAUTICAL MILE,  
<500 FEET

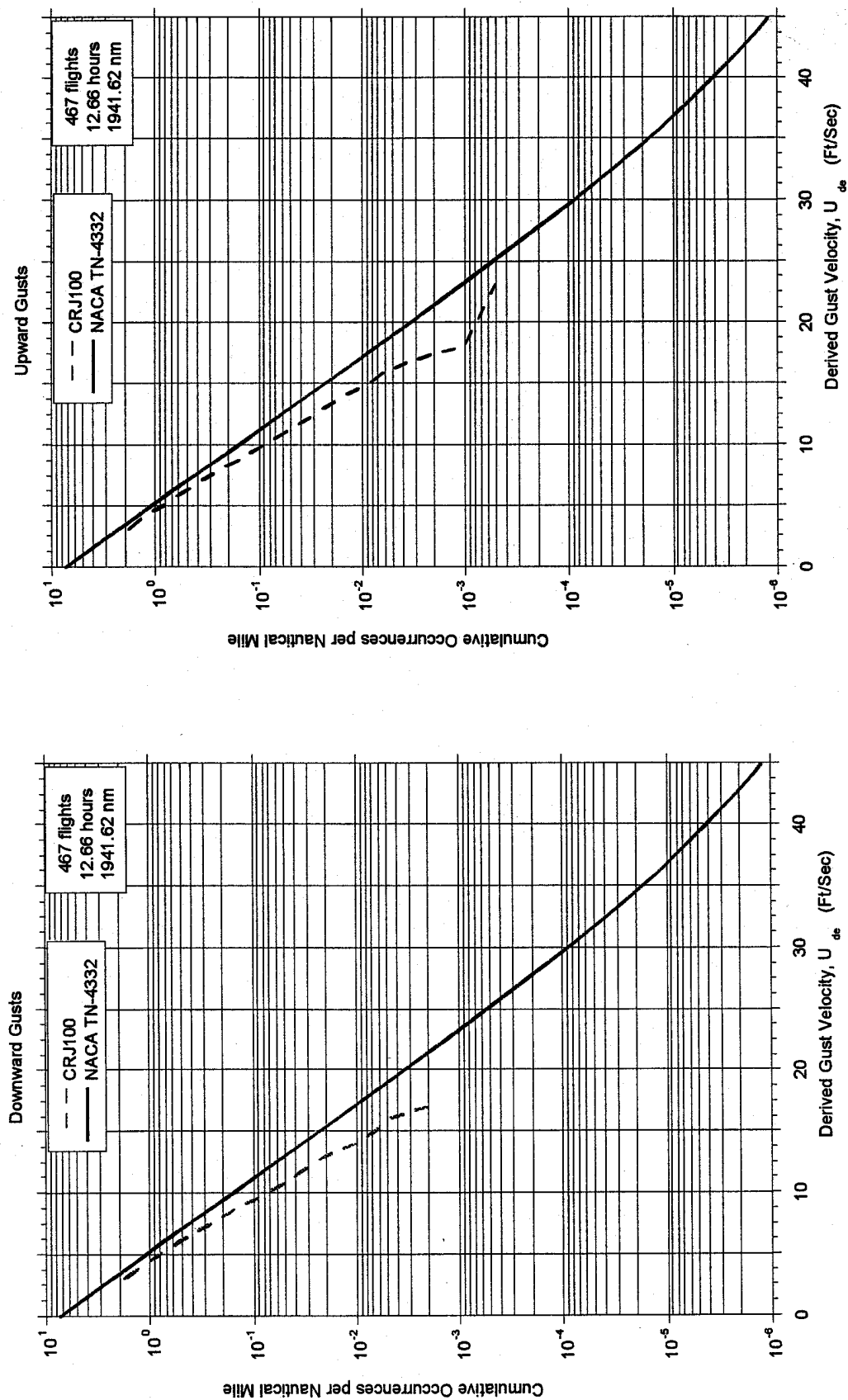


FIGURE A-50. CUMULATIVE OCCURRENCES OF DERIVED GUST VELOCITY PER NAUTICAL MILE,  
500-1500 FEET

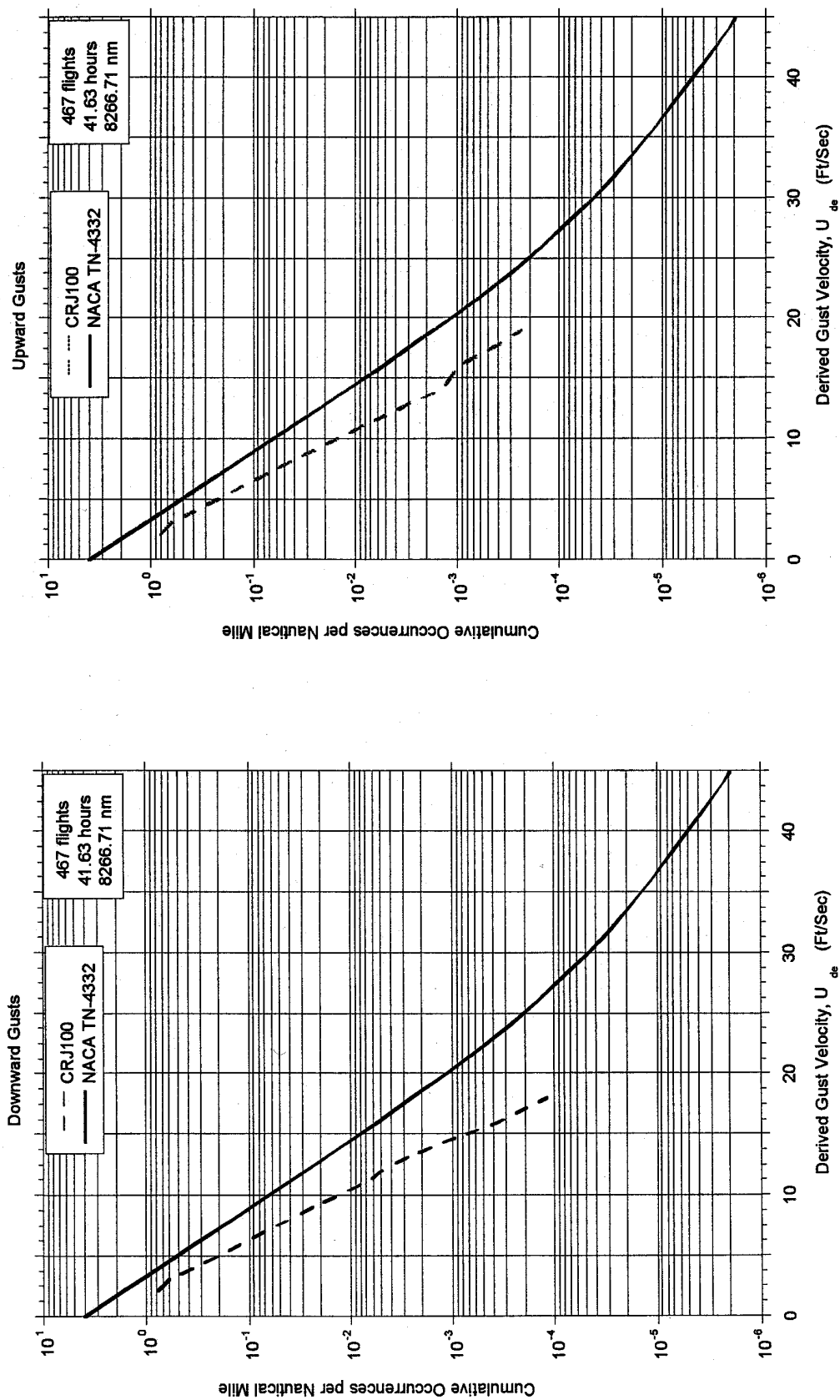


FIGURE A-51. CUMULATIVE OCCURRENCES OF DERIVED GUST VELOCITY PER NAUTICAL MILE,  
1500-4500 FEET

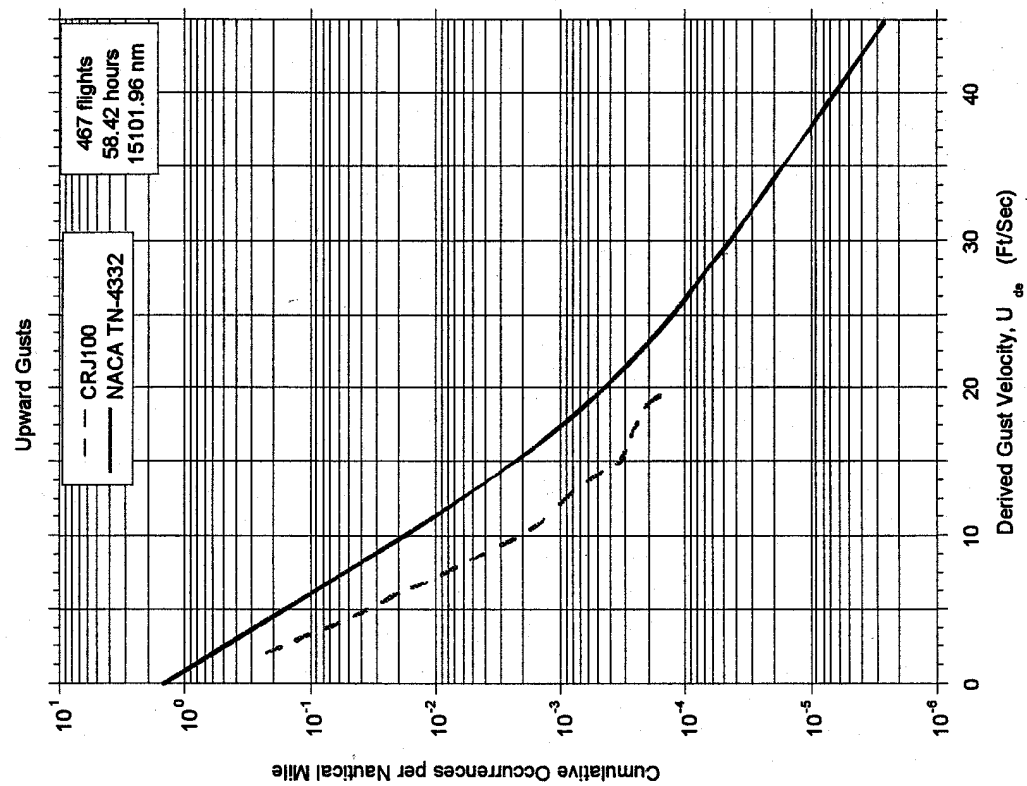
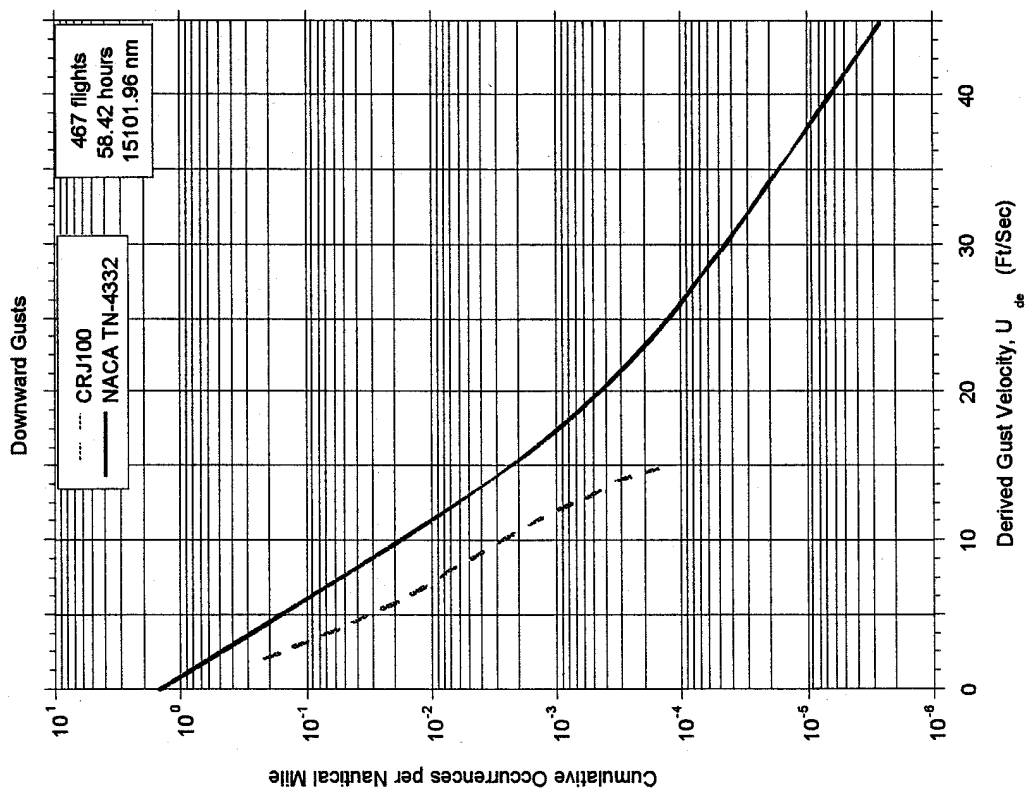


FIGURE A-52. CUMULATIVE OCCURRENCES OF DERIVED GUST VELOCITY PER NAUTICAL MILE,  
4500-9500 FEET

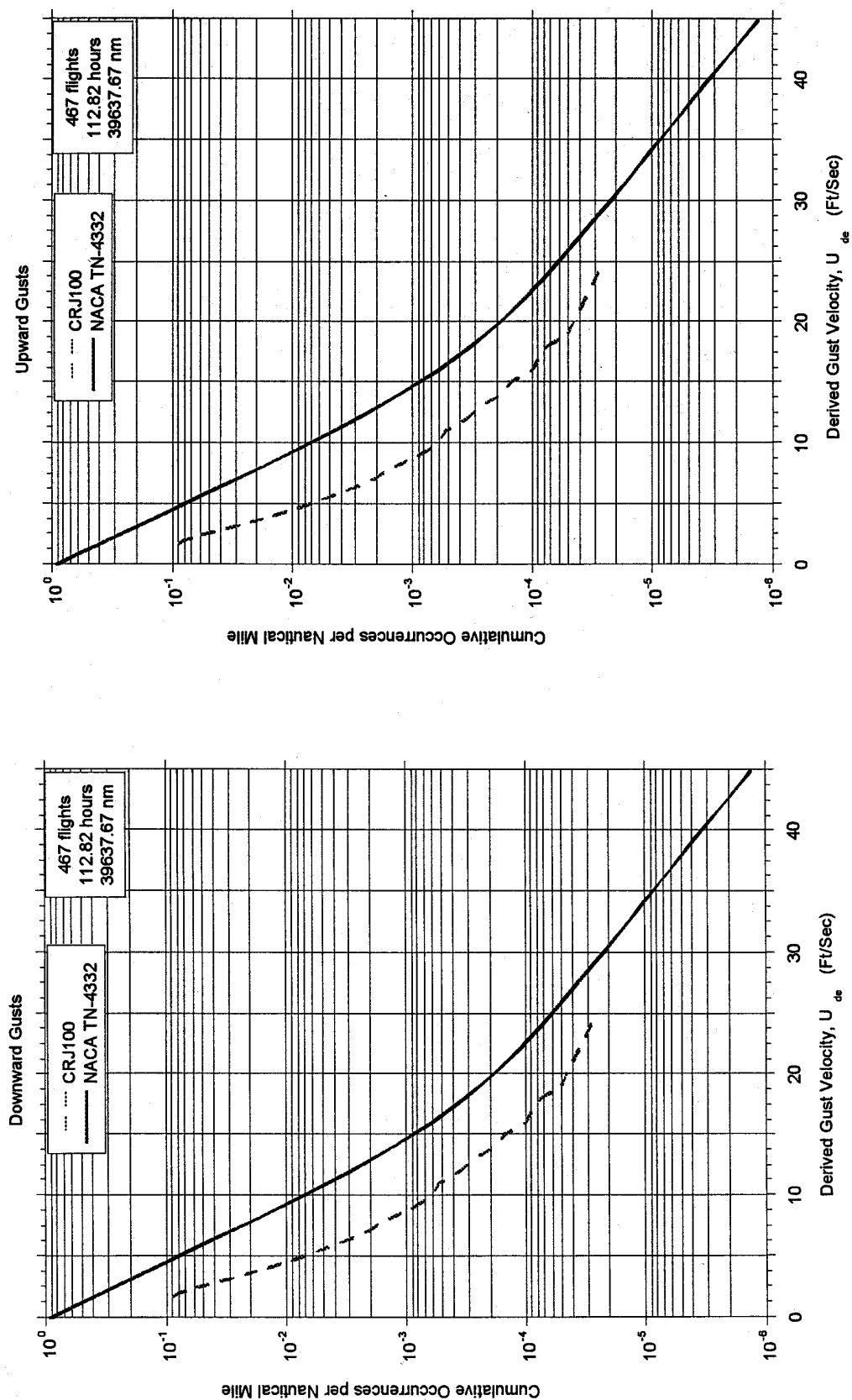


FIGURE A-53. CUMULATIVE OCCURRENCES OF DERIVED GUST VELOCITY PER NAUTICAL MILE,  
9,500-19,500 FEET

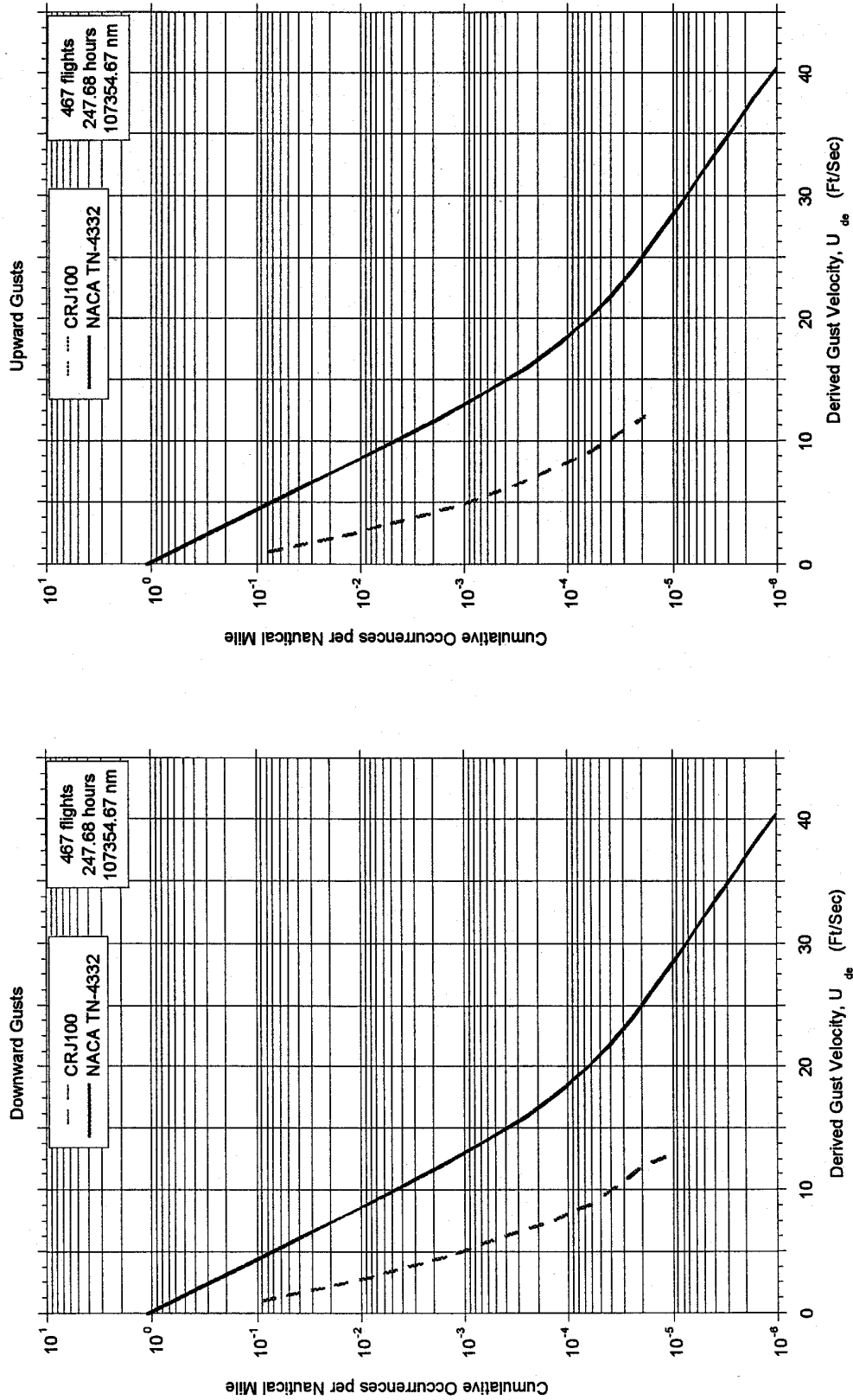


FIGURE A-54. CUMULATIVE OCCURRENCES OF DERIVED GUST VELOCITY PER NAUTICAL MILE,  
19,500-29,500 FEET

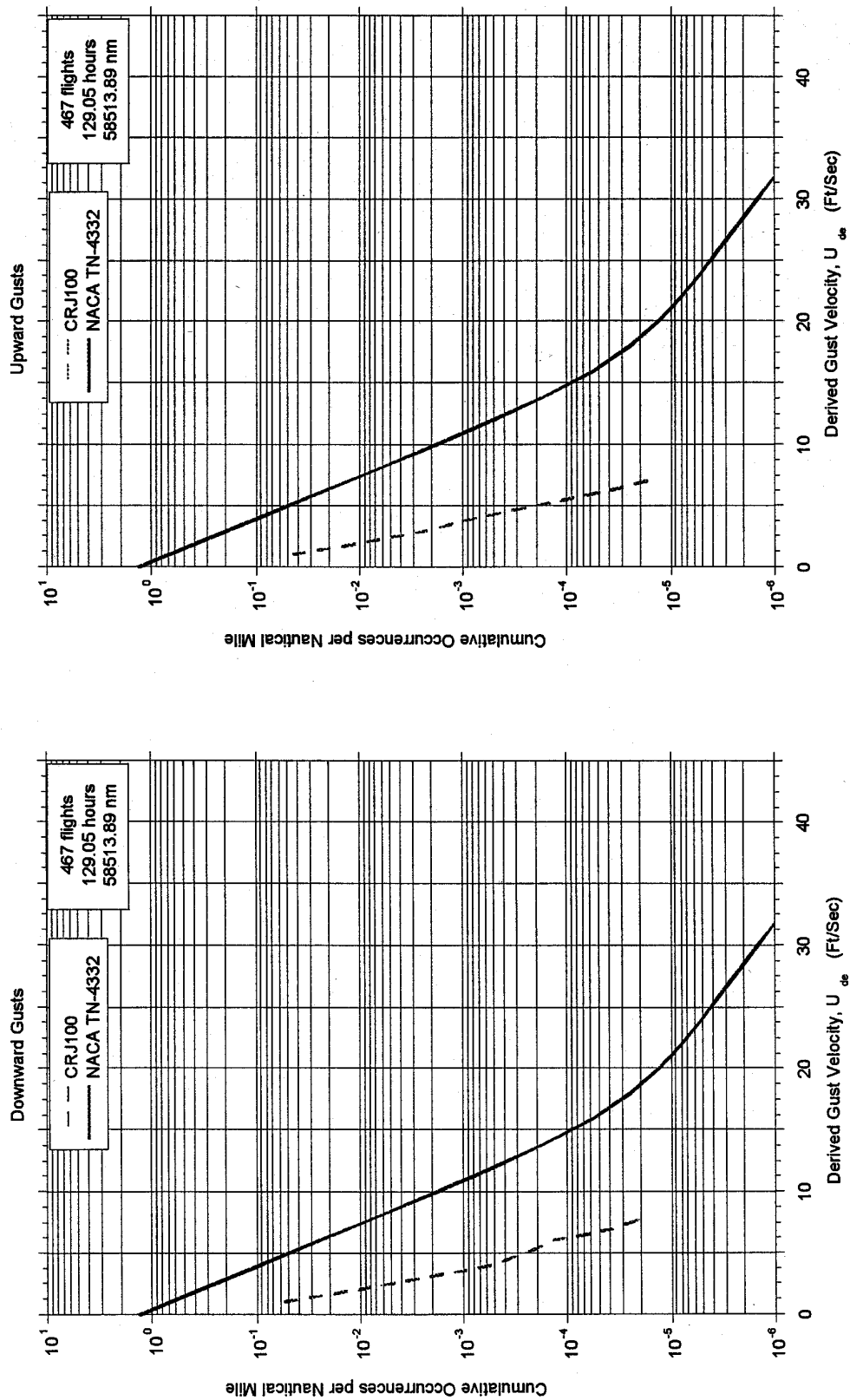


FIGURE A-55. CUMULATIVE OCCURRENCES OF DERIVED GUST VELOCITY PER NAUTICAL MILE,  
29,500-39,500 FEET

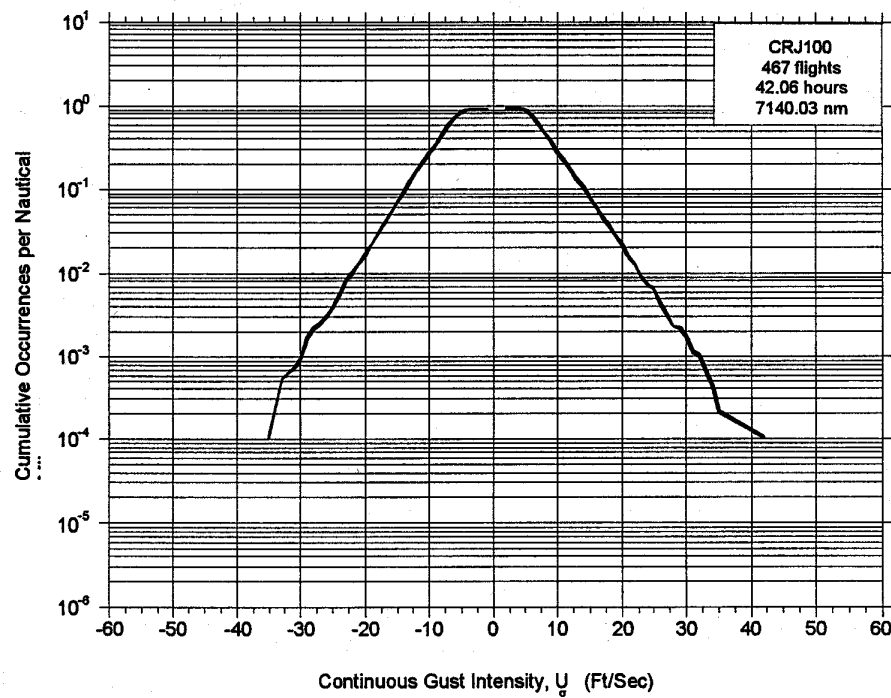


FIGURE A-56. CUMULATIVE OCCURRENCES OF DERIVED VELOCITY PER NAUTICLE MILE, FLAPS EXTENDED

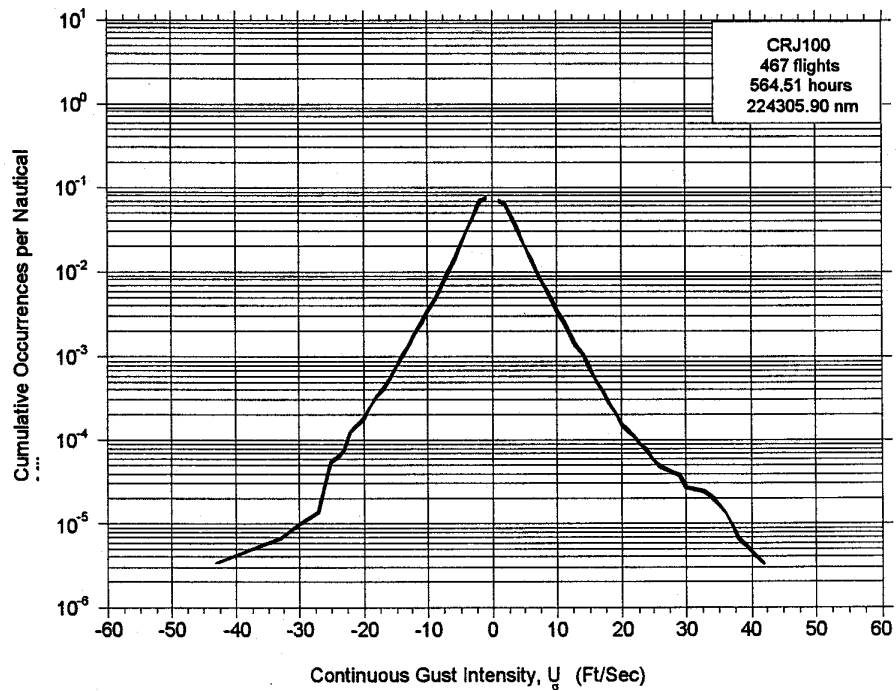


FIGURE A-57. CUMULATIVE OCCURRENCES OF DERIVED CUST VELOCITY PER NAUTICLE MILE, FLAPS RETRACTED

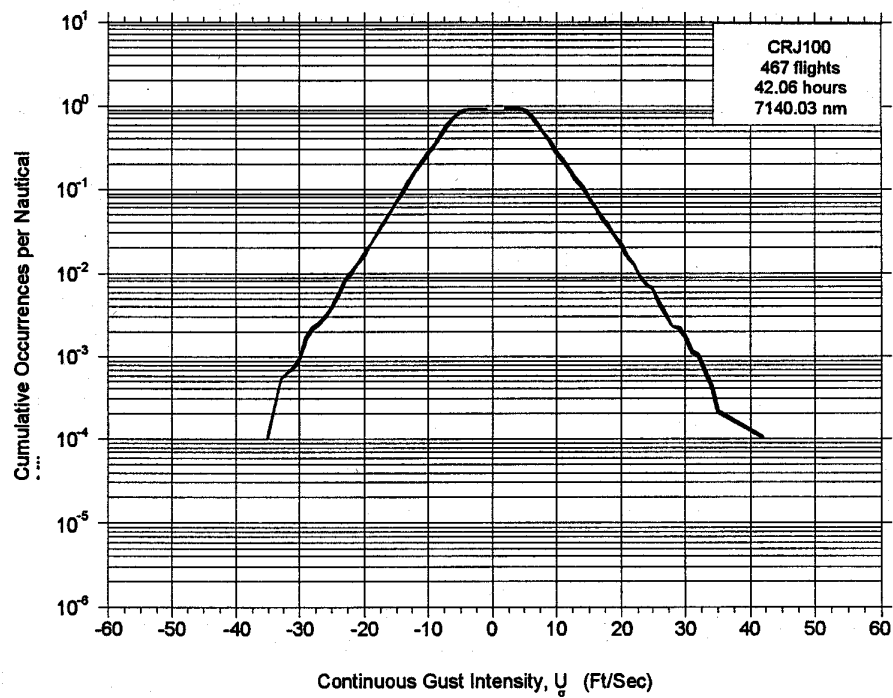


FIGURE A-58. CUMULATIVE OCCURRENCES OF CONTINUOUS GUST INTENSITY PER NAUTICLE MILE, FLAPS EXTENDED

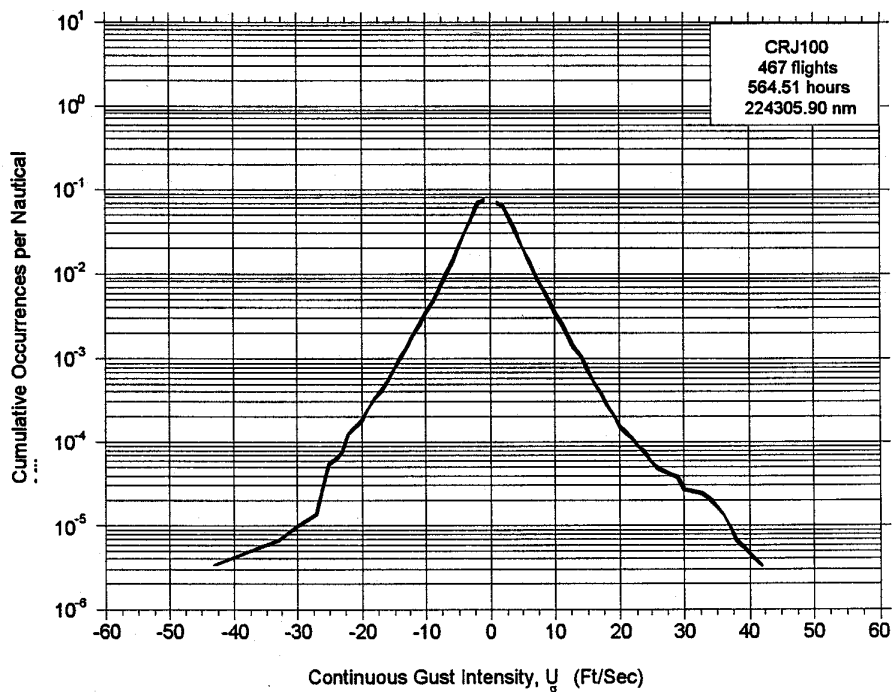


FIGURE A-59. CUMULATIVE OCCURRENCES OF CONTINUOUS GUST INTENSITY PER NAUTICLE MILE, FLAPS RETRACTED

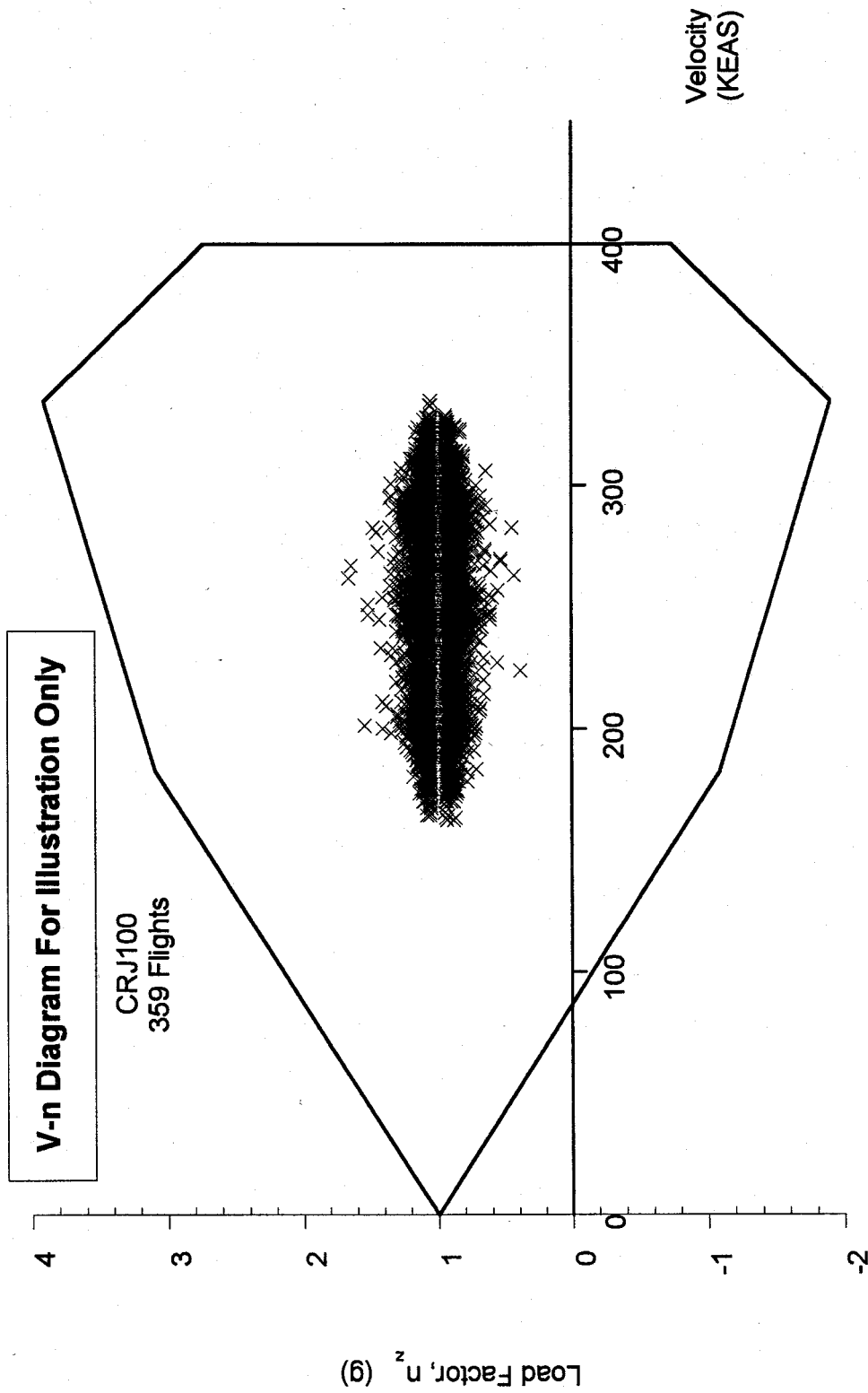


FIGURE A-60. GUST LOAD FACTOR AND COINCIDENT SPEED VS V-n DIAGRAM FOR FLAPS RETRACTED

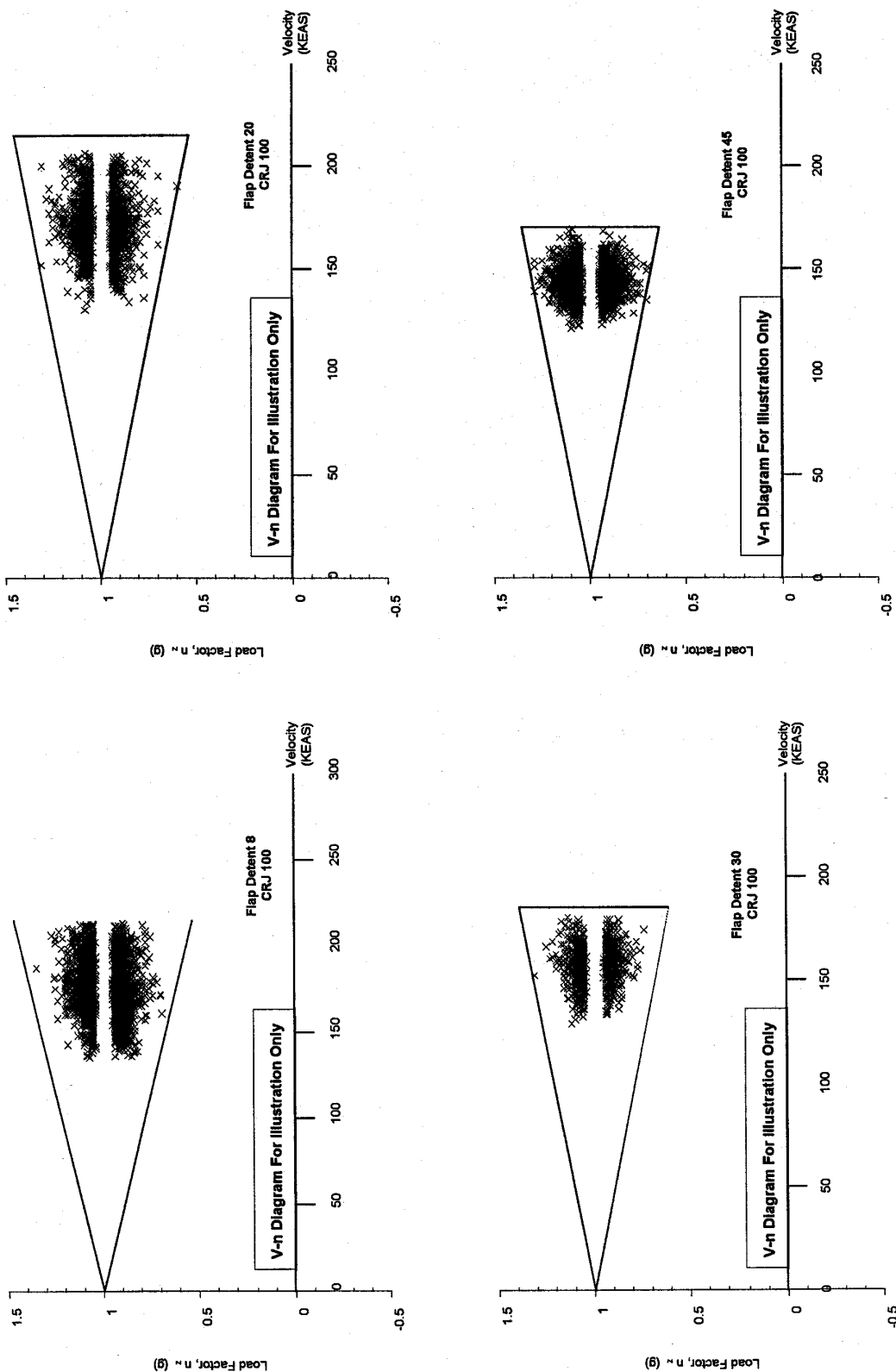


FIGURE A-61. GUST LOAD FACTOR AND COINCIDENT SPEED VS V-n DIAGRAMS FOR FLAPS EXTENDED, DETENTS 8, 20, 30, AND 45

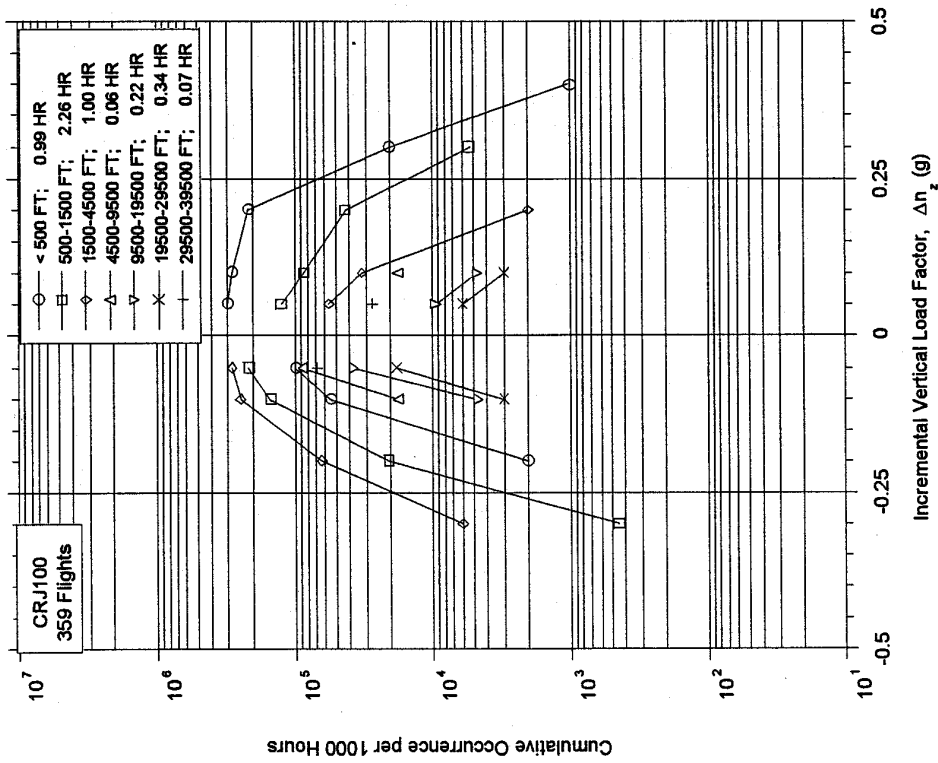


FIGURE A-62. CUMULATIVE OCCURRENCES OF INCREMENTAL VERTICAL MANEUVER LOAD FACTOR PER 1000 HOURS, DURING DEPARTURE BY ALTITUDE

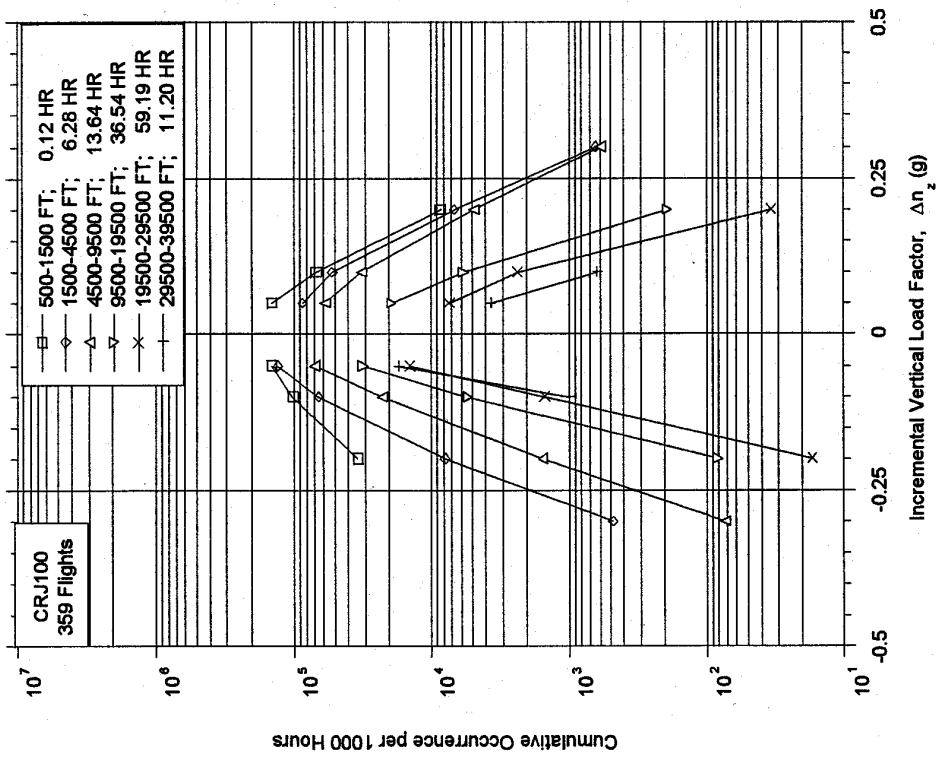


FIGURE A-63. CUMULATIVE OCCURRENCES OF INCREMENTAL VERTICAL MANEUVER LOAD FACTOR PER 1000 HOURS DURING CLIMB BY ALTITUDE

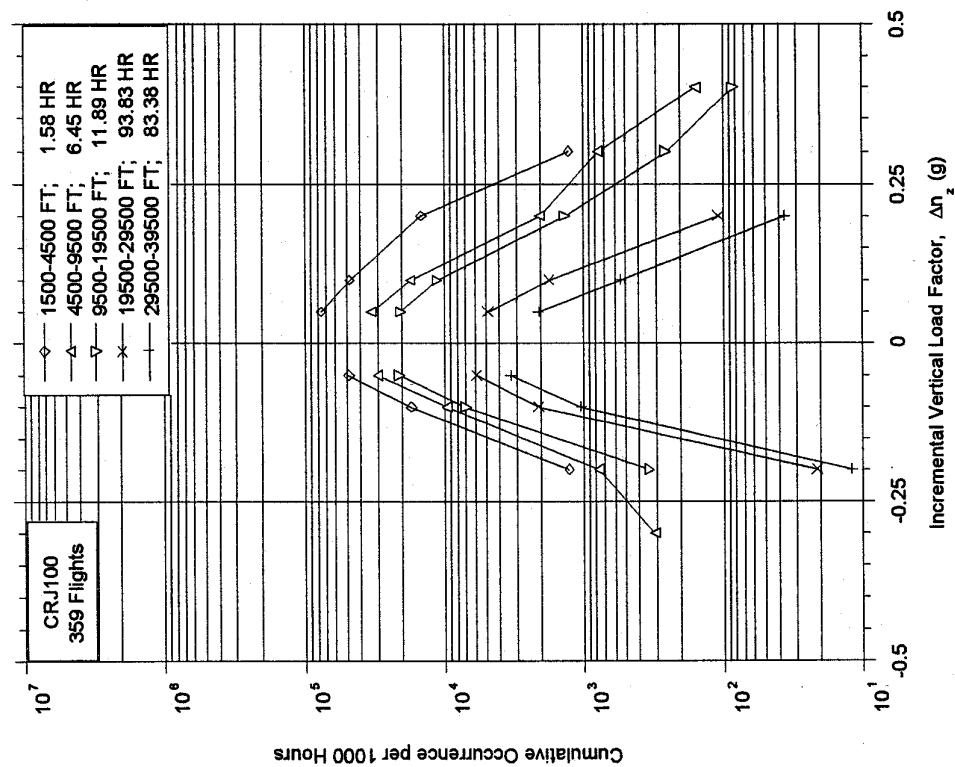


FIGURE A-64. CUMULATIVE OCCURRENCES OF INCREMENTAL VERTICAL MANEUVER LOAD FACTOR PER 1000 HOURS, DURING CRUISE BY ALTITUDE

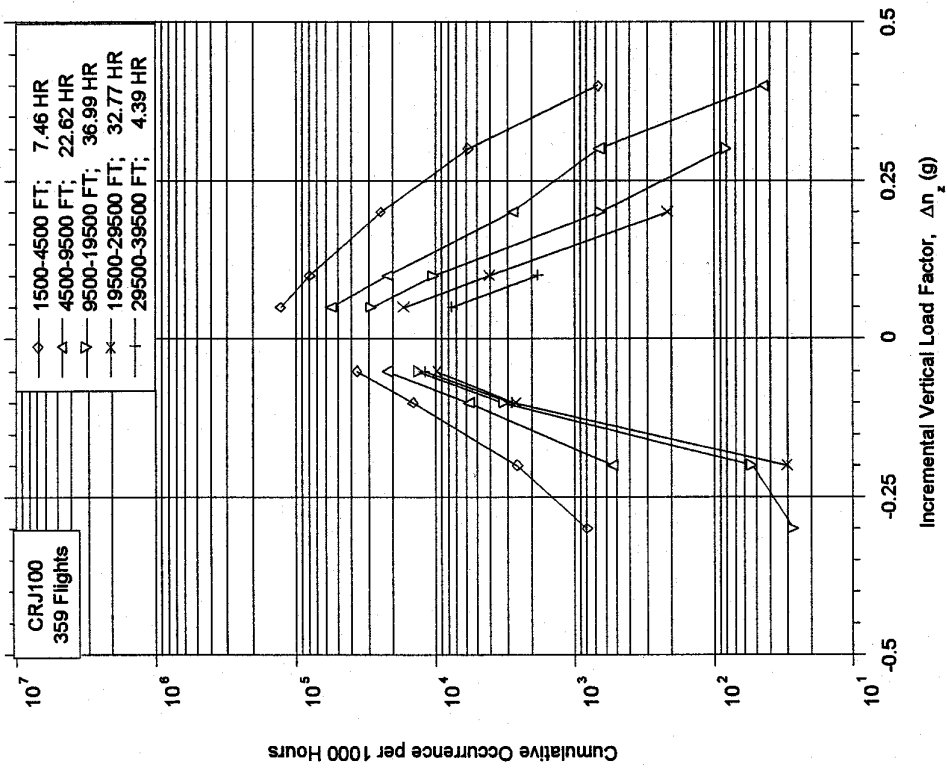


FIGURE A-65. CUMULATIVE OCCURRENCES OF INCREMENTAL VERTICAL MANEUVER LOAD FACTOR PER 1000 HOURS DURING DESCENT BY ALTITUDE

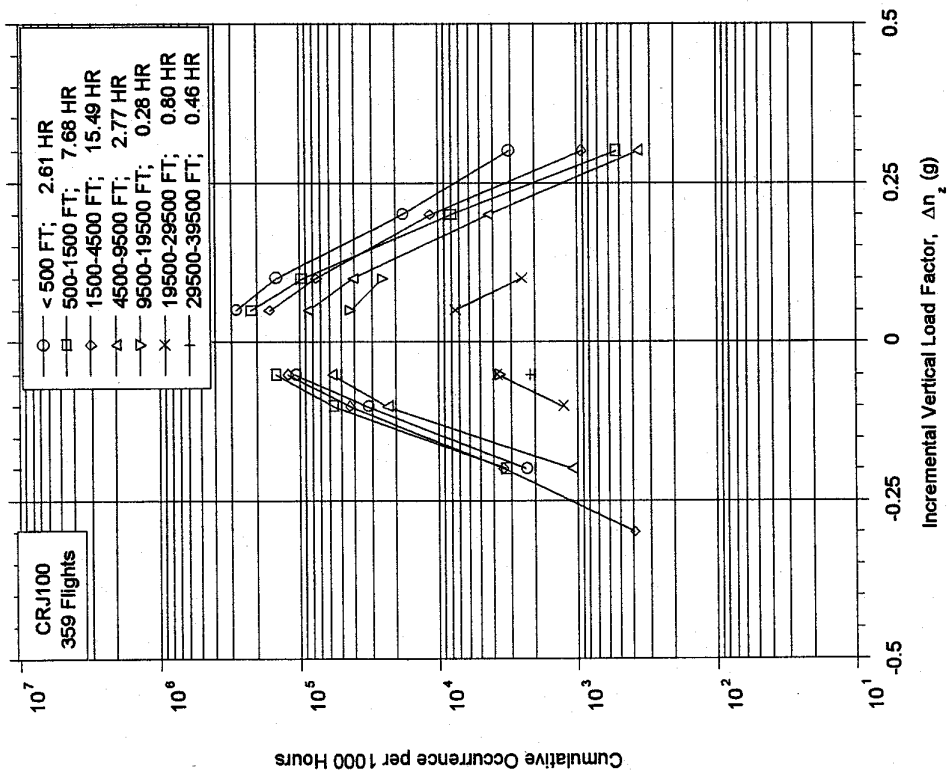


FIGURE A-66. CUMULATIVE OCCURRENCES OF INCREMENTAL VERTICAL MANEUVER LOAD FACTOR PER 1000 HOURS DURING APPROACH BY ALTITUDE

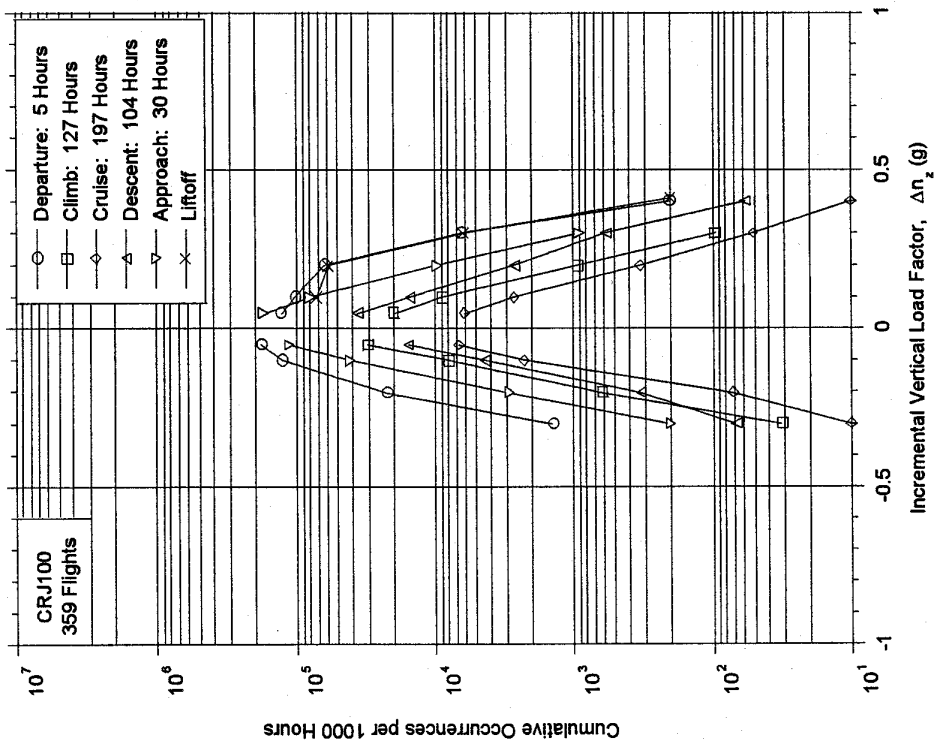


FIGURE A-67. CUMULATIVE OCCURRENCES OF INCREMENTAL VERTICAL MANEUVER LOAD FACTOR PER 1000 HOURS BY FLIGHT PHASE

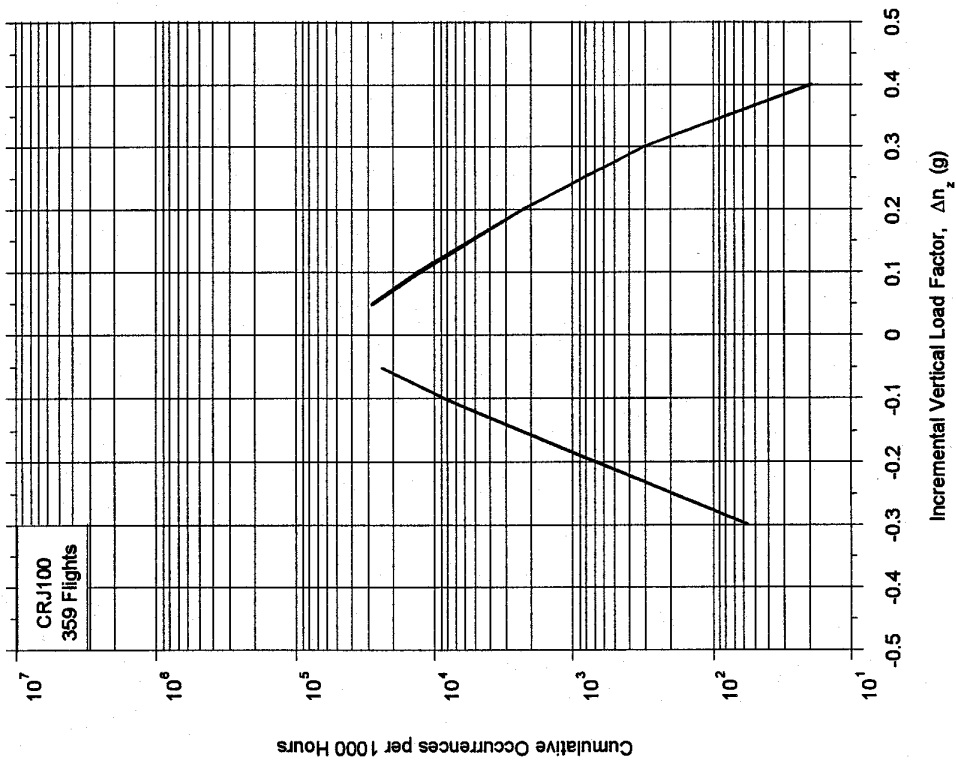


FIGURE A-68. CUMULATIVE OCCURRENCES OF INCREMENTAL VERTICAL MANEUVER LOAD FACTOR PER 1000 HOURS, COMBINED FLIGHT PHASES

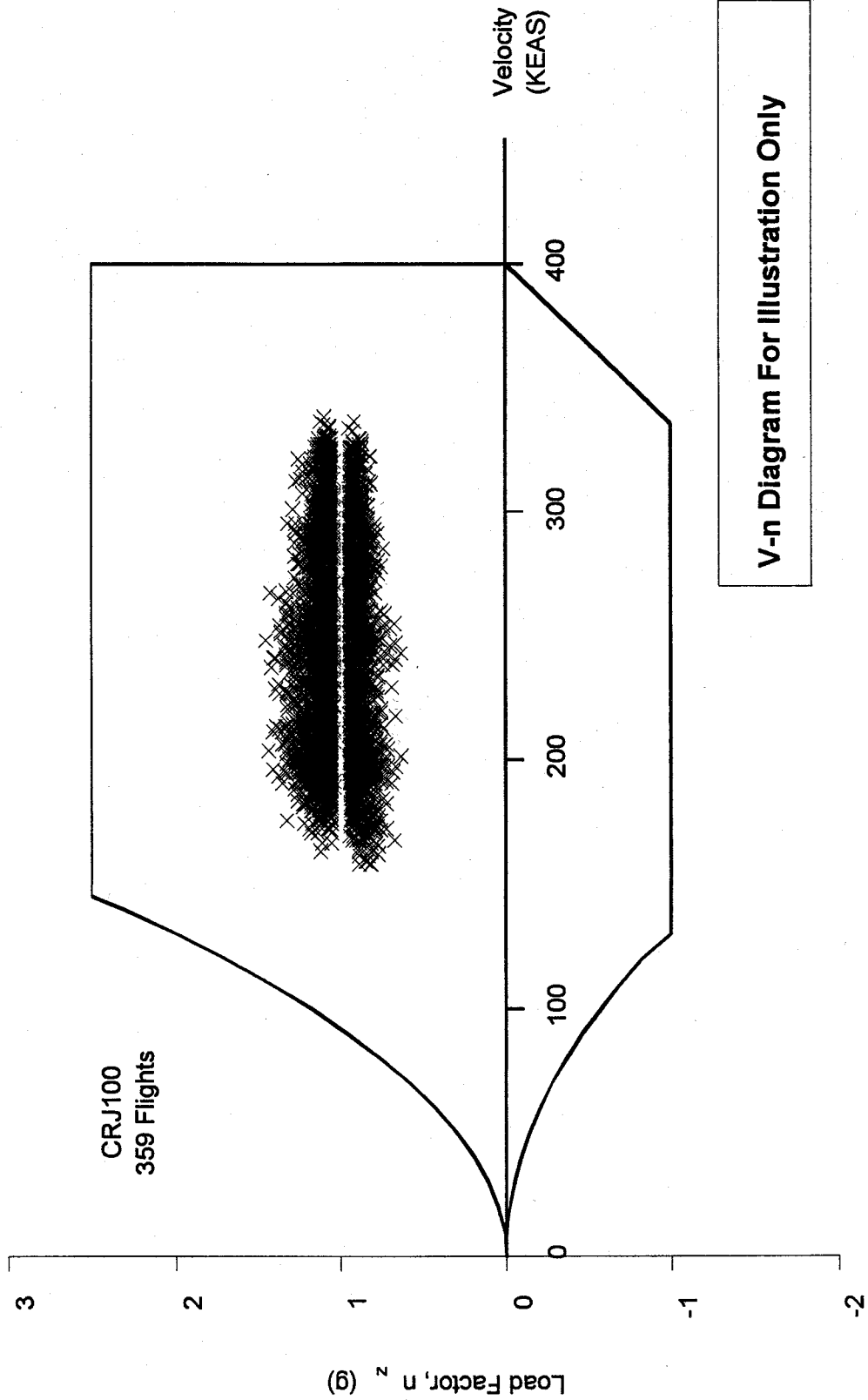


FIGURE A-69. MANEUVER LOAD FACTOR AND COINCIDENT SPEED VS V-n DIAGRAMS FOR FLAPS  
RETRACTED

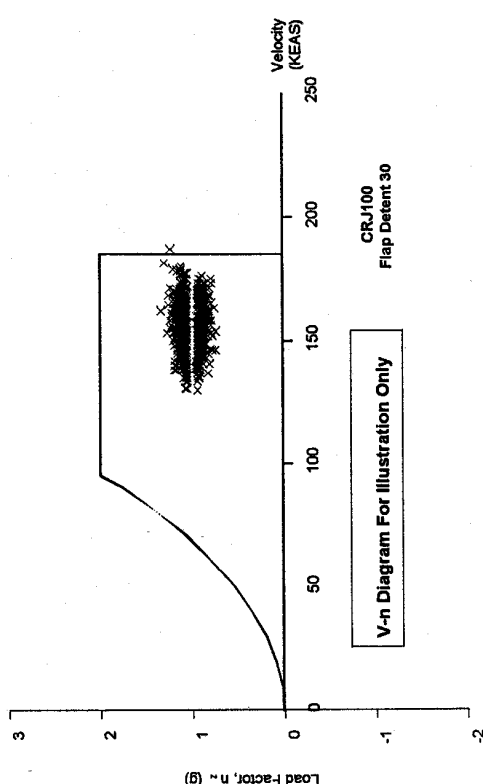
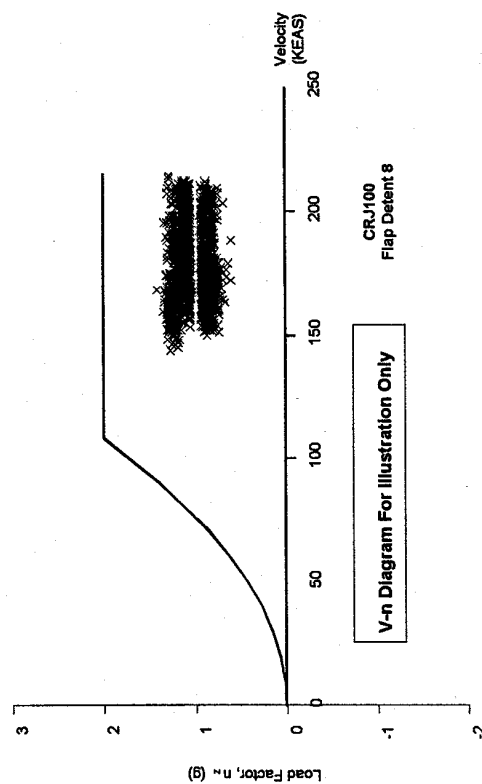
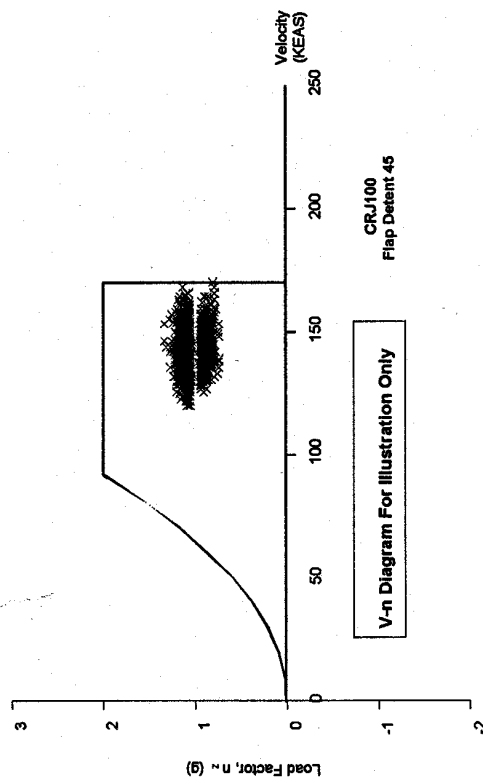
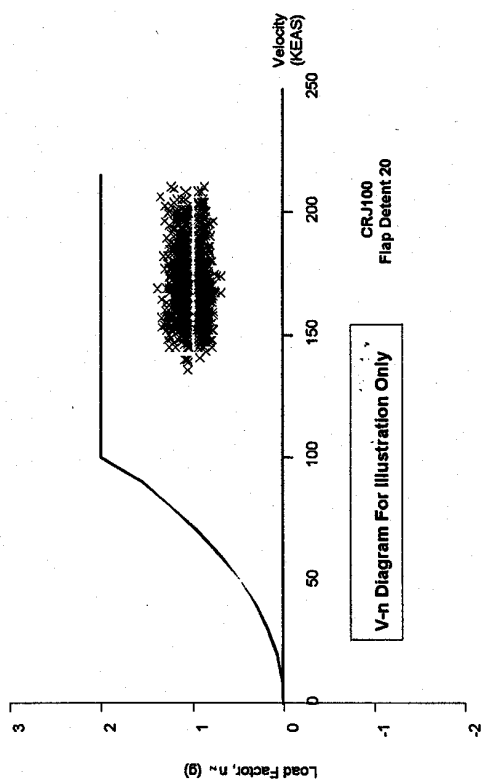


FIGURE A-70. MANEUVER LOAD FACTOR AND COINCIDENT SPEED VS V-n DIAGRAMS FOR FLAPS EXTENDED, DETENTS 8, 20, 30, AND 45

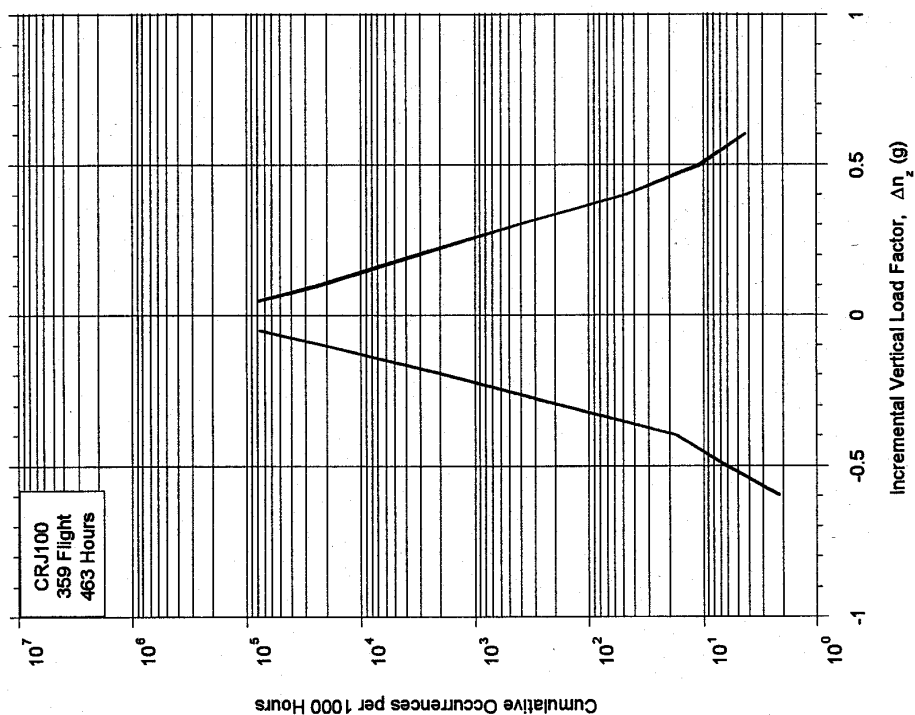


FIGURE A-71. CUMULATIVE OCCURRENCES OF INCREMENTAL VERTICAL LOAD FACTOR PER 1000 HOURS BY FLIGHT PHASE

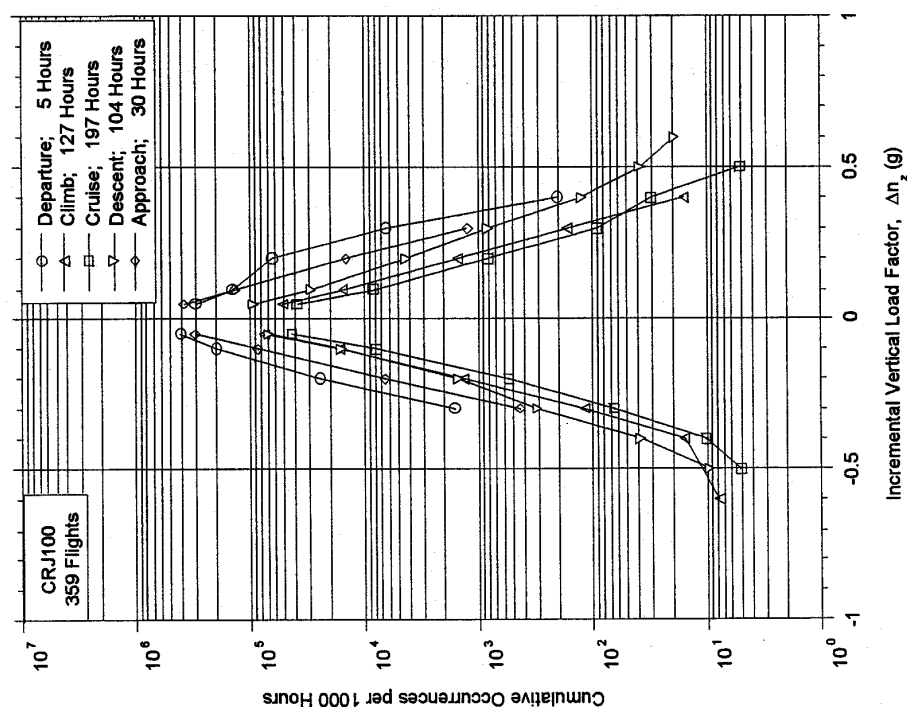


FIGURE A-72. CUMULATIVE OCCURRENCES OF INCREMENTAL VERTICAL LOAD FACTOR PER 1000 HOURS, COMBINED FLIGHT PHASES

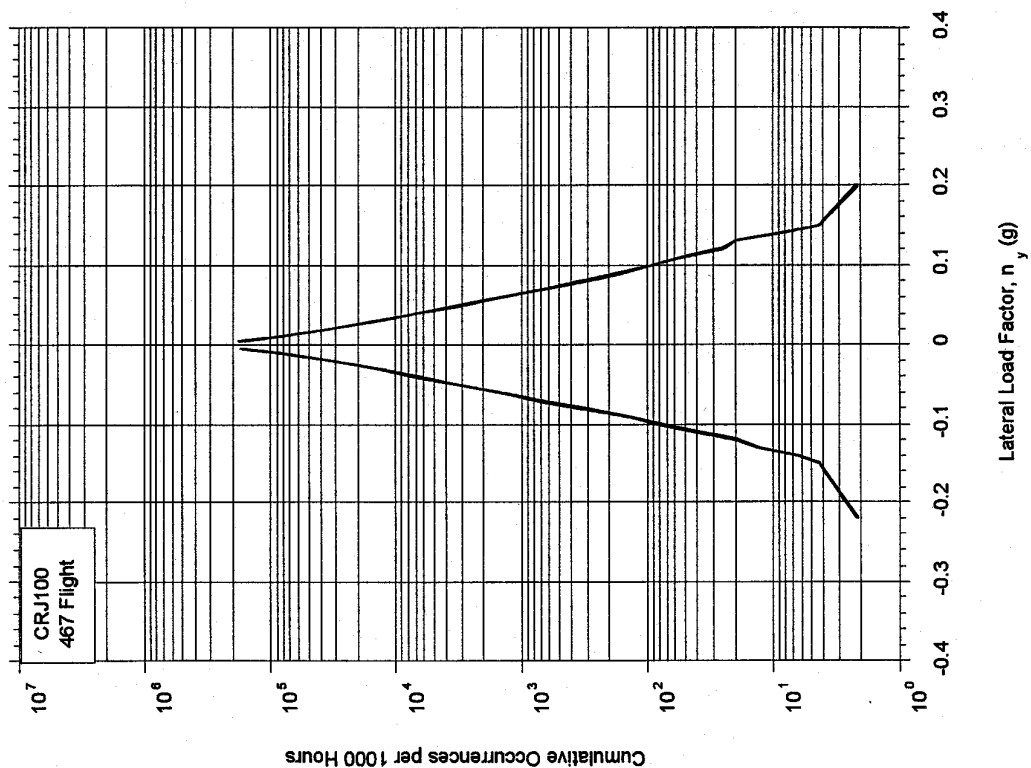


FIGURE A-73. CUMULATIVE OCCURRENCES OF LATERAL LOAD FACTOR PER 1000 HOURS BY FLIGHT PHASE

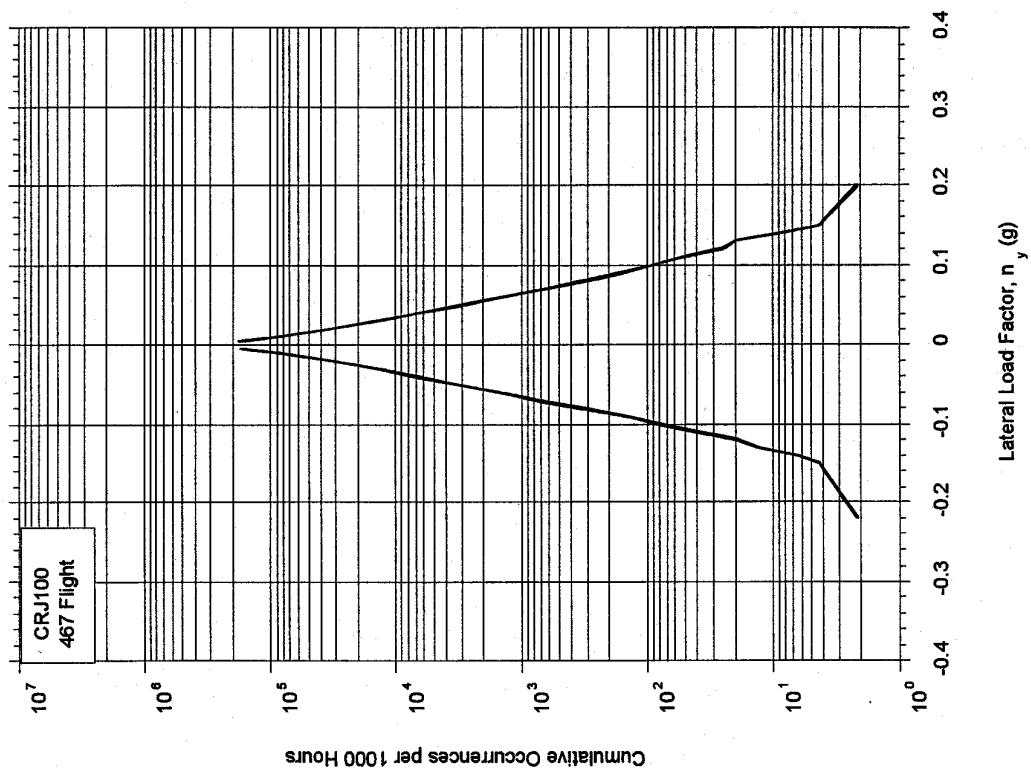


FIGURE A-74. CUMULATIVE OCCURRENCES OF LATERAL LOAD FACTOR PER 1000 HOURS, COMBINED FLIGHT PHASES

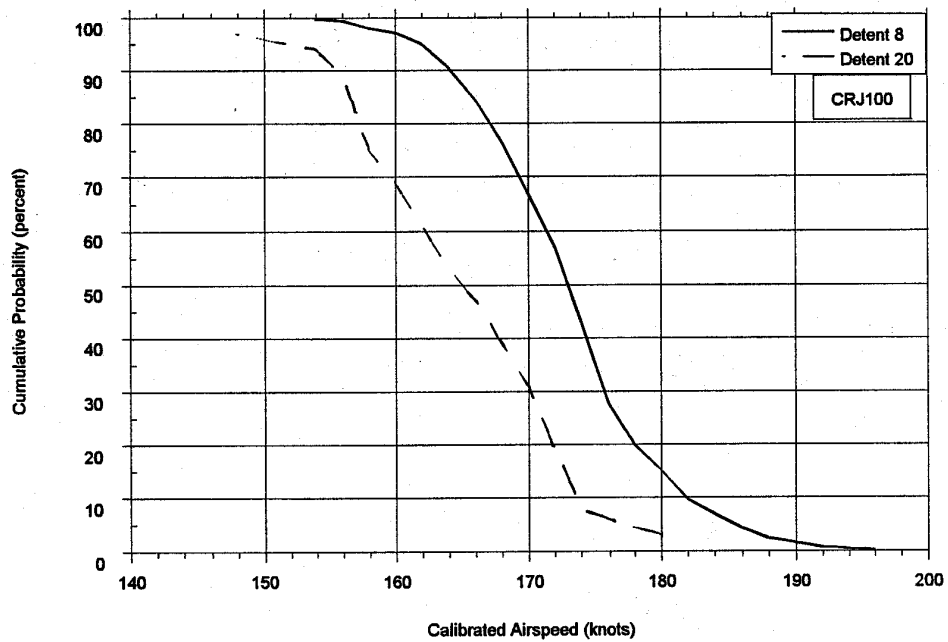


FIGURE A-75. CUMULATIVE PROBABILITY OF MAXIMUM AIRSPEED IN FLAP DETENT DURING DEPARTURE

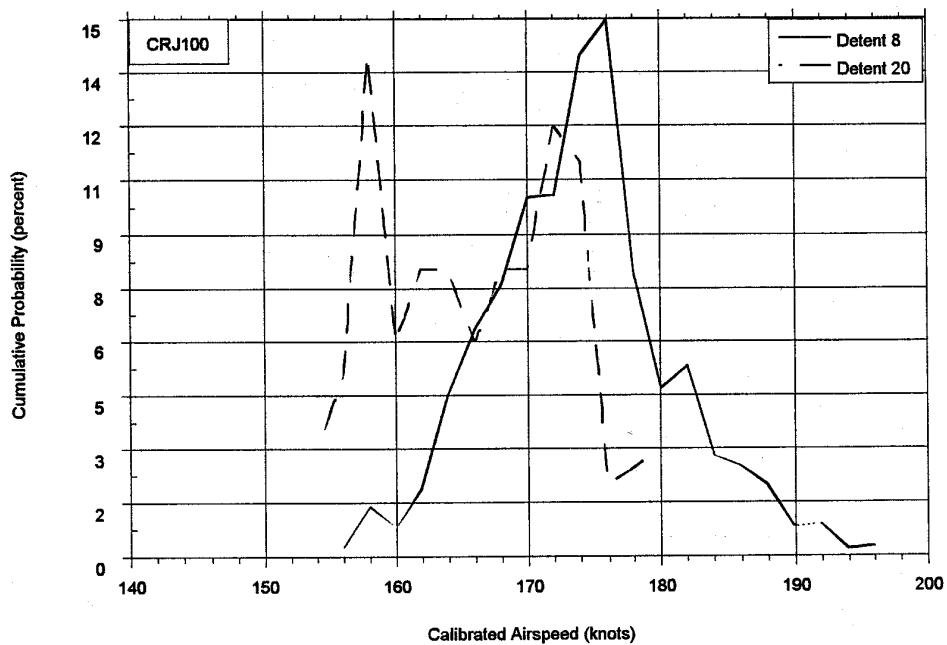


FIGURE A-76. RELATIVE PROBABILITY OF MAXIMUM AIRSPEED IN FLAP DETENT DURING DEPARTURE

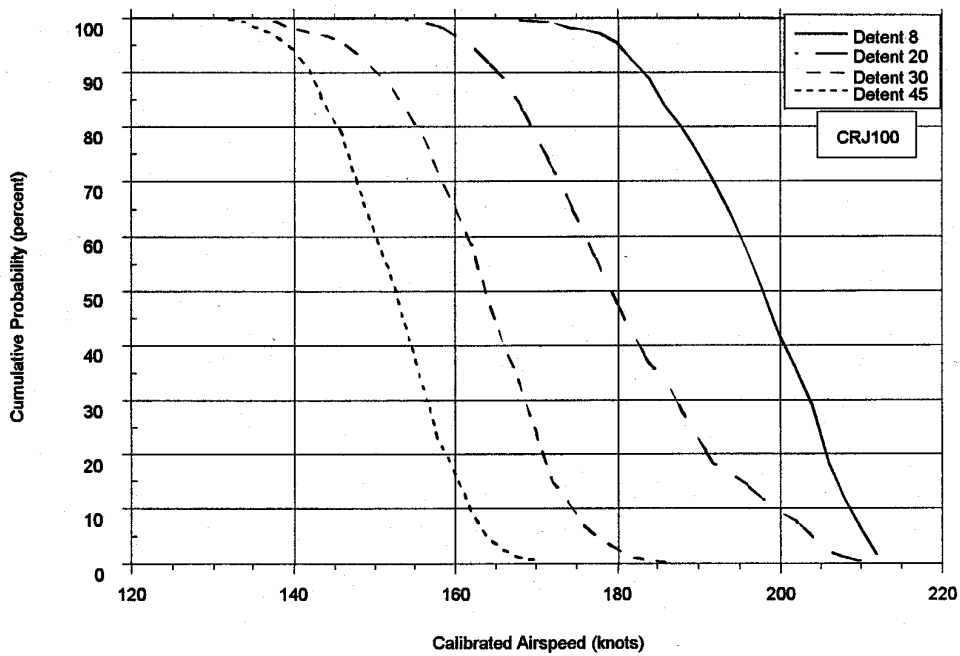


FIGURE A-77. CUMULATIVE PROBABILITY OF MAXIMUM AIRSPEED IN FLAP DETENT DURING APPROACH

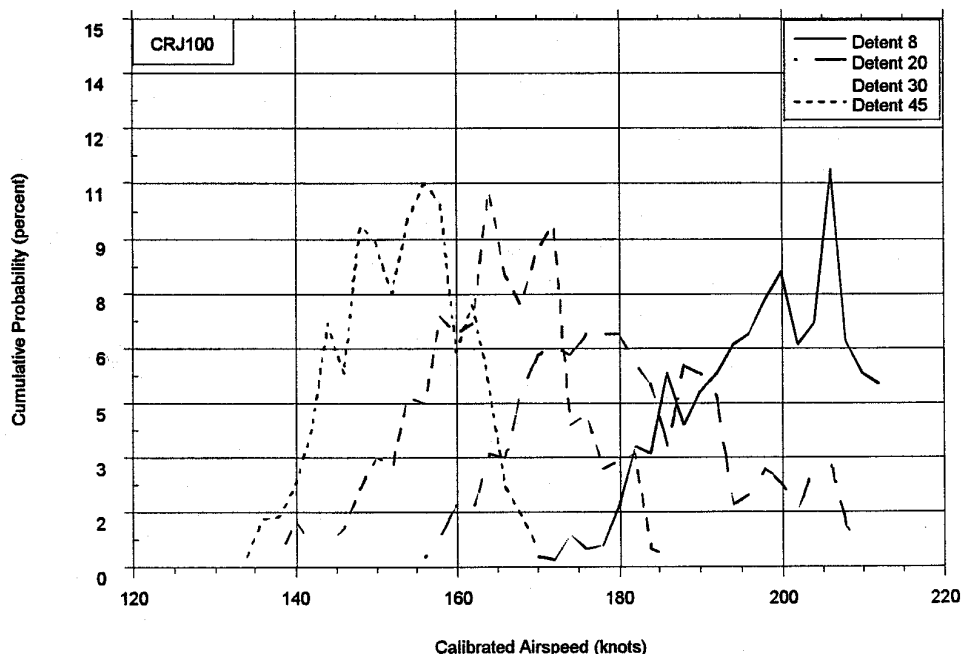


FIGURE A-78. RELATIVE PROBABILITY OF MAXIMUM AIRSPEED IN FLAP DETENT DURING APPROACH

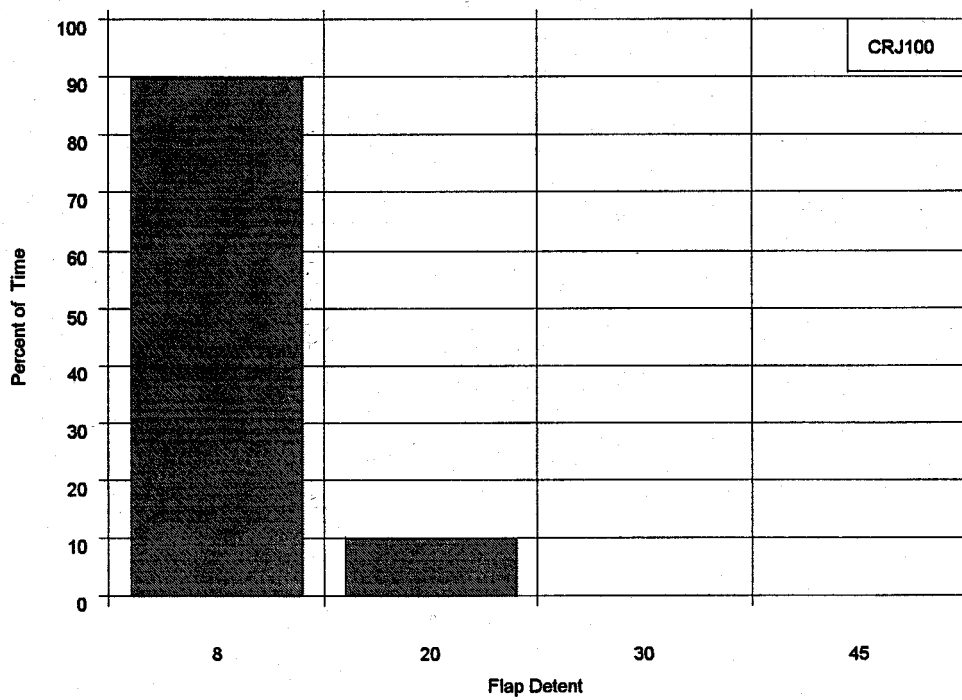


FIGURE A-79. PERCENT OF TIME IN FLAP DETENT DURING DEPARTURE

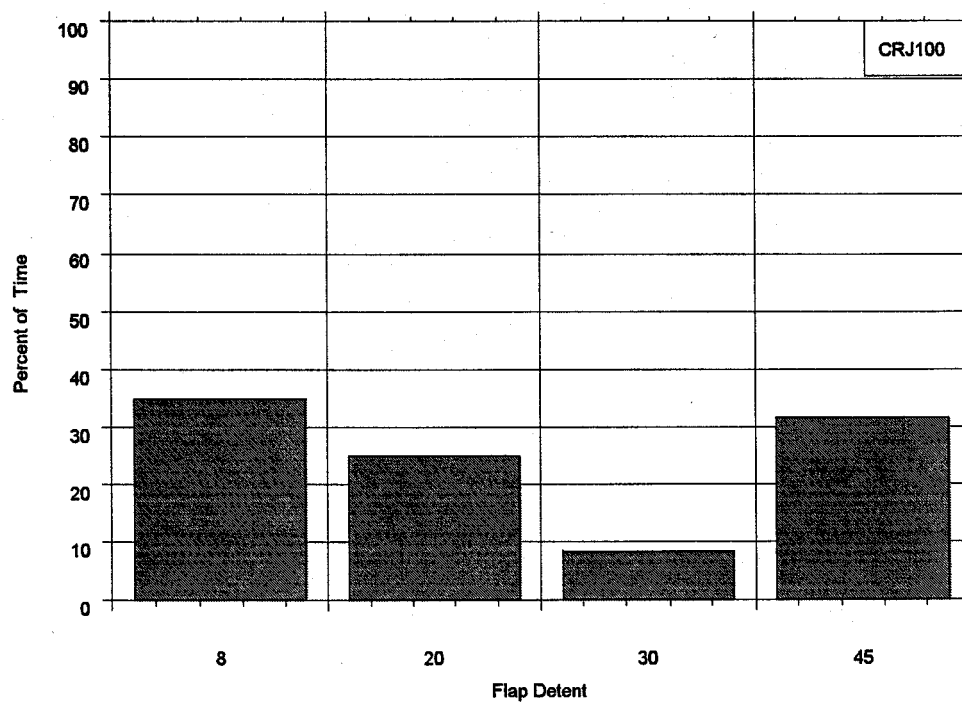


FIGURE A-80. PERCENT OF TIME IN FLAP DETENT DURING APPROACH

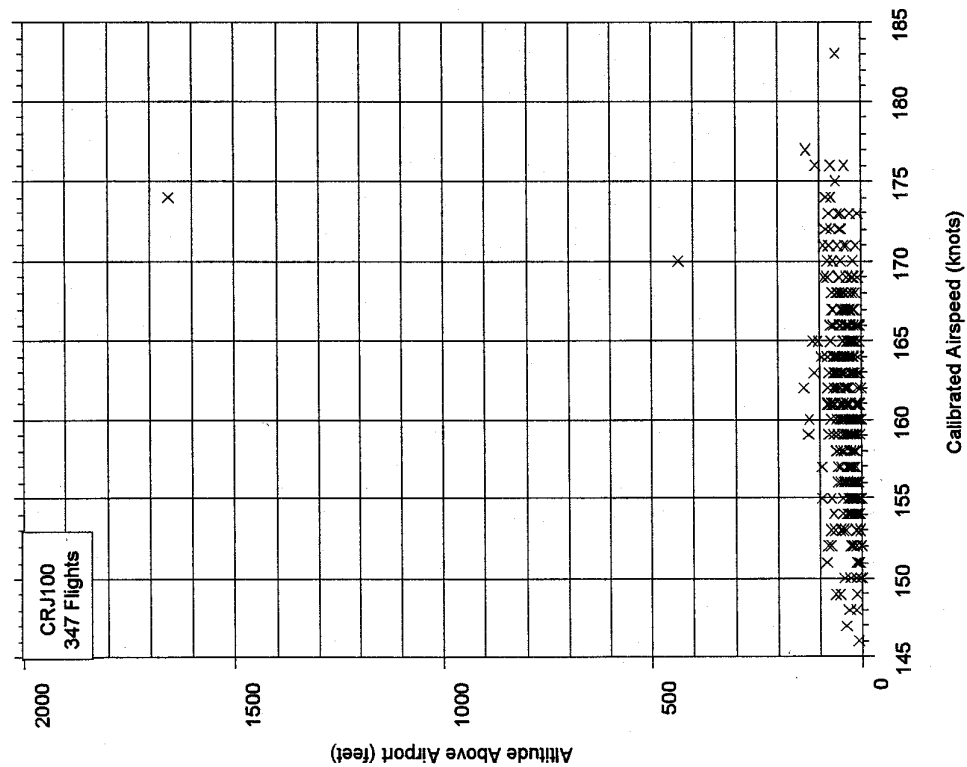


FIGURE A-81. COINCIDENT SPEED AND  
ALTITUDE ABOVE AIRPORT AT LANDING  
GEAR RETRACTION

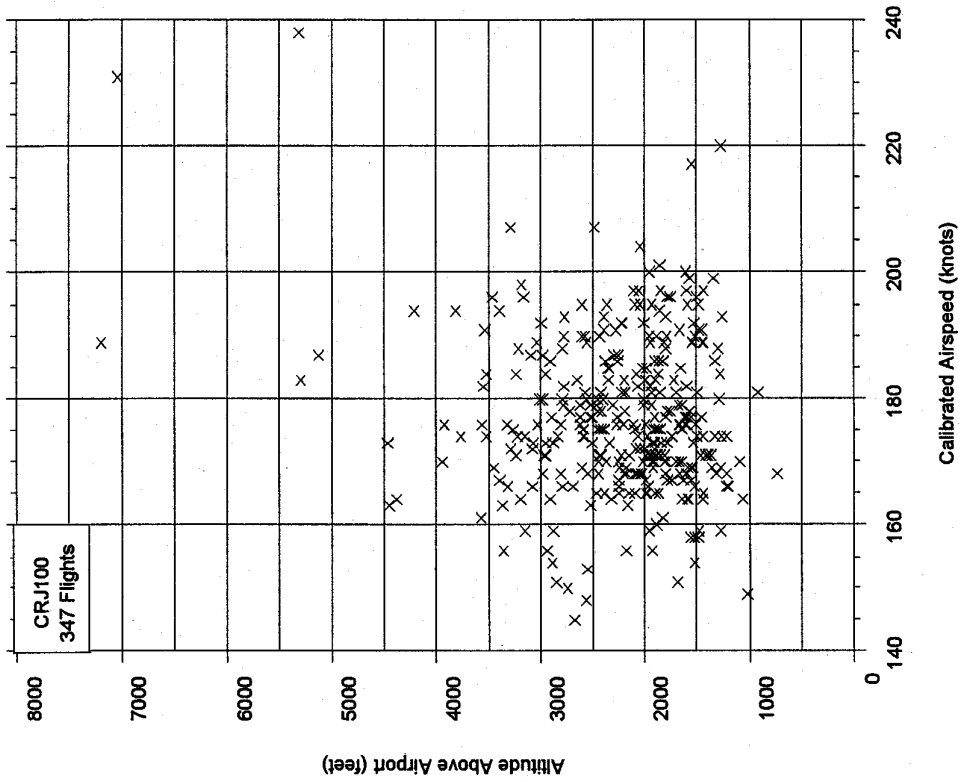


FIGURE A-82. COINCIDENT SPEED AND  
ALTITUDE ABOVE AIRPORT AT LANDING  
GEAR EXTENSION

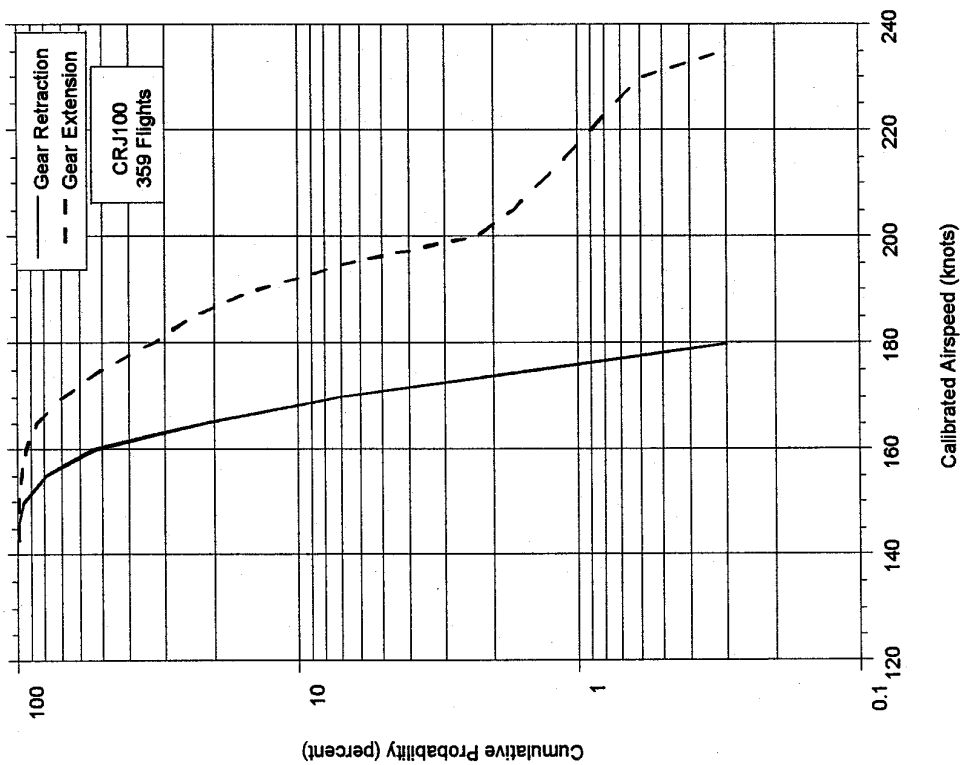


FIGURE A-83. CUMULATIVE PROBABILITY OF SPEED AT LANDING GEAR RETRACTION AND EXTENSION

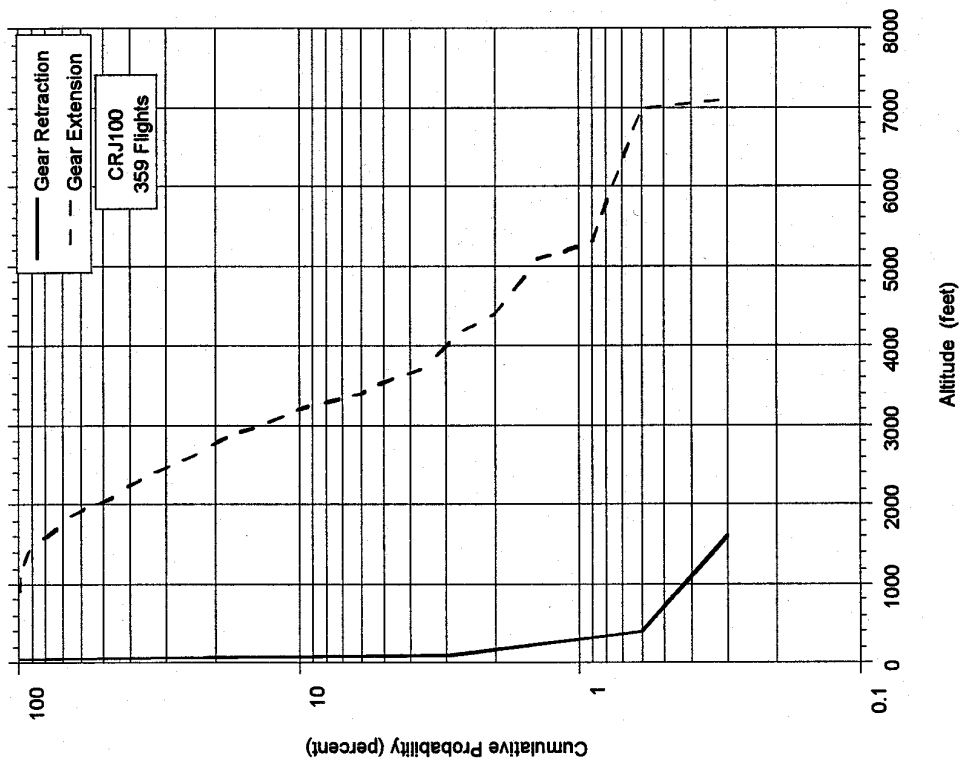


FIGURE A-84. CUMULATIVE PROBABILITY OF ALTITUDE ABOVE AIRPORT AT LANDING GEAR RETRACTION AND EXTENSION

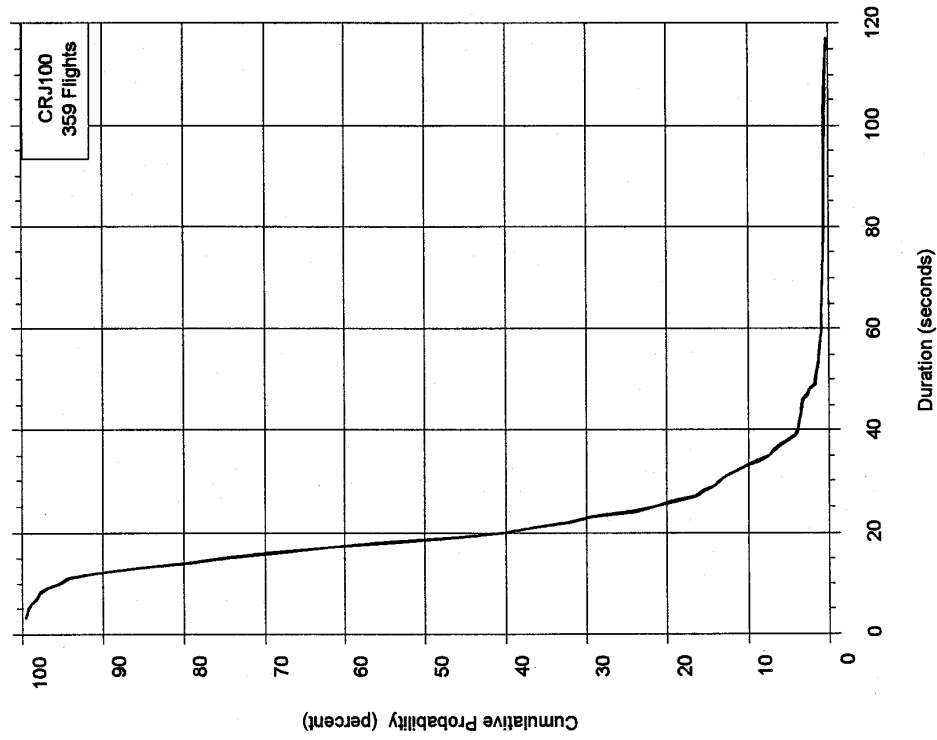


FIGURE A-85. CUMULATIVE PROBABILITY OF TIME AT WITH THRUST REVERSERS DEPLOYED

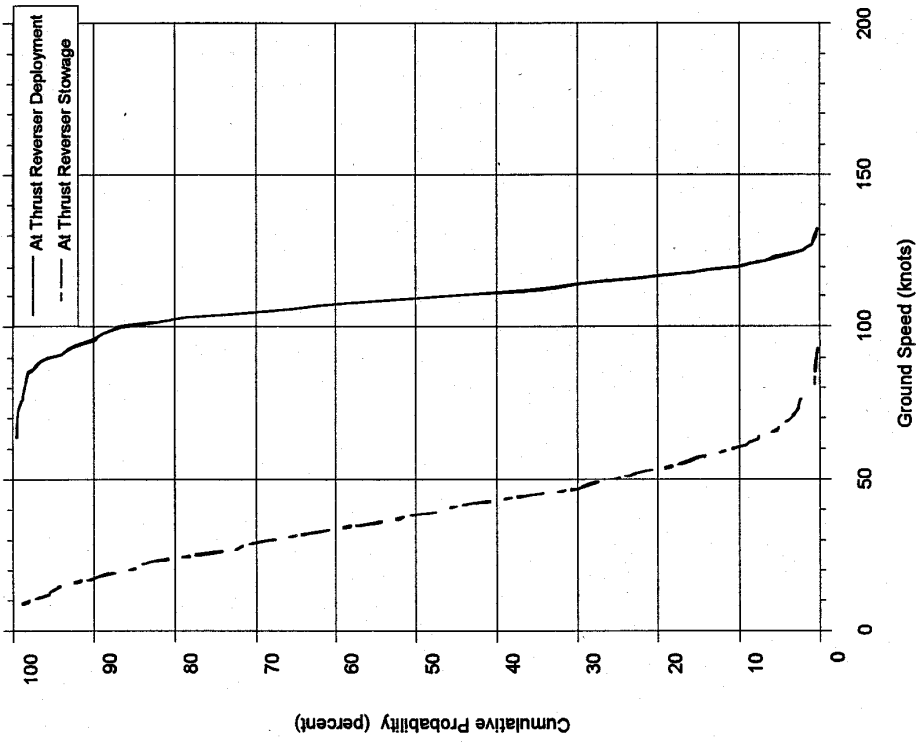


FIGURE A-86. CUMULATIVE PROBABILITY OF SPEED AT THRUST REVERSER DEPLOYMENT AND STOWAGE

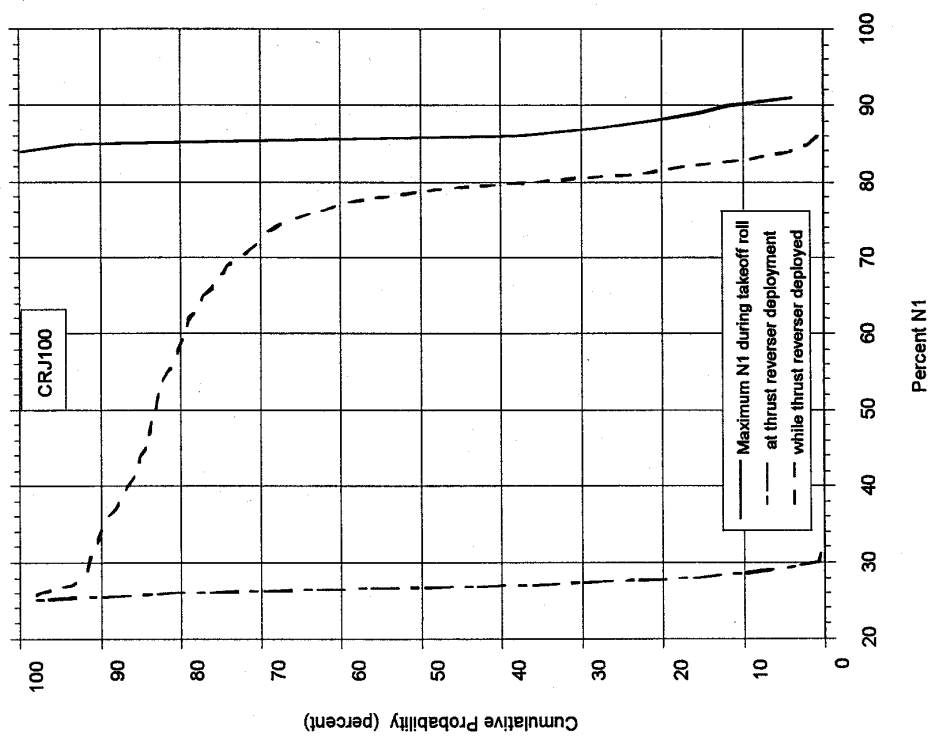


FIGURE A-87. CUMULATIVE PROBABILITY OF PERCENT OF  $N_1$  DURING TAKEOFF, AT THRUST REVERSER DEPLOYMENT, AND DURING THRUST REVERSER DEPLOYMENT